Compressible vs. incompressible pore water in fully-saturated poroelastic soil

Master thesis

F.P.M. Klein

TU Delft

Rijkswaterstaat
Ministerie van Infrastructuur en Waterstaat

Mark Klein Breteler. (02-2024). [Photo]. Deltares.

Compressible vs. incompressible pore water in fully-saturated poroelastic soil

Master thesis

by

F.P.M. Klein

Mark Klein Breteler. (02-2024). [Photo]. Deltares.

Student number:	4904125	
Project duration:	September 04, 2023 – May 23, 2024	
Thesis committee:	Prof. dr. ir. C. Vuik,	TU Delft, supervisor
	Prof. dr. H. M. Schuttelaars	TU Delft, committee member
	Dr. ir. M. van Damme,	Rijkswaterstaat WVL, supervisor
	Dr. ir. D. den Ouden-van der Horst,	TU Delft, daily supervisor

TU Delft

Rijkswaterstaat
Ministerie van Infrastructuur en Waterstaat

Abstract

This thesis aims to contribute to the understanding of how waves interact with soil. It is crucial for various applications in Civil Engineering to analyze the behaviour of soil and to understand the physics behind it. This master thesis contributes to this understanding via studying the impact of the boundary conditions on the model results with the aim of being able to model interaction between waves and soil.

We assume a media that is poroelastic and fully-saturated, unless stated otherwise. We also assume that the porous media consists of incompressible soil particles and pore water particles that may either be compressible or incompressible. The main goals of this thesis are (1) to describe the response of porous media to transient hydraulic loads using numerical methods like the Finite-Element Method, and (2) to apply it to a one-dimensional case whereby a sandbed is subjected to waves. Currently, it is common to predict the changes in pore water pressures in porous media subjected to transient hydraulic loads using Biot's model, which often assumes compressible pore water, assumes zero effective stresses on the surface of the seabed, and assumes that the wave load is completely carried by the pore water pressure only. Recently, a new model is proposed by Van Damme and Den Ouden-Van der Horst suggesting that transient hydraulic loads acting on a porous medium affect both the pore water pressures and effective stresses in soils. Note that this makes sure that the momentum balance equations are satisfied throughout the computational domain and its boundaries. The boundary conditions in this case do not satisfy Terzaghi's effective stress principle, whereas the standard has been to impose Terzaghi's effective stress principle when solving Biot's equations. Terzaghi's principle states that the sum of the effective stresses and pore water pressures must equal the hydraulic loads, whereas Biot's model is in line with this principle.

The model of Biot and the new model of Van Damme and Den Ouden-Van der Horst describe the physics differently which can have a large impact on the results. For example, the assumption of compressibility can significantly impact the distribution of the effective stress in the soil and thus the results. Biot's model is more sensitive for changing the compressibility parameter than the new model. Both models give similar solutions to the water pressure. However, they give different solutions to the other variables like the volumetric strain and displacements which appear in both models. Furthermore, the new model in one dimension is in line with the momentum balance equations and satisfies the volume balance equation. On the other hand, the standard is to solve Biot's model by imposing Terzaghi's principle at the boundary. For the new model we found promising results for the water pressure, when validating with the data of two experiments. At the end, which model predict the best solutions for volumetric strain, water pressure and displacements depends on what kind of problem the model is used for and the corresponding physics. The used code can be found at https://github.com/fpmklein/Compressible-vs.-incompressible-pore-water-in-fully-saturated-poroelastic-soil.

Preface

I am proud to present my master thesis ”Compressible vs. incompressible pore water in fully-saturated poroelastic soil”, which is an extension of the recently published paper by Myron van Damme and Dennis Den Ouden-van der Horst titled ”An alternative process-based approach to predicting the response of water saturated porous media to hydrodynamic loads”. This project took place between September 2023 and May 2024. This report is written to meet the graduate requirements of the master Applied Mathematics at the TU Delft with as specialization in numerical analysis and was done in collaboration with Rijkswaterstaat where I was able to do the project in form of a graduate internship. Applying mathematics to real problems in society has always been interesting to me. This is certainly the case with this project at Rijkswaterstaat, as the behavior of soil due to waves can also have implications for flood defences and a large part of the Netherlands is below sea level.

The research was very interesting, but also very challenging. Especially the literature review part was tough, since a lot of knowledge about the physical aspects was needed to truly understand the mathematical equations. This was quite new to me, as in my study the equations are usually just given rather than needing to be derived. Fortunately, I could always turn to my supervisors, Myron van Damme and Dennis den Ouden-van der Horst, when I got stuck or wanted feedback on written pieces. In particular, I could consult Myron for the physical aspects and Dennis for the mathematical part. I really appreciate the corporation between Myron and Dennis and their communication towards me. A huge thank you to them.

I would also like to thank some other people. First and foremost, I want to thank my parents for always being there, motivating me, and sometimes even holding me back when I studied too long. I would also like to thank some friends: Mirte, Nadine, Tamar, Xander and Ruben. They motivated me, gave occasional feedback, or helped me blow off some steam. I also want to thank Kees Vuik and Henk Schuttelaars for joining the thesis committee. Lastly, I would like to thank various close people for simply showing interest by asking how things were going now and then. In short, thank you everyone for the support and motivation!

I hope you enjoy reading my master thesis.

F.P.M. Klein
Delft, May 2024

Nomenclature

Table 1: Directions and their symbols.

Direction	Symbol
Horizontal	x
Vertical	z

Table 2: Symbols and their definitions and units.

Definition	Symbol		Units
Basis-finite-element functions	N		-
Basis-finite-element functions	$\tilde{N}$		-
Boundary domain	$\mathrm{d}\Omega$		-
Compressibility of the pore water	β		Pa^{-1}
Density of the soil	ρ_s		kg/m^3
Density of the pore water	ρ_f		kg/m^3
Displacement of the soil particles in the i-direction	u_i	(for $i = x, z$)	m
Displacement of the pore water in the i-direction	w_i	(for $i = x, z$)	m
Domain	Ω		-
Effective size of grains	d_{10}		m
Effective stress tensor	σ'_{ij}	(for $i, j = x, z$)	Pa
Elasticity modulus	E		Pa
Hydraulic conductivity	K_s		m/s
Functions in time	F_{xz}, F_{zz}		N
Geometric map	ϕ		-
Lamé's constants	λ, μ		Pa
Length in i-direction	n_i	(for $i = x, z$)	m
Normal unit vector to the boundary	η		-
Poisson ratio	ν_p		-
Pore water pressure	P		Pa
Porosity of the soil	p		-
Relative density	D_r		-
Specific weight of the pore water	γ_w		N/m^3
Stopping time	t_{end}		s
Strain tensor for soil	ϵ_{ij}	(for $i, j = x, z$)	-
Time	t		s
Time step	Δt		s
Total stress tensor	σ_{ij}	(for $i, j = x, z$)	Pa
Volumetric strain of the soil particles	ϵ_{vol}		-
Vorticity of the soil particles	ω		-

Contents

1 Introduction

Analyzing the behaviour of the soil and understanding the physics behind it is crucial for various application of Civil Engineering, like flood risk management and offshore Engineering. This is especially important for a country like the Netherlands, which for a large part is below sea level. To prevent flooding of the land we have to build and keep up flood defences and predict how their strength is affected by changes in hydraulic loads. An example of how the interaction between hydrodynamic loads and soils could influence levee safety is the case when a foreshore is experiencing loads due to the water waves which is shown in Figure 1.1. Due to the water waves, deformations of the foreshore could result in a decrease in resistance of the foreshore against erosion or shearing. Erosion of the foreshore leads to an increase in hydrodynamic loads on the levee cover and a decrease in resistance could cause deformation of the seaside toe structure of levees. On the other hand, foreshores reduce wave heights and loadings on the levee, if the erosion is limited. There are thus many factors that have an impact on flood defences.

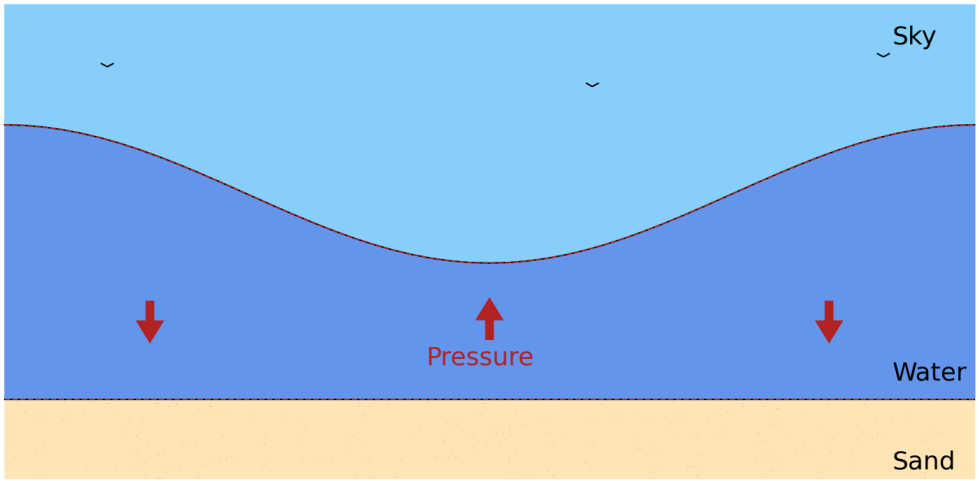

Figure 1.1: A flat foreshore subjected to water waves. The hydraulic load is denoted by the red arrows. When the red arrow is pointing downwards there is a positive pressure on the soil (pushing force) and when the red arrow is pointing upwards there is a negative pressure on the soil (pulling force).

To understand the relation between the soil and hydrodynamic loads and to be able to translate it to different real life scenarios, it is important to analyze and predict this relation for realistic scenarios such as a five metres thick layer of clay subjected to water waves with a period of hours or even days, and a sandy bed subjected to water waves with a period of only seconds. When adding vegetation to the soil we get another realistic scenario. To develop insights into the interaction between vegetated foreshores and water waves, Deltares has recently performed full-scale experiments [1]. For this project two lines

of salt-marsh vegetation were placed and for various wave conditions the pressure, the movement of the clay, the velocity of the water and the movement of the vegetation were monitored [1]. Monitoring these during the experiments gives a better physical understanding of the interaction between vegetated foreshores and water waves. Despite the costs, this remains essential for being able to translate the experimental results to foreshores with other types of soil. This way we can predict the impact of the water waves on the soil better for a certain case by doing these expensive experiments only once and translate it instead of analyzing for each specific case. Therefore, a general description of the interaction between the soil and the transient hydraulic loads is needed.

In this paper, the seabed is assumed to be fully-saturated and poroelastic, and the waves are assumed to be of Poisseuille type (pressure-induced flow) [2]. The soil particles in the seabed are assumed to be incompressible and the water particles could either be compressible or incompressible [3, 4]. In these cases it is common to use Biot's model. This model explains how fully-saturated poroelastic media deform [2] and have been studied extensively [3, 5]. However, in this model it is often assumed that the pore water is compressible [2] to better match the data obtained by experiments [6]. Unfortunately, this assumption of compressibility of pore water can significantly impact the distribution of the effective stress in the soil and thus also the deformation of the soil [4]. However, recent research has proposed a similar model that would not be impacted by the compressibility of the pore water [4]. These two models describe the physics differently, and thus can have a large impact on the results. Therefore, it is important to investigate the differences and validate with real case scenarios. In this thesis, the new model will be validated against two one-dimensional cases. We will compare the numerical results of the new model with data from two different experiments.

The aim of this master thesis is

1. to describe the response of porous media to transient hydraulic loads using numerical methods like the Finite-Element Method, and

2. to apply it to a one-dimensional case whereby a sandbed is subjected to waves.

Two models will be discussed: one is the well-known older model by Biot (1955) [2] and the other one is a recently published model by Van Damme and Den Ouden-Van der Horst (2023) [4]. For both models the acceleration terms and body forces like gravity will be ignored, the wave is assumed to be a standing wave and the soil properties are assumed to be constant in space and time. The main difference between the models lies in their boundary conditions at the surface. Biot's model aligns with the effective stress principle of Terzaghi which states that the total stress acting on a porous medium has to be equal to the pore water pressures added to the effective stresses [2, 3, 4]. Furthermore, Biot's model assumes that the full transient load due to the waves is carried by the dynamic pressure and that the effective stresses of the porous soil are zero at the surface boundary. Lastly, in Biot's model it is often assumed that the water is compressible.On the other hand, the new model is based on maintaining valid momentum balance equations within the computational domain and its boundaries [4] and considers instead the stress and the gradient of the stress, which follows from one of the momentum balance equations, at the surface boundary. While the new model then follows D'Alembert's principle of minimisation of virtual work [4], it does not satisfy the effective stress principle of Terzaghi at the surface in case of transient load which would be valid in the case of statics and linear stress [4]. The choice of boundary conditions can have a significantly impact on the results. For example, the choice of boundary conditions for Biot's model does not match observations of grass covers being pulled from the soil [7]. Due to the choice of boundary conditions for the new model, the solutions for the new model can explain this event [4]. Furthermore, the solutions of the new model could also help to explain the liquefaction of soil which is often observed when soil is subjected to water waves [4, 8].

Biot's model and the new model will be solved for variables that describe the deformation of the porous media by using numerical methods. In this report, we assume to have one homogeneous layer of soil as seabed, unless stated otherwise. We use the Finite-Element Method (FEM) for discretising in space. For discretising in time the Backward-Euler Method is used. This way a numerical model is derived for Biot's model and Van Damme and Den Ouden-Van der Horst. These numerical models for Biot's model and the new model will be solved for variables like the dynamic water pressure, volumetric strain and displacements. The volumetric strain and displacements are variables of minor importance compared to the pore water pressure. However, the impact of the volumetric strain and displacements on the effective stress and shear stress is very important, since the stability of the embankment is

determined by checking whether the effective stresses combined with shear stresses exceed a critical value. The shear strength is a function of the effective stress: when the effective stress increases, also the resistance to shearing grows. Similar to our literature report [9], we would like to answer the following questions:

1. Do Biot's model and Van Damme and Den Ouden-Van der Horst model in two dimensions differ in (numerical) solution?
2. Do the results of the two models get impacted by the assumption of (in)compressibility?
3. Can the numerical model correctly reproduce the physical behaviour observed during experiments?

We start in Chapter 2 with describing the stress and strain relations in a linear elastic medium. Then we extend these relations for the case of a fluid-solid system with a poroelastic fully-saturated medium. In Chapter 3 these constitutive equations describing the deformation of fully-saturated poroelastic media are stated in two dimensions. This set of equations is better known as Biot's model [2] where pore water is often assumed to be compressible. The numerical discretisation of Biot's model is stated in Chapter 4. In Section 4.1 we will look into the application of the Finite-Element Method and in Section 4.2 we will look into the application of the Backward-Euler method on the model of Biot in two dimensions in order to discretise the governing equations in space and time, respectively. In Chapter 5 the numerical discretisation of Biot's model in two dimensions is solved for three different but similar sets of boundary conditions. In Chapter 6 the governing equations of the new model of Van Damme and Den Ouden-Van der Horst in two dimensions are determined. In Chapter 7 these equations are discretised. In Section 7.1 the governing equations of the new model in two dimensions are first discretised in space by the Finite-Element Method and in Section 7.2 the resulting equations are descretised in time by the Backward-Euler method. In Chapter 8 the numerical descretisation of the model of Van Damme and Den Ouden-Van der Horst in two dimensions is solved in two dimensions for two different but similar boundary conditions sets. Then in Chapter 9 some more comparison is done between Biot's model and the new model in two dimensions by switching a set of boundary conditions. This way we want to investigate the influence of the model and of the boundary conditions separately. In Chapter 10 we validate the new model. We will first reduce the two-dimensional new model to one dimension in Section 10.1 and then compare the new model in one dimension to two different datasets. One dataset is obtained by measuring data in a one-dimensional set up with a vertical cylinder with first a sand deposit of 1.8 metres thick and then 0.2 metres water above the sand which is described in Section 10.2. The second dataset is obtained by measuring data in the middle of the width of the Twente channel when a ship passes by which is described in Section 10.3. Lastly, in Chapter 11 the conclusions are made, the research questions will be answered and ideas for further research are discussed.

2

Linear elastic medium (2D)

Following our literature report [9], we start with deriving the basic equations for a linear elastic medium, using Cartesian coordinates x, z, since this is a more simple case than the fluid-solid system with a fully-saturated poroelastic medium. We can write the stresses and strains as [2, 5]

$$\bar{\bar{\sigma}} := \begin{bmatrix} \sigma_{xx} & \sigma_{xz} \\ \sigma_{xz} & \sigma_{zz} \end{bmatrix} \text{ and} \tag{2.1}$$

$$\bar{\bar{\epsilon}} := \begin{bmatrix} \epsilon_{xx} & \epsilon_{xz} \\ \epsilon_{xz} & \epsilon_{zz} \end{bmatrix}, \tag{2.2}$$

where σ_{ij} [-] is the stress and ϵ_{ij} [-] is the strain for $i, j = x, z$. We will refer to $\bar{\bar{\sigma}}$ and $\bar{\bar{\epsilon}}$ as the stress tensor and strain tensor, respectively. The stress components σ_{ii} for $i = x, z$ are called normal stresses and σ_{ij} for $i, j = x, z$ and $i \neq j$ are called shear stresses. Two deformations with constant volume due to the normal stresses and the shear stresses are given by Figures 2.1 and 2.2, respectively. The strain components denote the change in length of an element divided by its original length [10]. For example, the horizontal strain ϵ_{xx} is the change of horizontal length of an element of original length Δx dived by that original length [10]. In Figure 2.3 the strain components are shown.

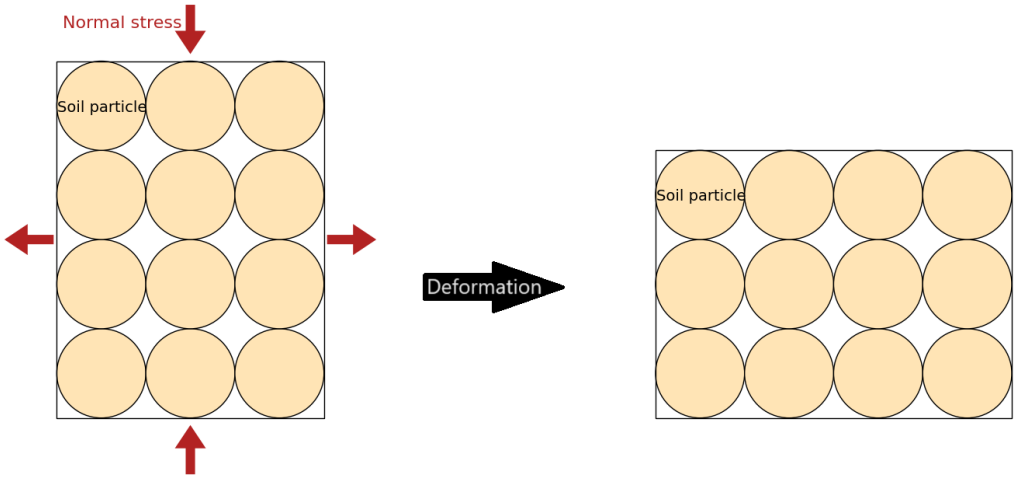

Figure 2.1: Deformation with constant volume due to normal stresses [10].

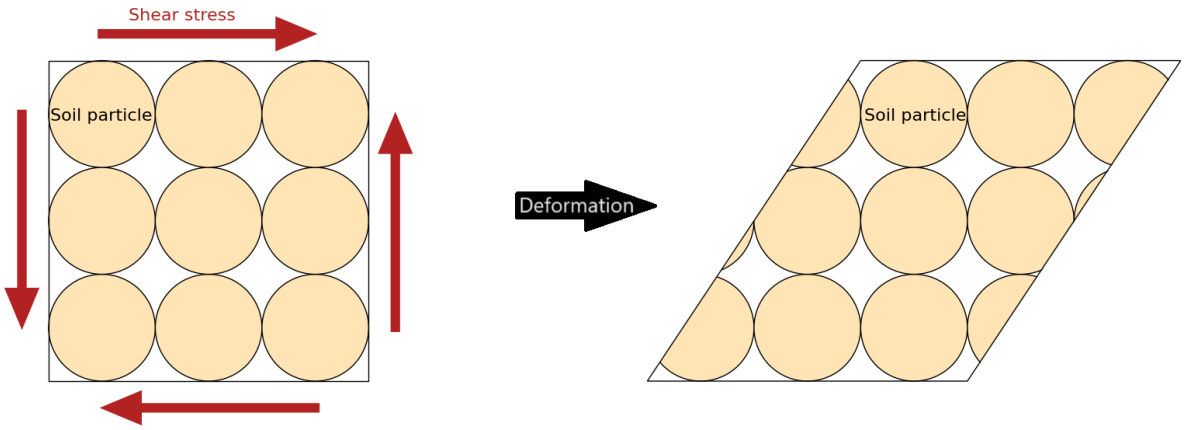

Figure 2.2: Deformation with constant volume due to shear stresses [10].

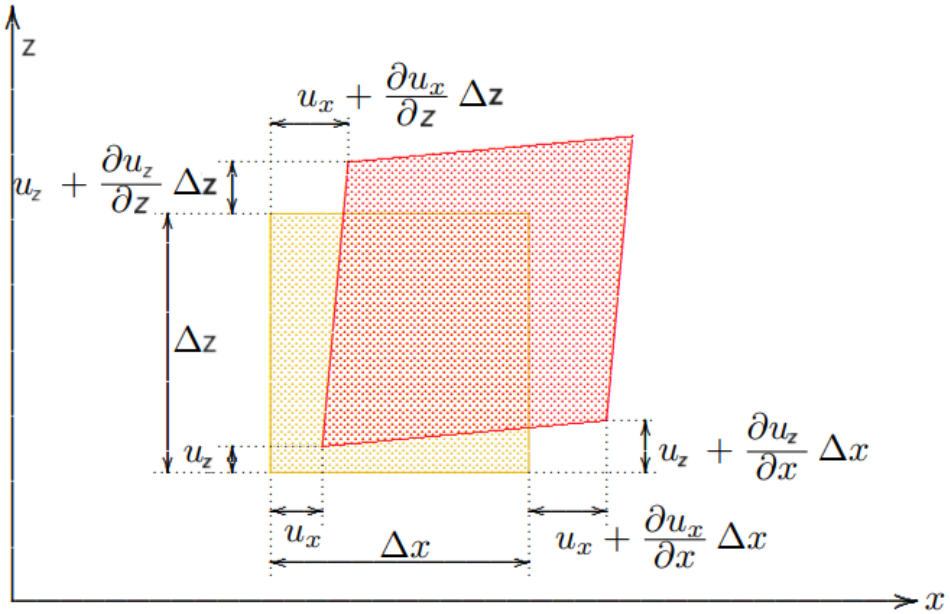

Figure 2.3: Strain components of ϵ acting on the computational domain Ω which is a rectangle [10]. This figure is from (Verruijt,2010).

In this section we assume a linear elastic medium of which a volume of the solid system will be represented by a rectangle of size $n_x \times n_z$. The domain $\Omega := n_x \times n_z$ is shown in Figure 2.4 together with the stress components pointing in positive direction.

Then we can use geometric equations, equations of motion and constitutive equations to represent the strain-displacement relations and stress-strain relations. In tensor form the geometric equations are given by [2, 5]

$$\epsilon_{ij} = \frac{1}{2}\left(\frac{\partial u_i}{\partial j} + \frac{\partial u_j}{\partial i}\right) \quad \text{for } i,j = x,z, \tag{2.3}$$

where u_i [m] denotes the displacement of the solid in the i-direction and $u_{i,j}$ means derivative of u_i with respect to the j-th component.

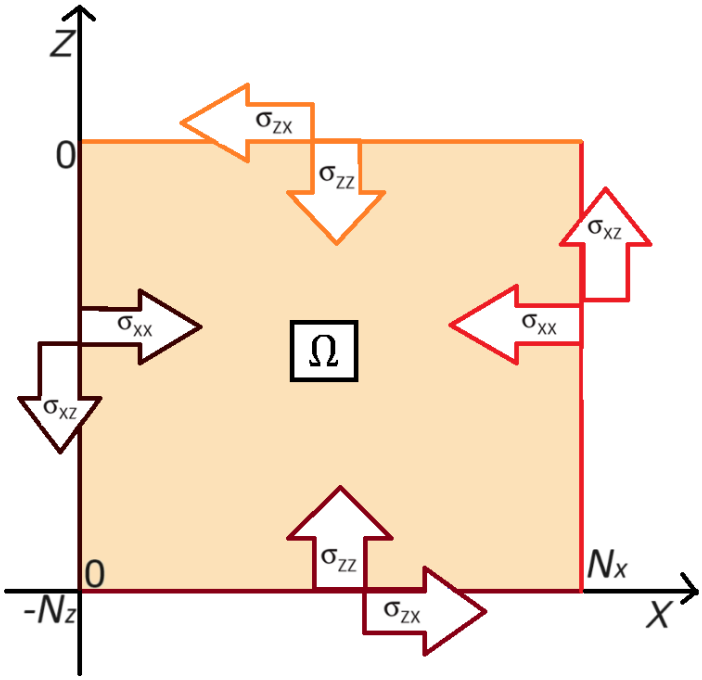

Figure 2.4: Stress components of σ acting on the computational domain Ω which is a rectangle.

According to [5], the constitutive equation which will be given in tensor form of Hooke's law:

$$\sigma_{ij} = -\sum_{k=x,z}\sum_{l=x,z} c_{ijkl}\epsilon_{kl} \quad \text{for } i,j = x,z, \tag{2.4}$$

where c_{ijkl} are components of a fourth-rank tensor including 81 components. Since stress tensors and strain tensors are symmetric, we have first minor symmetry and second minor symmetry, i.e. $c_{ijkl} = c_{jikl}$ and $c_{ijkl} = c_{ijlk}$. Furthermore, for a homogeneous medium, we also have major symmetry, i.e. $c_{ijkl} = c_{klij}$ [5]. Because of these symmetries, the number of independent components decreases to 2 so that Equation (2.4) becomes [3]

$$\sigma_{ij} = -2\mu\epsilon_{ij} - \lambda\delta_{ij}\epsilon_{\text{vol}} \quad \text{for } i,j = x,z,$$

where $\epsilon_{\text{vol}} = \epsilon_{xx} + \epsilon_{yy} + \epsilon_{zz}$ for $i = x,y,z$, δ_{ij} is the kronecker delta function ($\delta_{ij} = 1$ if $i = j$, otherwise 0) and λ [Pa] and μ [Pa] are Lame's constants. Lamé's constants are defind as

$$\begin{cases} \lambda &= \frac{v_p E}{(1+v_p)(1-2v_p)}, \\ \mu &= \frac{E}{2(1+v_p)}, \end{cases} \tag{2.5}$$

where E represents Young's modulus and v_p Poisson's ratio [5, 10]. Rewriting this in matrix-vector form [5] gives

$$\boldsymbol{\sigma} = -C\boldsymbol{\epsilon},$$

where

$$\boldsymbol{\sigma} = \begin{bmatrix} \sigma_{xx} \\ \sigma_{zz} \\ \sigma_{xz} \end{bmatrix}, \quad \boldsymbol{\epsilon} = \begin{bmatrix} \epsilon_{xx} \\ \epsilon_{zz} \\ \epsilon_{xz} \end{bmatrix}, \quad C = \begin{bmatrix} \lambda + 2\mu & \lambda & 0 \\ \lambda & \lambda + 2\mu & 0 \\ 0 & 0 & \mu \end{bmatrix}.$$

Note that matrix C is non-singular and invertible.
These conclude the relations of stresses and strains for a linear elastic medium.

3

Biot's model (2D)

We will now look into the governing equations of a fully-saturated poroelastic medium in line with Biot's model. Following our literature report [9], we consider a volume of a solid-fluid system which will be described by a unit size rectangle and assume that the principal stress and strain directions are the same. Furthermore, we ignore the acceleration terms of the fluid relative to the solid for now. And last, the body forces are also ignored.

In this chapter we will describe the stress and strain relations in this fluid-solid system by the governing equations of Biot's model in two dimensions together with the corresponding boundary conditions. In order to derive Biot's model we follow the steps presented by Verruijt [3, 10] and use their final set of equations instead of the equations of the new model of Van Damme and Den Ouden-Van der Horst stated in Chapter 4 of our literature report [9] (and in Chapter 6 of this master thesis). This Biot's model uses one governing equation less and one boundary condition more than the new model which is described in Chapter 6.

3.1. Conservation of mass equation

First of all, we need the equations of conservation of mass of the solids and the pore water. As described in our literature report [9], according to [3] the resulting mass balance equation for the pore water (fluid) is given by

$$\frac{\partial p\rho_f}{\partial t} + \frac{\partial}{\partial x}\left(p\rho_f \frac{\partial w_x}{\partial t}\right) + \frac{\partial}{\partial z}\left(p\rho_f \frac{\partial w_z}{\partial t}\right) = 0, \tag{3.1}$$

where ρ_f [kg/m^3] is the density of the fluid, w_x [m] is the displacement of the pore water in x-direction, w_z [m] is the displacements of the pore water in z-direction and p [-] the porosity of the medium. The mass balance equation for the soil is given by [3]

$$\frac{\partial (1-p)\rho_s}{\partial t} + \frac{\partial}{\partial x}\left([1-p]\rho_s \frac{\partial u_x}{\partial t}\right) + \frac{\partial}{\partial z}\left([1-p]\rho_s \frac{\partial u_x}{\partial t}\right) = 0, \tag{3.2}$$

where ρ_s [kg/m^3] is the density of the soil, u_x [m] is the displacement of the soil in x-direction and u_z [m] is the displacements of the soil in z-direction.

When assuming that the pore fluid depends on the fluid pressure by the following equation

$$\rho_f = \rho_0 \exp\left[\beta(P - P_0)\right],$$

where β is the compressibility of the fluid, P the pore fluid pressure, and ρ_0 and P_0 are reference quantities [10]. This means that

$$\begin{aligned} \frac{\partial p\rho_f}{\partial t} &= p\frac{\partial \rho_f}{\partial t} + \rho_f \frac{\partial p}{\partial t} \\ &= p\beta\rho_f \frac{\partial P}{\partial t} + \rho_f \frac{\partial p}{\partial t}. \end{aligned} \tag{3.3}$$

When substituting Equation (3.3) into Equation (3.1), we can rewrite the mass balance equation of the pore water as

$$\frac{\partial p}{\partial t} + p\beta\frac{\partial P}{\partial t} + \frac{\partial}{\partial x}\left(p\frac{\partial w_x}{\partial t}\right) + \frac{\partial}{\partial z}\left(p\frac{\partial w_z}{\partial t}\right) = 0, \tag{3.4}$$

where P [Pa] denotes the pore water pressure and β [Pa^{-1}] the compressibility. Note that the water is incompressible if $\beta = 0.0$ and compressible if $\beta > 0$. We assume that the soil particles are incompressible. Then we have that the density ρ_s is constant. Therefore, we have that Equation (3.2) becomes

$$-\frac{\partial p}{\partial t} + \frac{\partial}{\partial x}\left([1-p]\frac{\partial u_x}{\partial t}\right) + \frac{\partial}{\partial z}\left([1-p]\frac{\partial u_z}{\partial t}\right) = 0. \tag{3.5}$$

When adding Equations (3.4) and (3.5), we get [3]

$$p\beta\frac{\partial P}{\partial t} + \frac{\partial}{\partial x}\left(p\frac{\partial(w_x-u_x)}{\partial t}\right) + \frac{\partial}{\partial z}\left(p\frac{\partial(w_z-u_z)}{\partial t}\right) + \frac{\partial}{\partial x}\left(\frac{\partial u_x}{\partial t}\right) + \frac{\partial}{\partial z}\left(\frac{\partial u_z}{\partial t}\right) = 0. \tag{3.6}$$

Using $\epsilon_{\text{vol}} = \frac{\partial u_x}{\partial x} + \frac{\partial u_z}{\partial z}$, we can write Equation (3.6) as [3]

$$p\beta\frac{\partial P}{\partial t} + \frac{\partial}{\partial x}\left(p\frac{\partial(w_x-u_x)}{\partial t}\right) + \frac{\partial}{\partial z}\left(p\frac{\partial(w_z-u_z)}{\partial t}\right) + \frac{\partial \epsilon_{\text{vol}}}{\partial t} = 0. \tag{3.7}$$

The quantity $q_i := \frac{\partial p(w_i-u_i)}{\partial t}$ for $i = x, z$ is the porosity multiplied by the difference of the velocities of the pore water and soil particles. The specific discharge denotes this and appears in Darcy's law for fluid motion [3]. Using Darcy's law, we can also write that $q_i = -\frac{K_s}{\gamma_w}\frac{\partial P}{\partial i}$ for $i = x, z$, where K_s [m/s] denotes the hydraulic conductivity and γ_w [N/m^3] the specific weight [3]. Therefore, we have that

$$-\nabla\cdot\left(\frac{K_s}{\gamma_w}\nabla P\right) = \nabla\cdot\left(p\frac{\partial(\boldsymbol{w}-\boldsymbol{u})}{\partial t}\right), \tag{3.8}$$

where $\nabla\cdot = \frac{\partial v_x}{\partial x} + \frac{\partial v_z}{\partial z}$ for all vectors $\boldsymbol{v} = \begin{bmatrix} v_x \\ v_z \end{bmatrix}$. After substituting Equation (3.8) into Equation (3.7) and assuming K_s and γ_w are constants, we get

$$\frac{\gamma_w}{K_s}p\beta\frac{\partial P}{\partial t} - \nabla^2 P + \frac{\gamma_w}{K_s}\frac{\partial \epsilon_{\text{vol}}}{\partial t} = 0. \tag{3.9}$$

We can rewrite Equation (3.9) in terms of u_x, u_z and P as follows

$$\frac{\gamma_w}{K_s}p\beta\frac{\partial P}{\partial t} - \nabla^2 P + \frac{\gamma_w}{K_s}\frac{\partial}{\partial t}\left(\frac{\partial u_x}{\partial x} + \frac{\partial u_z}{\partial z}\right) = 0. \tag{3.10}$$

3.2. Momentum balance equation

The stress tensor can be separated into two parts, since we now have a fluid and a solid part. The stress acting on a rectangular domain in Figure 2.4 can be denoted as Equation (2.1) [2] and the stress acting on the fluid part the rectangle domain in Figure 2.4 can be described by the diagonal tensor [2]

$$\bar{\bar{s}} := \begin{bmatrix} s & 0 \\ 0 & s \end{bmatrix}, \tag{3.11}$$

where s [Pa] can be calculated by $s = \alpha P$ [2, 5] with P the fluid pressure and α the Biot constant that depends on the geometry of the medium. Usually $\alpha \approx 1$ can be assumed in Civil Engineering problems [5]. We will assume from now on that $\alpha = 1$. Note the plus-signs in the relation $s = \alpha P$ which describes that scalar s must be positive when the force acting on the fluid is a pressure and the stress tensors σ_x, σ_y and σ_z are negative due to the positive compression convention in the formulation. Note that in [2]

a minus-sign is placed before s, since they assume negative pressure when the stresses are positive. The strain tensor in the solid is denoted by Equation (2.2), where ϵ_{ij} for $i,j = x,z$ are described by Equation (2.3) [2, 3]. For a linear solid medium the total stress and effective stress coincided. However, since we now have a saturated medium, there is also the pore pressure in the relation between total and effective stress which is in tensor form [2, 3]

$$\sigma_{ij} = \sigma'_{ij} + \delta_{ij}P \quad \text{for } i,j = x,z,$$

where σ'_{ij} [-] denotes the effective stress tensor of the solid medium, σ_{ij} [Pa] the total stress tensor, δ_{ij} the Kronecker delta function and P the pore water pressure. Since $\sigma'_{ij} = -2\mu\epsilon_{ij} - \lambda\delta_{ij}\epsilon_{\text{vol}}$, we have that

$$\sigma_{ij} = -2\mu\epsilon_{ij} - \lambda\delta_{ij}\epsilon_{\text{vol}} + \delta_{ij}P \quad \text{for } i,j = x,z, \tag{3.12}$$

where δ_{ij} is the kronecker delta and λ and μ are Lamé's constant.

The equilibrium equations for a fully saturated poroelastic medium are made out of the stresses acting upon the rectangle which is given by [2, 5]

$$\frac{\partial\sigma_{ix}}{\partial x} + \frac{\partial\sigma_{iz}}{\partial z} = 0 \quad \text{for } i = x,z. \tag{3.13}$$

Then substituting Equation (3.12) into Equation (3.13) gives

$$-2\mu\frac{\partial\epsilon_{ix}}{\partial x} - \lambda\delta_{ix}\frac{\partial\epsilon_{\text{vol}}}{\partial x} + \delta_{ix}\frac{\partial P}{\partial x} - 2\mu\frac{\partial\epsilon_{iz}}{\partial z} - \lambda\delta_{iz}\frac{\partial\epsilon_{\text{vol}}}{\partial z} + \delta_{iz}\frac{\partial P}{\partial z} = 0 \quad \text{for } i = x,z. \tag{3.14}$$

We can rewrite this as [3]

$$\begin{cases} -(\lambda+\mu)\frac{\partial\epsilon_{\text{vol}}}{\partial x} - \mu\nabla^2 u_x + \frac{\partial P}{\partial x} = 0 \\ -(\lambda+\mu)\frac{\partial\epsilon_{\text{vol}}}{\partial z} - \mu\nabla^2 u_z + \frac{\partial P}{\partial z} = 0 \end{cases}, \tag{3.15}$$

where $\nabla^2\boldsymbol{v} = \frac{\partial^v_x}{\partial x^2} + \frac{\partial^2 v_z}{\partial z^2}$ for all vectors $\boldsymbol{v} = \begin{bmatrix} v_x \\ v_z \end{bmatrix}$. We can also rewrite Equation (3.14) as

$$\begin{cases} -\mu\frac{\partial\omega}{\partial z} - (\lambda+2\mu)\frac{\partial\epsilon_{\text{vol}}}{\partial x} + \frac{\partial P}{\partial x} = 0 \\ \mu\frac{\partial\omega}{\partial x} - (\lambda+2\mu)\frac{\partial\epsilon_{\text{vol}}}{\partial z} + \frac{\partial P}{\partial z} = 0 \end{cases}, \tag{3.16}$$

where $\omega := \frac{\partial u_x}{\partial z} - \frac{\partial u_z}{\partial x}$. which is used in [4]. Note that ω and ϵ are not independent variables, since they depend on the displacements. Therefore, we will solve the set of equations given by Equation (3.16) expressed in only the displacements and the pore water pressure, i.e.

$$\begin{cases} (\lambda+\mu)\mu\frac{\partial}{\partial z}\left(\frac{\partial u_x}{\partial z} - \frac{\partial u_z}{\partial x}\right) - (\lambda+2\mu)\nabla^2 u_x + \frac{\partial P}{\partial x} = 0 \\ -(\lambda+\mu)\frac{\partial}{\partial x}\left(\frac{\partial u_x}{\partial z} - \frac{\partial u_z}{\partial x}\right) - (\lambda+2\mu)\nabla^2 u_z + \frac{\partial P}{\partial z} = 0 \end{cases}, \tag{3.17}$$

Note that Equations (3.15) and (3.17) have second order derivatives. Equation (3.15) depends on ϵ, P and u_x or u_z while Equation (3.17) depends on P, u_x and u_z. Using Equation (3.17), we already used the definition of the dependant variables (ϵ, ω) and do not need an extra equation(s) for these variables. Furthermore, it can be analytically shown that the vorticity ω is zero everywhere on the domain and its boundaries and therefore the first term of Equations (3.17) disappears which simplifies the two momentum balance equations significantly. Equation (3.17) will be used further in this chapter.

3.3. Boundary conditions

At the surface, it is common in Biot's model to set the normal stress equal to the hydrodynamic load and to suppose that the normal effective stress equals zero. This means that the water pressure at the surface must equal the hydrodynamic load, since the normal stress is defined to be the sum of the normal effective stress and the water pressure [9]. In other words, at the surface we have that

$\sigma_{zz} := \sigma'_{zz} + P = F_{zz}$ where $\sigma'_{zz} = 0$, $P = F_{zz}$ and where F_{zz} is a function depending only on time and horizontal displacement. However, according to [4], the assumption of $\sigma'_{zz} + P = F_{zz}$ gives a pressure at the surface that is much larger than the pressure of the waves on the surface caused by water running over the porous medium [9]. Note that since $\sigma_{zz} = F_{zz} = \sigma'_{zz} + P$, Terzaghi's principle is met. Another condition at boundary $z = 0$ [9] is that the shear stress equals also a function $\sigma_{xz} = F_{xz}$ [3], where F_{xz} is a function only depending on time and horizontal displacement. Recall that the formula of shear stress is given by $\sigma_{xz} = -2\mu\epsilon_{xz} = -\mu\left(\frac{\partial u_x}{\partial z} + \frac{\partial u_z}{\partial x}\right)$.

At $z = -n_z$ we assume that the displacement for the soil and pore water in z-direction is zero for a deep enough seabed [9] which implies that $u_z = 0$ and that there is no gradient for the pore water pressure which is defined as $\frac{\partial P}{\partial z} = 0$ [6, 7] at $z = -n_z$, respectively.

Similarly, at $x = 0$ and $x = -n_x$ it is assumed that the displacements will smoothen out according to [11]. Then we get that $\frac{\partial u_z}{\partial x} = 0$ and $\frac{\partial u_x}{\partial z} = 0$ at $x = 0, L$ [6]. Assuming that the displacements on the sides of the domain are negligible, we have that $u_x = 0$ at $x = 0, n_x$ [6]. Therefore, we also have that the volumetric strain does not have a gradient $\frac{\partial \epsilon_{\text{vol}}}{\partial x} = 0$ at $x = 0, n_x$. Furthermore, we have that the pore water has no gradient at $x = 0$ and $x = n_x$, which is defined by $\frac{\partial P}{\partial x} = 0$, since the water displacements are also assumed to be negligible [6]. Furthermore, since $\frac{\partial u_x}{\partial z} = 0$ and $\frac{\partial u_z}{\partial x} = 0$, we have that $\omega = 0$ at $x = 0$ and $x = n_x$ which agrees when assuming $\omega = 0$ everywhere beforehand.

In conclusion, we have the following boundary conditions

$$\text{for } z = 0: \begin{cases} -\mu\left(\frac{\partial u_x}{\partial z} + \frac{\partial u_z}{\partial x}\right) = F_{xz} \\ P = F_{zz} \\ -\lambda\frac{\partial u_x}{\partial x} - (\lambda + 2\mu)\frac{\partial u_z}{\partial z} = 0 \end{cases}, \tag{3.18}$$

$$\text{for } z = -n_z: \left\{ u_z = \frac{\partial u_x}{\partial z} = \frac{\partial P}{\partial z} = 0 \right. , \tag{3.19}$$

$$\text{and for } x = 0 \text{ and } x = n_x: \left\{ u_x = \frac{\partial u_z}{\partial x} = \frac{\partial P}{\partial x} = 0 \right. , \tag{3.20}$$

3.4. Initial conditions

Following our literature paper [9], we assume that at the beginning, $t = 0$, everything is at rest. Therefore, it is assumed that no stresses act on the surface in the beginning, so there are no stresses and displacements at time $t = 0$ [4]. Since we have no displacement and stresses, the volumetric strain and pressure must be zero too. Then we have that [4]

$$\omega|_{t=0} = u_x|_{t=0} = u_z|_{t=0} = \epsilon_{\text{vol}}|_{t=0} = P|_{t=0} = 0.$$

4

Numerical model of Biot (2D)

In this chapter, the numerical approximation of the two-dimensional physical model of Biot described in Chapter 3 will be derived. We will use the Finite-Element Method for discretisation in space and the Euler method for discretisation in time which are described in Sections 4.1 and 4.2, respectively. After applying the discretisation first in space and second in time, the final numerical model is derived.

4.1. Discretisation in space

In the following sections we will discretise the mass and momentum balance equations which are given in Section 3. First we will discretise these four equations with respect to space using the Finite-Element Method (FEM) in order to derive the Galerkin equations. We do this per equation. In this numerical approach we assume that $\Omega = (0, n_x) \times (-n_z, 0) \subseteq \mathbb{R}^2$ is the space domain and that $\mathbb{T} = (0, t_{\text{end}})$ is the time domain, with $n_x, n_z, t_{\text{end}} > 0$.

The two-dimensional domain and its boundaries are given as in Figure 4.1, each with their own color. The normal unit vectors with respect to this boundaries are also given in Figure 4.1, These have corresponding colors to their boundary. The normal unit vectors in two dimensions are given by

$$\eta_1 = \begin{bmatrix} 0 \\ -1 \end{bmatrix}, \quad \eta_2 = \begin{bmatrix} 1 \\ 0 \end{bmatrix}, \quad \eta_3 = \begin{bmatrix} 0 \\ 1 \end{bmatrix}, \quad \eta_4 = \begin{bmatrix} -1 \\ 0 \end{bmatrix}.$$

Note that the first entry represents the x-direction (horizontal) and the second entry represents the z-direction (vertical).

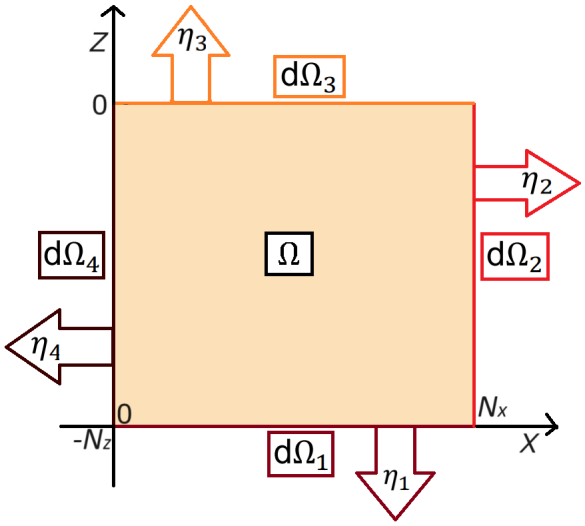

Figure 4.1: Rectangle domain with boundaries and their normal unit vectors. The domain is given by the color blue. The subdomains $d\Omega_1, d\Omega_2, d\Omega_3$ and $d\Omega_4$ with their normal unit vectors are given by the colors bordeaux red, light red, orange and dark red, respectively.

We define n to be the dimension of the space and N_i are the basis-functions for $i = 1, \dots, n$ that form a basis for the space. Note that in the next few sections N_i has a superscript which can be the symbol of the volumetric strain, pore water pressure or displacement in horizontal or vertical direction. In this case, N_i for $i = 1, \dots, n$ are defined for the space of that unknown variable specifically. n is assumed to be the same for all spaces.

4.1.1. Conservation of mass equation

We will derive the weak form of the pressure equation and its matrix-vector form. Suppose that the test and trial functions are given by

$$v^{u_x}(x,z,t) = \sum_{i=1}^{n} N_i^{u_x}(x,z)\bar{v}_i^{u_x}(t), \tag{4.1}$$

$$v^{u_z}(x,z,t) = \sum_{i=1}^{n} N_i^{u_z}(x,z)\bar{v}_i^{u_z}(t), \tag{4.2}$$

$$v^{P}(x,z,t) = \sum_{i=1}^{n} N_i^{P}(x,z)\bar{v}_i^{P}(t), \tag{4.3}$$

$$u_x(x,z,t) = \sum_{j=1}^{n} N_j^{u_x}(x,z)\bar{u}_j^{x}(t), \tag{4.4}$$

$$u_z(x,z,t) = \sum_{j=1}^{n} N_j^{u_z}(x,z)\bar{u}_j^{z}(t), \tag{4.5}$$

$$P(x,z,t) = \sum_{l=1}^{n} N_l^{P}(x,z)\bar{P}_l(t). \tag{4.6}$$

Note that the basis-functions only depend on the domain Ω and the parameters with a bar above depend only on time $\mathbb{T}$.

After multiplying Equation (3.10) by test function v^P and integrating over the domain Ω, we have that

$$\int_{\Omega} v^{P}\left[\frac{\gamma_w}{K_s}p\beta\frac{\partial P}{\partial t} - \frac{\partial^2 P}{\partial x^2} - \frac{\partial^2 P}{\partial z^2} + \frac{\gamma_w}{K_s}\frac{\partial}{\partial t}\left(\frac{\partial u_x}{\partial x} + \frac{\partial u_z}{\partial z}\right)\right]\mathrm{d}\Omega = 0. \tag{4.7}$$

Since $\frac{\partial^2 P}{\partial x^2} + \frac{\partial^2 P}{\partial z^2} = \nabla\cdot(\nabla P)$, we can apply integration by parts on the $-\frac{\partial^2 P}{\partial x^2} - \frac{\partial^2 P}{\partial z^2}$ part followed by the divergence theorem. Then Equation (4.7) becomes

$$-\int_{\mathrm{d}\Omega} v^{P}\,(\nabla P\cdot\boldsymbol{\eta})\,\mathrm{d}\Gamma + \int_{\Omega} v^{P}\frac{\gamma_w}{K_s}\left[p\beta\frac{\partial P}{\partial t} + \frac{\partial}{\partial t}\left(\frac{\partial u_x}{\partial x} + \frac{\partial u_z}{\partial z}\right)\right] + \left(\nabla v^{P}\cdot\nabla P\right)\mathrm{d}\Omega = 0. \tag{4.8}$$

After setting $v^P(x,z,t) = 0$ for $z = 0$ because of the boundary condition given by Equation (3.18) and using the other boundary conditions given by Equations (3.19) and (3.20), we get that

$$\begin{aligned}\int_{\mathrm{d}\Omega} v^{P}\,(\nabla P\cdot\boldsymbol{\eta})\,\mathrm{d}\Gamma = &\int_{\mathrm{d}\Omega_1} v^{P}\,(\nabla P\cdot\boldsymbol{\eta}_1)\,\mathrm{d}\Gamma + \int_{\mathrm{d}\Omega_2} v^{P}\,(\nabla P\cdot\boldsymbol{\eta}_2)\,\mathrm{d}\Gamma \\ &+ \int_{\mathrm{d}\Omega_3} v^{P}\,(\nabla P\cdot\boldsymbol{\eta}_3)\,\mathrm{d}\Gamma + \int_{\mathrm{d}\Omega_4} v^{P}\,(\nabla P\cdot\boldsymbol{\eta}_4)\,\mathrm{d}\Gamma \\ &= 0.\end{aligned} \tag{4.9}$$

When substituting the test and trial functions given by Equations (4.1), (4.2), (4.3) (4.4), (4.5) and (4.6), and boundary integral given by Equation (4.9) into Equation (4.8), we get the following Galerkin

equations

$$0 = \int_\Omega \sum_{i=1}^{n} N_i^P \bar{v}_i^P \frac{\gamma_w}{K_s} \left[p\beta \frac{\partial}{\partial t} \left(\sum_{l=1}^{n} N_l^P \bar{P}_l \right) + \frac{\partial}{\partial t} \left(\sum_{j=1}^{n} \frac{\partial N_j^{u_x}}{\partial x} \bar{u}_j^x + \sum_{l=1}^{n} \frac{\partial N_l^{u_z}}{\partial z} \bar{u}_l^z \right) \right] + \left[\nabla \left(\sum_{i=1}^{n} N_i^P \bar{v}_i^P \right) \cdot \nabla \left(\sum_{l=1}^{n} N_l^P \bar{P}_l \right) \right] \mathrm{d}\Omega$$
$$= \sum_{i=1}^{n} \bar{v}_i^P \int_\Omega N_i^P \frac{\gamma_w}{K_s} \left[p\beta \sum_{l=1}^{n} N_l^P \frac{\partial \bar{P}_l}{\partial t} + \sum_{j=1}^{n} N_j^\epsilon \frac{\partial \bar{\epsilon}_j}{\partial t} \right] + \left[\nabla N_i^P \cdot \left(\sum_{l=1}^{n} \bar{P}_l \nabla N_l^P \right) \right] \mathrm{d}\Omega. \quad (4.10)$$

Since it must hold for arbitrary $\bar{v}_i^P$ with $i = 1, \dots, n$, we have that Equation (4.10) still holds as

$$0 = \int_\Omega N_i^P \frac{\gamma_w}{K_s} \left[p\beta \sum_{l=1}^{n} N_l^P \frac{\partial \bar{P}_l}{\partial t} + \left(\sum_{j=1}^{n} \frac{\partial N_j^{u_x}}{\partial x} \frac{\partial \bar{u}_j^x}{\partial t} + \sum_{l=1}^{n} \frac{\partial N_l^{u_z}}{\partial z} \frac{\partial \bar{u}_l^z}{\partial t} \right) \right] + \left[\nabla N_i^P \cdot \left(\sum_{l=1}^{n} \bar{P}_l \nabla N_l^P \right) \right] \mathrm{d}\Omega. \quad (4.11)$$

We can write Equation (4.11) as matrix-vector multiplication

$$A^{PP} \bar{\boldsymbol{P}}_t + C^{Pu_x} \bar{\boldsymbol{u}}_t^x + D^{Pu_z} \bar{\boldsymbol{u}}_t^z + B^P \bar{\boldsymbol{P}} = 0, \quad (4.12)$$

where

$$A_{ij}^{PP} = \int_\Omega \frac{\gamma_w}{K_s} p\beta N_i^P N_j^P \mathrm{d}\Omega, \quad B_{ij}^P = \int_\Omega \nabla N_i^P \cdot \nabla N_j^P \mathrm{d}\Omega, \quad C_{ij}^{Pu_x} = \int_\Omega \frac{\gamma_w}{K_s} N_i^P \frac{\partial N_j^{u_x}}{\partial x} \mathrm{d}\Omega, \quad D_{ij}^{Pu_z} = \int_\Omega \frac{\gamma_w}{K_s} N_i^P \frac{\partial N_j^{u_z}}{\partial z} \mathrm{d}\Omega,$$
$$\bar{\boldsymbol{P}} = \begin{bmatrix} \bar{P}_1 \\ \vdots \\ \bar{P}_n \end{bmatrix}, \quad \bar{\boldsymbol{P}}_t = \begin{bmatrix} \frac{\partial \bar{P}_1}{\partial t} \\ \vdots \\ \frac{\partial \bar{P}_n}{\partial t} \end{bmatrix}, \quad \bar{\boldsymbol{u}}_t^x = \begin{bmatrix} \frac{\partial \bar{u}_1^x}{\partial t} \\ \vdots \\ \frac{\partial \bar{u}_n^x}{\partial t} \end{bmatrix}, \quad \bar{\boldsymbol{u}}_t^z = \begin{bmatrix} \frac{\partial \bar{u}_1^z}{\partial t} \\ \vdots \\ \frac{\partial \bar{u}_n^z}{\partial t} \end{bmatrix},$$

for $i, j = 1, \dots, n$. Equation (4.12) is our first matrix problem to solve.

4.1.2. Momentum balance equations

We will derive the weak form of the displacement equations and its matrix-vector form. Suppose that the test functions are given by Equations (4.1), (4.2) and (4.3), and the trial functions are given by (4.4), (4.5) and (4.6) for u_x, u_z and P, respectively.

After multiplying Equations (3.17) by test functions v^{u_x} and v^{u_z}, respectively, and integrating over the domain Ω we get

$$0 = \int_\Omega v^{u_x} \left[-(\lambda + 2\mu) \left(\frac{\partial^2 u_x}{\partial x^2} + \frac{\partial^2 u_x}{\partial z^2} \right) + (\lambda + \mu) \frac{\partial}{\partial z} \left(\frac{\partial u_x}{\partial z} - \frac{\partial u_z}{\partial x} \right) + \frac{\partial P}{\partial x} \right] \mathrm{d}\Omega, \quad (4.13)$$
$$0 = \int_\Omega v^{u_z} \left[-(\lambda + 2\mu) \left(\frac{\partial^2 u_z}{\partial x^2} + \frac{\partial^2 u_z}{\partial z^2} \right) - (\lambda + \mu) \frac{\partial}{\partial x} \left(\frac{\partial u_x}{\partial z} - \frac{\partial u_z}{\partial x} \right) + \frac{\partial P}{\partial z} \right] \mathrm{d}\Omega. \quad (4.14)$$

Since $\frac{\partial^2 u_i}{\partial x^2} + \frac{\partial^2 u_i}{\partial z^2} = \nabla \cdot (\nabla u_i)$ for $i = x, z$, applying integration by parts and divergence theorem to Equations (4.13) and (4.14) gives

$$0 = -\int_{\mathrm{d}\Omega} v^{u_x} \left[(\lambda + 2\mu) \nabla u_x \cdot \boldsymbol{\eta} \right] \mathrm{d}\Gamma + \int_\Omega v^{u_x} \left((\lambda + \mu) \frac{\partial}{\partial z} \left(\frac{\partial u_x}{\partial z} - \frac{\partial u_z}{\partial x} \right) + \frac{\partial P}{\partial x} \right) + (\lambda + 2\mu) \left[\nabla v^{u_x} \cdot \nabla u_x \right] \mathrm{d}\Omega, \quad (4.15)$$

$$0 = -\int_{\mathrm{d}\Omega} v^{u_z} \left[(\lambda + 2\mu) \nabla u_z \cdot \boldsymbol{\eta} \right] \mathrm{d}\Gamma + \int_\Omega v^{u_z} \left(-(\lambda + \mu) \frac{\partial}{\partial x} \left(\frac{\partial u_x}{\partial z} - \frac{\partial u_z}{\partial x} \right) + \frac{\partial P}{\partial z} \right) + (\lambda + 2\mu) \left[\nabla v^{u_z} \cdot \nabla u_z \right] \mathrm{d}\Omega. \quad (4.16)$$

After substituting the boundary conditions given by Equations (3.18), (3.19) and (3.20) into Equations

(4.15) and (4.16), we get that

$$\begin{aligned}\int_{d\Omega} v^{u_x}\left[\nabla u_x \cdot \boldsymbol{\eta}\right] d\Gamma &= \int_{d\Omega_1} v^{u_x}\left[\nabla u_x \cdot \boldsymbol{\eta}_1\right] d\Gamma + \int_{d\Omega_2} v^{u_x}\left[\nabla u_x \cdot \boldsymbol{\eta}_2\right] d\Gamma \\ &\quad + \int_{d\Omega_3} v^{u_x}\left[\nabla u_x \cdot \boldsymbol{\eta}_3\right] d\Gamma + \int_{d\Omega_4} v^{u_x}\left[\nabla u_x \cdot \boldsymbol{\eta}_4\right] d\Gamma \\ &= -\int_{d\Omega_3} v^{u_x}\left(\frac{\partial u_z}{\partial x} + \frac{1}{\mu}F_{xz}\right) d\Gamma, \end{aligned} \tag{4.17}$$

$$\begin{aligned}\int_{d\Omega} v^{u_z}\left[\nabla u_z \cdot \boldsymbol{\eta}\right] d\Gamma &= \int_{d\Omega_1} v^{u_z}\left[\nabla u_z \cdot \boldsymbol{\eta}_1\right] d\Gamma + \int_{d\Omega_2} v^{u_z}\left[\nabla u_z \cdot \boldsymbol{\eta}_2\right] d\Gamma \\ &\quad + \int_{d\Omega_3} v^{u_z}\left[\nabla u_z \cdot \boldsymbol{\eta}_3\right] d\Gamma + \int_{d\Omega_4} v^{u_z}\left[\nabla u_z \cdot \boldsymbol{\eta}_4\right] d\Gamma \\ &= -\int_{d\Omega_3} v^{u_z}\frac{\lambda}{\lambda+2\mu}\frac{\partial u_x}{\partial x} d\Gamma. \end{aligned} \tag{4.18}$$

Substituting the test and trial functions given by Equations (4.1), (4.2), (4.3) (4.4), (4.5) and (4.6), and boundary integrals given by Equations (4.17) and (4.18) into Equations (4.15) and (4.16) gives the following Galerkin equations

$$\begin{aligned} 0 = &\int_{d\Omega_3} (\lambda+2\mu)\sum_{i=1}^{n} N_i^{u_x}\bar{v}_i^{u_x}\left[\frac{\partial}{\partial x}\left(\sum_{i=1}^{n} N_i^{u_z}\bar{u}_i^{z}\right) + \frac{1}{\mu}F_{xz}\right] d\Gamma \\ &+ \int_{\Omega}\sum_{i=1}^{n} N_i^{u_x}\bar{v}_i^{u_x}\left((\lambda+\mu)\frac{\partial}{\partial z}\left[\frac{\partial}{\partial z}\left(\sum_{j=1}^{n} N_j^{u_x}\bar{u}_j^{x}\right) - \frac{\partial}{\partial x}\left(\sum_{j=1}^{n} N_j^{u_z}\bar{u}_j^{z}\right)\right] + \frac{\partial}{\partial x}\left(\sum_{l=1}^{n} N_l^{P}\bar{P}_l\right)\right) \\ &+ (\lambda+2\mu)\left[\nabla\left(\sum_{i=1}^{n} N_i^{u_x}\bar{v}_i^{u_x}\right)\cdot\nabla\left(\sum_{j=1}^{n} N_j^{u_x}\bar{u}_j^{x}\right)\right] d\Omega, \end{aligned} \tag{4.19}$$

$$\begin{aligned} 0 = &\int_{d\Omega_3} (\lambda+2\mu)\sum_{i=1}^{n} N_i^{u_z}\bar{v}_i^{u_z}\frac{\lambda}{\lambda+2\mu}\frac{\partial}{\partial x}\left(\sum_{i=1}^{n} N_i^{u_x}\bar{u}_i^{x}\right) d\Gamma \\ &+ \int_{\Omega}\sum_{i=1}^{n} N_i^{u_z}\bar{v}_i^{u_z}\left(-(\lambda+\mu)\frac{\partial}{\partial x}\left[\frac{\partial}{\partial z}\left(\sum_{j=1}^{n} N_j^{u_x}\bar{u}_j^{x}\right) - \frac{\partial}{\partial x}\left(\sum_{j=1}^{n} N_j^{u_z}\bar{u}_j^{z}\right)\right] + \frac{\partial}{\partial z}\left(\sum_{l=1}^{n} N_l^{P}\bar{P}_l\right)\right) \\ &+ (\lambda+2\mu)\left[\nabla\left(\sum_{i=1}^{n} N_i^{u_z}\bar{v}_i^{u_z}\right)\cdot\nabla\left(\sum_{j=1}^{n} N_j^{u_z}\bar{u}_j^{z}\right)\right] d\Omega,. \end{aligned} \tag{4.20}$$

Equations (4.19) and (4.20) can be written as

$$
\begin{aligned}
0 = &\int_{\mathrm{d}\Omega_3} (\lambda+2\mu)\sum_{i=1}^{n} N_i^{u_x}\bar{v}_i^{u_x}\left[\sum_{i=1}^{n}\frac{\partial N_i^{u_z}}{\partial x}\bar{u}_i^z + \frac{1}{\mu}F_{xz}\right]\mathrm{d}\Gamma \\
&+ \int_{\Omega}\sum_{i=1}^{n} N_i^{u_x}\bar{v}_i^{u_x}\left((\lambda+\mu)\left[\sum_{j=1}^{n}\frac{\partial^2 N_j^{u_x}}{\partial z^2}\bar{u}_j^x - \sum_{j=1}^{n}\frac{\partial^2 N_j^{u_z}}{\partial z\partial x}\bar{u}_j^z\right] + \sum_{l=1}^{n}\frac{\partial N_l^P}{\partial x}\bar{P}_l\right) \\
&\quad + (\lambda+2\mu)\left[\sum_{i=1}^{n}\nabla N_i^{u_x}\bar{v}_i^{u_x}\cdot\sum_{j=1}^{n}\nabla N_j^{u_x}\bar{u}_j^x\right]\mathrm{d}\Omega, \qquad (4.21)\\
0 = &\int_{\mathrm{d}\Omega_3} (\lambda+2\mu)\sum_{i=1}^{n} N_i^{u_z}\bar{v}_i^{u_z}\frac{\lambda}{\lambda+2\mu}\sum_{i=1}^{n}\frac{\partial N_i^{u_x}}{\partial x}\bar{u}_i^x\mathrm{d}\Gamma \\
&+ \int_{\Omega}\sum_{i=1}^{n} N_i^{u_z}\bar{v}_i^{u_z}\left(-(\lambda+\mu)\left[\sum_{j=1}^{n}\frac{\partial^2 N_j^{u_x}}{\partial x\partial z}\bar{u}_j^x - \sum_{j=1}^{n}\frac{\partial^2 N_j^{u_z}}{\partial x^2}\bar{u}_j^z\right] + \sum_{l=1}^{n}\frac{\partial N_l^P}{\partial z}\bar{P}_l\right) \\
&\quad + (\lambda+2\mu)\left[\sum_{i=1}^{n}\nabla N_i^{u_z}\bar{v}_i^{u_z}\cdot\sum_{j=1}^{n}\nabla N_j^{u_z}\bar{u}_j^z\right]\mathrm{d}\Omega,. \qquad (4.22)
\end{aligned}
$$

Since it must hold for arbitrary $\bar{v}_i^{u_x}$ and $\bar{v}_i^{u_z}$ with $i = 1, \dots, n$, we have that Equations (4.21) and (4.22) still hold as

$$
\begin{aligned}
0 = &\int_{\mathrm{d}\Omega_3} (\lambda+2\mu) N_i^{u_x}\left[\sum_{i=1}^{n}\frac{\partial N_i^{u_z}}{\partial x}\bar{u}_i^z + \frac{1}{\mu}F_{xz}\right]\mathrm{d}\Gamma \\
&+ \int_{\Omega} N_i^{u_x}\left((\lambda+\mu)\left[\sum_{j=1}^{n}\frac{\partial^2 N_j^{u_x}}{\partial z^2}\bar{u}_j^x - \sum_{j=1}^{n}\frac{\partial^2 N_j^{u_z}}{\partial z\partial x}\bar{u}_j^z\right] + \sum_{l=1}^{n}\frac{\partial N_l^P}{\partial x}\bar{P}_l\right) \\
&\quad + (\lambda+2\mu)\left[\nabla N_i^{u_x}\cdot\sum_{j=1}^{n}\nabla N_j^{u_x}\bar{u}_j^x\right]\mathrm{d}\Omega, \qquad (4.23)\\
0 = &\int_{\mathrm{d}\Omega_3} (\lambda+2\mu) N_i^{u_z}\frac{\lambda}{\lambda+2\mu}\sum_{i=1}^{n}\frac{\partial N_i^{u_x}}{\partial x}\bar{u}_i^x\mathrm{d}\Gamma \\
&+ \int_{\Omega} N_i^{u_z}\left(-(\lambda+\mu)\left[\sum_{j=1}^{n}\frac{\partial^2 N_j^{u_x}}{\partial x\partial z}\bar{u}_j^x - \sum_{j=1}^{n}\frac{\partial^2 N_j^{u_z}}{\partial x^2}\bar{u}_j^z\right] + \sum_{l=1}^{n}\frac{\partial N_l^P}{\partial z}\bar{P}_l\right) \\
&\quad + (\lambda+2\mu)\left[\nabla N_i^{u_z}\cdot\sum_{j=1}^{n}\nabla N_j^{u_z}\bar{u}_j^z\right]\mathrm{d}\Omega,. \qquad (4.24)
\end{aligned}
$$

We can write Equations (4.23) and (4.24) as matrix-vector multiplications,

$$
\begin{cases}
(B^{u_x} + DD^{u_x})\bar{\boldsymbol{u}}^x + (-CD^{u_z} + SC^{u_z})\bar{\boldsymbol{u}}^z + C^{u_x}\bar{\boldsymbol{P}} &= -\mathbf{F}^{xz} \\
(B^{u_z} + CC^{u_z})\bar{\boldsymbol{u}}^z + (-CD^{u_x} + SC^{u_x})\bar{\boldsymbol{u}}^x + D^{u_z}\bar{\boldsymbol{P}} &= 0
\end{cases}, \qquad (4.25)
$$

where

$$SC_{ij}^{u_x} = \int_{\mathrm{d}\Omega_3} (\lambda + 2\mu) N_i^{u_x} \frac{\partial N_j^{u_z}}{\partial x} \mathrm{d}\Gamma, \quad SC_{ij}^{u_z} = \int_{\mathrm{d}\Omega_3} \lambda N_i^{u_z} \frac{\partial N_j^{u_x}}{\partial x} \mathrm{d}\Gamma,$$
$$B_{ij}^{u_x} = \int_{\Omega} (\lambda + 2\mu) \nabla N_i^{u_x} \cdot \nabla N_j^{u_x} \mathrm{d}\Omega, \quad B_{ij}^{u_z} = \int_{\Omega} (\lambda + 2\mu) \nabla N_i^{u_z} \cdot \nabla N_j^{u_z} \mathrm{d}\Omega,$$
$$C_{ij}^{u_x} = \int_{\Omega} N_i^{u_x} \frac{\partial N_j^{P}}{\partial x} \mathrm{d}\Omega, \quad D_{ij}^{u_z} = \int_{\Omega} N_i^{u_z} \frac{\partial N_j^{P}}{\partial z} \mathrm{d}\Omega,$$
$$CD_{ij}^{u_x} = \int_{\Omega} (\lambda + \mu) N_i^{u_x} \frac{\partial^2 N_j^{u_x}}{\partial x \partial z} \mathrm{d}\Omega, \quad CD_{ij}^{u_z} = \int_{\Omega} (\lambda + \mu) N_i^{u_z} \frac{\partial^2 N_j^{u_z}}{\partial z \partial x} \mathrm{d}\Omega,$$
$$CC_{ij}^{u_z} = \int_{\Omega} (\lambda + \mu) N_i^{u_z} \frac{\partial^2 N_j^{u_z}}{\partial x^2} \mathrm{d}\Omega, \quad DD_{ij}^{u_x} = \int_{\Omega} (\lambda + \mu) N_i^{u_x} \frac{\partial^2 N_j^{u_x}}{\partial z^2} \mathrm{d}\Omega,$$
$$F_i^{xz} = \int_{\Omega_3} N_i^{u_x} \frac{1}{2\mu} F_{xz} \mathrm{d}\Gamma,$$

for $i, j = 1, \dots, n$.

4.1.3. Final FEM Model

We assume that $N_i^{\epsilon} = N_i^{\omega} = N_i^{P} = N_i^{u_x} = N_i^{u_z} =: N_i$ for all $i = 1, \dots, n$. After collecting the governing equations given by Equations (4.12) and (4.25), we get the following set of Galerkin equations:

$$\begin{cases} \frac{\gamma_w}{K_s} p\beta A \bar{\boldsymbol{P}}_t + \frac{\gamma_w}{K_s} C \bar{\boldsymbol{u}}_t^x + \frac{\gamma_w}{K_s} D \bar{\boldsymbol{u}}_t^z + B \bar{\boldsymbol{P}} & = 0 \\ [(\lambda + 2\mu) B + DD] \bar{\boldsymbol{u}}^x + [-CD + (\lambda + 2\mu) SC] \bar{\boldsymbol{u}}^z + C \bar{\boldsymbol{P}} & = -\mathbf{F}^{xz}, \\ [(\lambda + 2\mu) B + CC] \bar{\boldsymbol{u}}^z + [-CD + \lambda SC] \bar{\boldsymbol{u}}^x + D \bar{\boldsymbol{P}} & = 0 \end{cases} \tag{4.26}$$

where
$A_{ij} = \int_{\Omega} N_i N_j \mathrm{d}\Omega$, $B_{ij} = \int_{\Omega} \nabla N_i \cdot \nabla N_j \mathrm{d}\Omega$, $C_{ij} = \int_{\Omega} N_i \frac{\partial N_j}{\partial x} \mathrm{d}\Omega$, $SC_{ij} = \int_{\mathrm{d}\Omega_3} N_i \frac{\partial N_j}{\partial x} \mathrm{d}\Gamma$, $D_{ij} = \int_{\Omega} N_i \frac{\partial N_j}{\partial z} \mathrm{d}\Omega$,
$CD_{ij} = \int_{\Omega} (\lambda + \mu) N_i \frac{\partial^2 N_j}{\partial z \partial x} \mathrm{d}\Omega$, $CC_{ij} = \int_{\Omega} (\lambda + \mu) N_i \frac{\partial^2 N_j}{\partial x^2} \mathrm{d}\Omega$, $DD_{ij} = \int_{\Omega} (\lambda + \mu) N_i \frac{\partial^2 N_j}{\partial z^2} \mathrm{d}\Omega$
for all $i, j = 1, \dots, n$.

We can write Equation (4.26) as one system of matrix-vector multiplication

$$M^t \boldsymbol{\theta}_t + M \boldsymbol{\theta} = \boldsymbol{f}, \tag{4.27}$$

where

$$M^t = \begin{bmatrix} \frac{\gamma_w}{K_s} p\beta A & \frac{\gamma_w}{K_s} C & \frac{\gamma_w}{K_s} D \\ \emptyset & \emptyset & \emptyset \\ \emptyset & \emptyset & \emptyset \end{bmatrix} \in \mathbb{R}^{3n \times 3n}, \quad M = \begin{bmatrix} B & \emptyset & \emptyset \\ \emptyset & (\lambda + 2\mu) B + DD & -CD + (\lambda + 2\mu) SC \\ \emptyset & -CD + \lambda SC & (\lambda + 2\mu) B + CC \end{bmatrix} \in \mathbb{R}^{3n \times 3n},$$

$$\boldsymbol{\theta} = \begin{bmatrix} \bar{\boldsymbol{P}} \\ \bar{\boldsymbol{u}}^x \\ \bar{\boldsymbol{u}}^z \end{bmatrix} \in \mathbb{R}^{3n}, \boldsymbol{\theta}_t = \begin{bmatrix} \frac{\partial \bar{\boldsymbol{P}}}{\partial t} \\ \frac{\partial \bar{\boldsymbol{u}}^x}{\partial t} \\ \frac{\partial \bar{\boldsymbol{u}}^z}{\partial t} \end{bmatrix} \in \mathbb{R}^{3n}, \quad \boldsymbol{f} = \begin{bmatrix} \mathbf{0} \\ -\mathbf{F}^{xz} \\ \mathbf{0} \end{bmatrix} \in \mathbb{R}^{3n}.$$

Note that the Neumann boundary conditions are included. The Dirichlet boundary conditions will be included after time discretisation.

4.2. Discretisation in time

For discretising the Galerkin equations in matrix-vector form given by Equation (4.27) we use the Backward-Euler method. This method is an implicit method which is needed, since some of the governing equations are not time dependent but the equations are all coupled. Furthermore, an implicit

method is unconditionally stable which we prioritize over accuracy. The Backward-Euler method is given by

$$\boldsymbol{\theta}_t = \frac{1}{\Delta t}\left(\boldsymbol{\theta}^{k+1} - \boldsymbol{\theta}^k\right) = g\left(t^{k+1}, \boldsymbol{\theta}\left(t^{k+1}\right)\right), \tag{4.28}$$

where $\boldsymbol{\theta}^{k+1} = \boldsymbol{\theta}\left(t^{k+1}\right)$, $\Delta t = t^{k+1} - t^k$ is the time step, and $g\left(t^{k+1}, \boldsymbol{\theta}\left(t^{k+1}\right)\right) = \boldsymbol{f}^{k+1} - M\boldsymbol{\theta}^{k+1}$ and $\boldsymbol{f}^{k+1} = \boldsymbol{f}\left(t^{k+1}\right)$. Applying Equation (4.28) to Equation (4.27) gives

$$\left(M^t + \Delta t M\right)\boldsymbol{\theta}^{k+1} = M^t\boldsymbol{\theta}^k + \Delta t\boldsymbol{f}^{k+1}. \tag{4.29}$$

Assuming that $\left(M^t + \Delta t M\right)$ is invertible, Equation (4.29) can be written as

$$\boldsymbol{\theta}^{k+1} = \left(M^t + \Delta t M\right)^{-1}\left(M^t\boldsymbol{\theta}^k + \Delta t\boldsymbol{f}^{k+1}\right). \tag{4.30}$$

The Dirichlet boundary conditions are included by setting the corresponding rows to zero of matrices $\left(M^t + \Delta t M\right)$ and M^t, and the right entry in these rows of matrix M to one and of the right-hand side vector to the Dirichlet value.

5

Solving the numerical model of Biot (2D)

In this chapter, the solutions to the numerical model described in 4 are solved using two different sets of boundary conditions. We assume that $\omega(x,z) = 0$ for all $x,z \in [0,L]x[-Z,0]$ which can be proven analytically under the assumption that the influence of the acceleration terms are negligible [4].

5.1. Numerical model to solve

Recall that $\omega = \frac{\partial u_x}{\partial z} - \frac{\partial u_z}{\partial x}$. Then by substituting $\frac{\partial u_x}{\partial z} - \frac{\partial u_z}{\partial x} = 0$ (or its equivalent $\omega = 0$), we get the following discretisation in space model

$$\begin{cases} \frac{\gamma_w}{K_s} p\beta A\bar{\boldsymbol{P}}_t + \frac{\gamma_w}{K_s} A\bar{\boldsymbol{u}}_t^x + \frac{\gamma_w}{K_s} A\bar{\boldsymbol{u}}_t^z + B\bar{\boldsymbol{P}} & = 0 \\ (\lambda + 2\mu)\, B\bar{\boldsymbol{u}}^x + (\lambda + 2\mu)\, SC\bar{\boldsymbol{u}}^z + C\bar{\boldsymbol{P}} & = -\mathbf{F}^{xz}, \\ (\lambda + 2\mu)\, B\bar{\boldsymbol{u}}^z + \lambda\, SC\bar{\boldsymbol{u}}^x + D\bar{\boldsymbol{P}} & = 0 \end{cases} \tag{5.1}$$

where
$A_{ij} = \int_\Omega N_i N_j \mathrm{d}\Omega$, $B_{ij} = \int_\Omega \nabla N_i \cdot \nabla N_j \mathrm{d}\Omega$, $C_{ij} = \int_\Omega N_i \frac{\partial N_j}{\partial x} \mathrm{d}\Omega$, $SC_{ij} = \int_{\mathrm{d}\Omega_3} N_i \frac{\partial N_j}{\partial x} \mathrm{d}\Gamma$, $D_{ij} = \int_\Omega N_i \frac{\partial N_j}{\partial z} \mathrm{d}\Omega$, for all $i,j = 1,\dots,n$.

After discretising Equation (5.1) also in time, the system can be written in the following matrix-vector multiplication form

$$\boldsymbol{\theta}^{k+1} = \left(M^t + \Delta t M\right)^{-1} \left(M^t \boldsymbol{\theta}^k + \Delta t \boldsymbol{f}^{k+1}\right), \tag{5.2}$$

where

$$M^t = \begin{bmatrix} \frac{\gamma_w}{K_s} p\beta A & \frac{\gamma_w}{K_s} C & \frac{\gamma_w}{K_s} D \\ \emptyset & \emptyset & \emptyset \\ \emptyset & \emptyset & \emptyset \end{bmatrix} \in \mathbb{R}^{3n \times 3n}, \quad M = \begin{bmatrix} B & \emptyset & \emptyset \\ \emptyset & (\lambda + 2\mu)\, B & (\lambda + 2\mu) SC \\ \emptyset & \lambda\, SC & (\lambda + 2\mu)\, B \end{bmatrix} \in \mathbb{R}^{3n \times 3n},$$

$$\boldsymbol{\theta} = \begin{bmatrix} \bar{\boldsymbol{P}} \\ \bar{\boldsymbol{u}}^x \\ \bar{\boldsymbol{u}}^z \end{bmatrix} \in \mathbb{R}^{3n}, \boldsymbol{\theta}_t = \begin{bmatrix} \frac{\partial \bar{\boldsymbol{P}}}{\partial t} \\ \frac{\partial \bar{\boldsymbol{u}}^x}{\partial t} \\ \frac{\partial \bar{\boldsymbol{u}}^z}{\partial t} \end{bmatrix} \in \mathbb{R}^{3n}, \quad \boldsymbol{f} = \begin{bmatrix} \mathbf{0} \\ -\mathbf{F}^{xz} \\ \mathbf{0} \end{bmatrix} \in \mathbb{R}^{3n}.$$

We will now define some terms we used for discretising with Finite-Element Method starting with the kind of geometric maps we used. For each Ω_i, there exists points (X_{ji}, Z_{ji}), $j = 1,\dots,(p_x+1)(p_z+1)$, such that

$$\phi_i(\xi,\eta) = \left(\sum_{j=1}^{(p_x+1)(p_z+1)} X_{ji}\tilde{N}_{i,j}(\xi,\eta), \quad \sum_{j=1}^{(p_x+1)(p_z+1)} Z_{ji}\tilde{N}_{i,j}(\xi,\eta)\right), \tag{5.3}$$

with $i = 1,\dots,m$, which maps the reference domain $\tilde{\Omega} := [0,1] \times [0,1]$ to the physical subdomain $\Omega_i := [(i_x - 1)\frac{n_x}{m_x}, i_x\frac{n_x}{m_x}] \times [-(i_z - 1)\frac{n_z}{m_z}, -i_z\frac{n_z}{m_z}]$. Here m_x and m_z are the amount of subdomains

chosen in x- and z-direction with $i_x = 1, \dots, m_x$ and $i_z = 1, \dots, m_z$ respectively. So the total amount of subdomains is given by $m := m_x m_z$. Note that $\Omega_i \subseteq \Omega := [0, n_x] \times [-n_z, 0]$ for all $i = 1, \dots, m$. Note that in order to map a unit square domain, by counting the reference points each row from left to right and from bottom to top, the points (X_{ij}, Z_{ij}) become the physical points. This is shown in Figure 5.1, where as example $n_x = 1$, $n_z = 2$, $m_x = 2$, $m_z = 4$, $p_x = p_z = 1$ and $k_x = k_z = 0$.

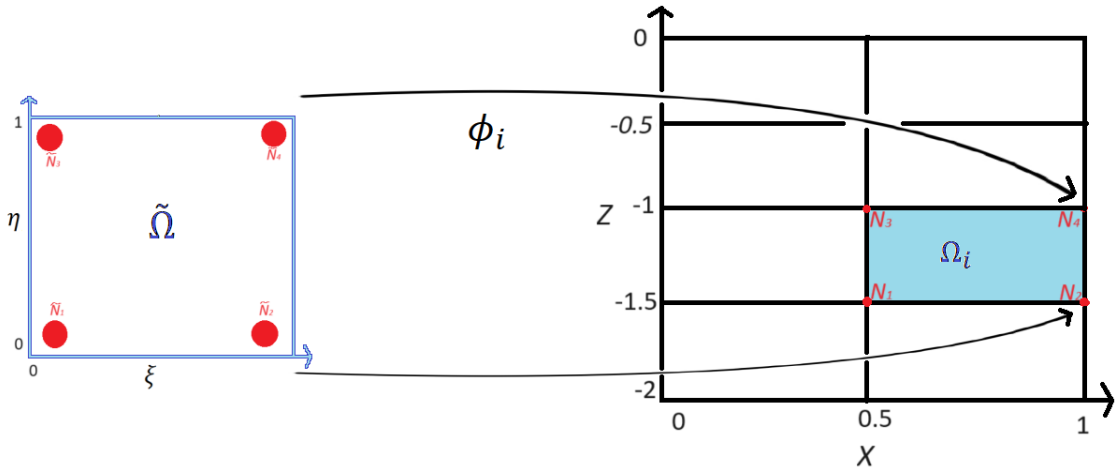

Figure 5.1: Mapping the reference domain to the physical (sub)domain.

We use piece-wise linear basis-functions in both x- and z-directions which is of degree 1 and smoothness 0 in both x- and z-directions, say $p_x = p_z = 1$ and $k_x = k_z = 0$, respectively, denoted by N_j, $j = 1, \dots, (p_x + 1)(p_z + 1)$. These basis element functions are given by

$$N_j|_{\Omega_i} = \sum_{l=1}^{(p_x+1)(p_z+1)} e_{ijk} \tilde{N}_{li}, \tag{5.4}$$

for $i = 1, \dots, m$ with $e_{ijk} = 1$ if $j = k$ and otherwise 0, and $\tilde{N}_{li}(x, z) = \tilde{N}_j \circ \phi_i(x, z)$. Note that this is specific the case for $p_x = p_z = 1$ with $k_x = k_z = 0$.

Furthermore, for integration of a subdomain we use 50×50 integration points, the space step is chosen as $\Delta x = \Delta z = 0.04$ and the time step is chosen as $\Delta t = 0.01$. We choose these steps in space and time such that the computation time would be reasonable which is approximately 3 minutes when $t_{textend} = 2.25$. For accuracy we could increase the number of subdomains (i.e. decrease the step in space) and decrease the time step. However, this requires an more efficient code and better equipment for computation.

The porosity, Poisson ratio, hydraulic conductivity, the shear modulus and specific weight are given by Table 5.1. The compressibility parameter β is often determined by [10]

$$\beta = s\beta_0 + \frac{1 - s}{P_0}, \tag{5.5}$$

where s the degree of saturation, β_0 the compressibility of pure water, P_0 the absolute pressure in the water. These parameters are given by Table 5.2. In this case, it is assumed that the water contains some small bubbles of gas, like air, and is almost fully-saturated. The amount of air in the water is usually derived from calibrating the outcomes of the model to the experimental data and is not experimentally determined by itself [8]. Note that fully-saturated soil would have a degree of saturation equal to one. However, then the water would be practically incompressible [10] while Biot's assumes compressible water. The wave parameters are set as in Table 5.3 unless stated otherwise.

We recall that λ is given by Equation (2.5). At last, we set $n_x = 1$ and $n_z = 2$, i.e. $\tilde{\Omega} = [0, 1] \times [-2, 0]$. Lastly, we set the stopping time t_{end} equal to 2.25 seconds at which the results will be shown.

Table 5.1: Parameters of one layer of sandy deposit [8].

Soil properties	Symbols	Values
Hydraulic conductivity [m/s]	K_s	$1.8 \cdot 10^{-4}$
Porosity	p	0.425
Poisson ratio	v_p	0.3
Shear modulus [Pa]	μ	$1.27 \cdot 10^{7}$
Specific weight of water [N/m^3]	γ_w	10^4

Table 5.2: Parameters of compressibility equation given by Equation (5.5) .

Soil properties	Symbols	Values
Degree of saturation [8]	s	0.996
Compressibility of pure water [10]	β_0	$0.5 \cdot 10^{-9}$
Absolute pressure in the water [Pa] [10]	P_0	10^5

Table 5.3: Parameters of the waves [8].

Wave properties	Symbols	Values
Wave period [s]	T	9
Wave height [m]	H	3.5
Water depth [m]	D	5.2
Wave length [m]	L	n_x

In the next three sections we will define some sets of boundary conditions. Boundary conditions B-I is the one used in the computations in the previous sections. Boundary conditions B-II similar to B-I but the first boundary condition at $z = 0$ is written differently, when assumed that $\omega = 0$. The third set of boundary conditions B-Is set to investigate the relation with the assumption $\omega = 0$ on Ω and the boundary condition $\sigma'_{xz} = 0$ at $z = 0$ better. For all sets of boundary conditions, we set $F_{zz} = 0.5\gamma_w H \cos\left(2\pi\frac{x}{L}\right)\sin\left(2\pi\frac{t}{T}\right)$, where γ_w [N/m^3] the specific weight of the pore water, H [m] is the wave height, L [m] the length of the wave, T [s] the wave period. The values of these wave parameters can be found in Table 5.3. The function F_{zz} at 2.25 seconds is shown in Figure 5.2. In Figure 5.2 it shown that when the wave is at it largest, the load on the sandy bed is also at its largest (red arrow pointing downwards). As the wave goes low, the load decreases and the pressure becomes negative which can be referred to as a pulling force (red arrow pointing upwards). Furthermore, we set $F_{xz} = 0$ which means that we assume that the shear stress at the surface is negligible.

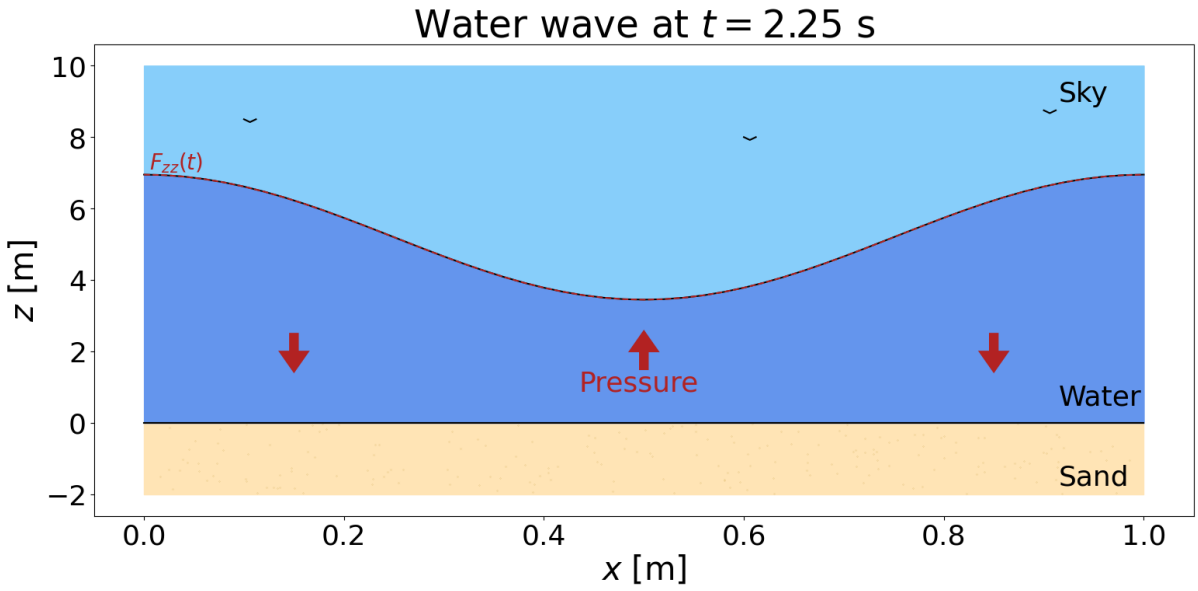

Figure 5.2: A sandy bed experiencing transient loads due to water waves at $t = 2.25$ s. The hydraulic load is visualised by the red color and at the surface of the sandy bed ($z = 0$) assumed to equal $F_{zz}(t)$. A red arrow pointing downwards means a positive pressure and a red arrow pointing upwards means a negative pressure (pulling force).

5.1.1. Boundary conditions B-I

Regardless of $\omega = 0$, we define boundary conditions B-I as

$$\begin{aligned}
\text{for } z = 0 : &\begin{cases} -\mu\left(\frac{\partial u_x}{\partial z} + \frac{\partial u_z}{\partial x}\right) & = F_{xz} \\ P & = F_{zz} \\ -\lambda\frac{\partial u_x}{\partial x} - (\lambda + 2\mu)\frac{\partial u_z}{\partial z} & = 0 \end{cases}, \\
\text{for } z = -n_z : &\left\{u_z = \frac{\partial u_x}{\partial z} = \frac{\partial P}{\partial z} = \frac{\partial \epsilon_{\text{vol}}}{\partial z} = 0\right. \quad , \\
\text{and for } x = 0 \text{ and } x = n_x : &\left\{u_x = \frac{\partial u_z}{\partial x} = \frac{\partial P}{\partial x} = \frac{\partial \epsilon_{\text{vol}}}{\partial x} = 0\right. .
\end{aligned}$$

Note that the definition of shear stress at $z = 0$ is used without using the assumption of $\omega = 0$, i.e. setting $\sigma_{xz} := -\mu\left(\frac{\partial u_x}{\partial z} + \frac{\partial u_z}{\partial x}\right)$ equal to F_{xz}. However, note that since in our case we assume $\omega = 0$, we expect that $\frac{\partial u_x}{\partial z} = \frac{\partial u_z}{\partial x} = 0$ at $z = 0$.

5.1.2. Boundary conditions B-II

Assuming $\omega = 0$, we define boundary conditions B-II as

$$\begin{aligned}
\text{for } z = 0 : &\begin{cases} -2\mu\frac{\partial u_x}{\partial z} & = F_{xz} \\ P & = F_{zz} \\ -\lambda\frac{\partial u_x}{\partial x} - (\lambda + 2\mu)\frac{\partial u_z}{\partial z} & = 0 \end{cases}, \\
\text{for } z = -n_z : &\left\{u_z = \frac{\partial u_x}{\partial z} = \frac{\partial P}{\partial z} = \frac{\partial \epsilon_{\text{vol}}}{\partial z} = 0\right. \quad , \\
\text{and for } x = 0 \text{ and } x = n_x : &\left\{u_x = \frac{\partial u_z}{\partial x} = \frac{\partial P}{\partial x} = \frac{\partial \epsilon_{\text{vol}}}{\partial x} = 0\right. .
\end{aligned}$$

Since $-\mu\left(\frac{\partial u_x}{\partial z} + \frac{\partial u_z}{\partial x}\right)$ can be rewritten to $-2\mu\frac{\partial u_x}{\partial z}$, when assuming $\omega = 0$ like we do, this boundary conditions set should theoretically give similar results as boundary conditions B-I.

5.1.3. Boundary conditions B-III

Assuming $\omega = 0$, we define boundary conditions B-III as

$$\text{for } z = 0: \begin{cases} \frac{\partial u_x}{\partial z} - \frac{\partial u_z}{\partial x} & = 0 \\ P & = F_{zz} \\ -\lambda \frac{\partial u_x}{\partial x} - (\lambda + 2\mu) \frac{\partial u_z}{\partial z} & = 0 \end{cases},$$

$$\text{for } z = -n_z: \left\{ u_z = \frac{\partial u_x}{\partial z} = \frac{\partial P}{\partial z} = \frac{\partial \epsilon_{\text{vol}}}{\partial z} = 0 \right. \quad ,$$

$$\text{and for } x = 0 \text{ and } x = n_x: \left\{ u_x = \frac{\partial u_z}{\partial x} = \frac{\partial P}{\partial x} = \frac{\partial \epsilon_{\text{vol}}}{\partial x} = 0 \right. .$$

Note that now the definition of vorticity at $z = 0$ used as boundary condition instead of setting the shear stress being zero at $z = 0$.

5.2. Solution to numerical model

In this section we assume that the water is slightly compressible and set $\beta = 4.05 \cdot 10^{-8}$. The solutions to completely incompressible water, i.e. $\beta = 0.5 \cdot 10^{-9}$, are really similar in two dimensions with only some minor differences in behaviour near the surface which are only noticeable when zoomed in. This can be expected since $4.05 \cdot 10^{-8}$ is already close to $0.5 \cdot 10^{-9}$. However, when setting the compressibility $\beta = 10^{-6}$, there are some small changes in behaviour of the solution visible, especially for the volumetric strain when using boundary conditions set B-I. This is shown in Appendix A. Given that these changes in value/behaviour are so small, the water is nearly incompressible but Biot's model is typically used with the assumption of compressible water, we will use $\beta = 4.05 \cdot 10^{-8}$ to solve Biot's equations which means that the degree of saturation is 0.996.

The three variables volumetric strain ϵ_{vol}, dynamic water pressure P, x-displacement u_x, z-displacement u_z and their derivatives are plotted at $t = 2.25$ for the case of compressible water. The effective stress σ'_{zz}, shear stress σ'_{xz}, vorticity ω and the volume balance equation, which is in form of the volumetric strain equation, are also shown.

In Figures 5.3, 5.4 and 5.5 the solutions for $\epsilon_{\text{vol}}, P, u_x$ and u_z, and their derivatives with respect to x and z, and in Figure 5.6 the corresponding solutions for $\omega, \sigma'_{zz}, \sigma_{xz}$ and volume balance, using boundary conditions B-I are shown. In Figures 5.7, 5.8 and 5.9 the solutions for $\epsilon_{\text{vol}}, P, u_x$ and u_z, and their derivatives with respect to x and z, and in Figure 5.10 the corresponding solutions for $\omega, \sigma'_{zz}, \sigma_{xz}$ and volume balance, using boundary conditions B-II are shown. In Figures 5.11, 5.12 and 5.13 the solutions for $\epsilon_{\text{vol}}, P, u_x$ and u_z, and their derivatives with respect to x and z, and in Figure 5.14 the corresponding solutions for $\omega, \sigma'_{zz}, \sigma_{xz}$ and volume balance, using boundary conditions B-III are shown.

Using boundary conditions B-I the relation between ϵ and P does not hold, i.e. the equations $(\lambda + 2\mu)\frac{\partial \epsilon}{\partial x} = \frac{\partial P}{\partial x}$ and $(\lambda + 2\mu)\frac{\partial \epsilon}{\partial z} = \frac{\partial P}{\partial z}$ do not hold. Furthermore, we also find that $\omega = \frac{\partial u_x}{\partial z} - \frac{\partial u_z}{\partial x}$ does not equal zero like we assumed which is shown in Figure 5.6. Since $\sigma'_{xz} = -2\mu\left(\frac{\partial u_x}{\partial z} + \frac{\partial u_z}{\partial x}\right)$ and assuming $\omega = 0$, we expect that $\frac{\partial u_x}{\partial z} = \frac{\partial u_z}{\partial x} = 0$ which we do not find in the corresponding Figures 5.4 and 5.5. And last, we will take a look at whether the volume is conserved. According to [4], the volume is only conserved, when the solution of the momentum balance equations given by Equation (3.17) is also a solution of the storage equation given by Equation (3.10) and the volumetric strain equation which is given by

$$\frac{\gamma_w}{K_s} p\beta \frac{\partial P}{\partial t} - (\lambda + 2\mu)\left(\frac{\partial^2 \epsilon_{\text{vol}}}{\partial x^2} + \frac{\partial^2 \epsilon_{\text{vol}}}{\partial z^2}\right) = -\frac{\gamma_w}{K_s} \frac{\partial \epsilon_{\text{vol}}}{\partial t}, \tag{5.6}$$

where $\epsilon_{\text{vol}} = \frac{\partial u_x}{\partial x} + \frac{\partial u_z}{\partial z}$. The volumetric strain equation can be derived by taking the divergence of the momentum balance equations given by Equation (3.17) and substituting the storage equation given by Equation (3.10). This is explained in more detail in Chapter 6, since the volumetric strain equation given by Equation (5.6) is part of the governing equations of the new model described in this chapter. In Biot's model the storage equation is part of the model and we need the volumetric strain equation to hold as well to conserve the volume. Therefore, we will check whether the weak equation of volumetric strain equation is indeed zero and refer to it by 'volume balance'. Therefore, when we say that the

volume balance is zero, we mean that the volumetric strain equation is satisfied which results in the volume being conserved (i.e. volume balance). The solution to Biot's model for the volumetric strain is only valid if it is a solution for both the momentum balance equations and volume balance equations. If the solution does not satisfy the volumetric strain equation given by Equation (5.6), then it is also not a solution to both the volume and momentum balance equations. Note that near the surface $z = 0$, we have that the volume balance equation does not hold. This can be seen in Figure 5.6.

Using boundary conditions B-II, we find that the relation between ϵ and P does not hold and that $\omega = \frac{\partial u_x}{\partial z} - \frac{\partial u_z}{\partial x}$ does not equal zero. Furthermore, the shear stress is also not zero at $z = 0$ like we wanted. Since $\sigma'_{xz} = -\mu\left(\frac{\partial u_x}{\partial z} + \frac{\partial u_z}{\partial x}\right)$ and $\omega = \frac{\partial u_x}{\partial z} + \frac{\partial u_z}{\partial x}$ must equal 0 and since we set $\frac{\partial u_x}{\partial z} = 0$, this means we do not get $\frac{\partial u_z}{\partial x} = 0$. This inequality indeed can be seen in the right bottom subplot of Figure 5.8. In Figure 5.10 we find that the volume balance equation given by Equation (5.6) approximately holds. However, note that this is probably because the solution of the volumetric strain is very small too.

When using boundary conditions B-III, we find that the relation between ϵ and P does hold and that $\omega = \frac{\partial u_x}{\partial z} - \frac{\partial u_z}{\partial x}$ equals zero. Furthermore, the volume balance given by Equation (5.6) does not hold which can be seen in Figure 5.14. However, now the shear stress is not zero at $z = 0$ which we originally wanted and is significantly larger than for the other boundary conditions sets. Furthermore, note that the other boundary conditions can also be found in Figures 5.3, 5.4 and 5.5 for boundary conditions B-I, in Figures 5.7, 5.8 and 5.9 for boundary conditions B-II and in Figures 5.11, 5.12 and 5.13 for boundary conditions B-III. Indeed, in the right top and bottom subplots of Figures 5.3, 5.7 and 5.11 one can see that $u_x = 0$ at the left and right boundary and $u_z = 0$ at the bottom boundary. Furthermore, in the left bottom subplot one can see that P is indeed a cosine in x-direction at the top boundary. We assumed that a positive pressure is the load pressing in the depth and thus negative pressure is a pulling force. Therefore, the water pressure subplots agree with the transient load shown in Figure 5.2: at the left having a large load which means a large positive pressure (a pushing force), followed by a small load which causes the pressure to become largely negative (a pulling force) and finished by again a large load resulting in a large positive pressure on the soil. This can also be noticed in the z-displacements figures, since negative z-displacement means displacement downwards in the soil and thus positive z-displacement means displacement upwards to the surface of the soil. In Figures 5.4, 5.8 and 5.12 one can also find that $\frac{\partial P}{\partial x} = 0$ and $\frac{\partial \epsilon}{\partial x} = 0$ at $x = 0, L$. Furthermore, in Figures 5.5, 5.9 and 5.13 one can find $\frac{\partial u_x}{\partial z} = 0$ at $z = 0, -n_z$, $\frac{\partial P}{\partial z} = 0$ and $\frac{\partial \epsilon}{\partial z} = 0$ at $z = -n_z$

In conclusion, this numerical model of Biot cannot determine the solution while satisfying all assumptions and boundary conditions. This suggests that the numerical model of Biot's model together with boundary conditions B-I, B-II or B-III is ill-posed. This can be due to the the equations of the numerical model itself and/or the boundary conditions. An example is that the volume balance equation is now not satisfied. An other example is that the effective stress being equal to zero in combination with the shear stresses being zero could be an incorrect boundary condition physically. In Section 9 we will look into this by using a similar model with the volume balance equation and by setting the vertical momentum balance equation at $z = 0$ in stead of the effective stress being equal to zero at $z = 0$ in the current numerical model of Biot, respectively.

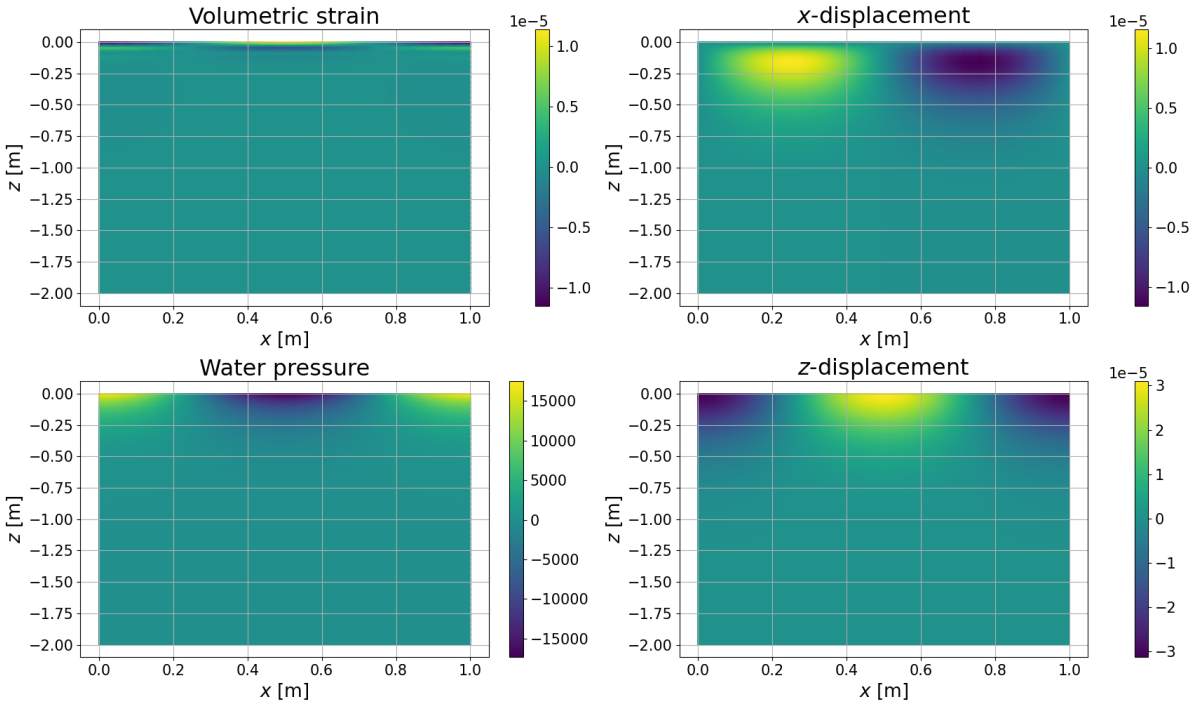

Figure 5.3: Solutions to Biot's model for ϵ_{vol} [-], P [Pa], u_x [m], u_z [m] at $t_{\text{end}} = 2.25$ s, when water is assumed to be compressible with $\beta = 4.05 \cdot 10^{-8}$ Pa^{-1} and using boundary conditions B-I. In this thesis, a negative pressure is pointing upwards (a pulling force), and a positive pressure is pointing downwards (a pushing force). The soil displacement upwards or to the right is positive and downwards or to the left is negative.

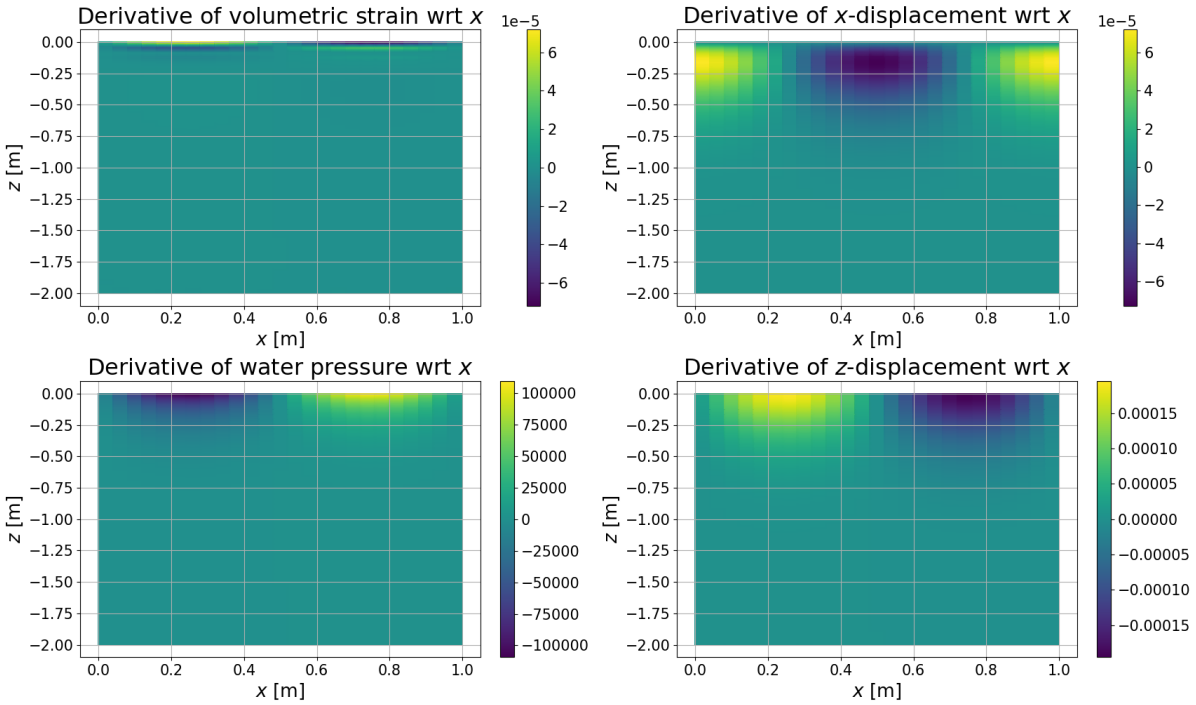

Figure 5.4: Solutions to Biot's model for $\frac{\partial \epsilon_{\text{vol}}}{\partial x}$ [m^{-1}], $\frac{\partial P}{\partial x}$ [N/m^3], $\frac{\partial u_x}{\partial x}$ [-], $\frac{\partial u_z}{\partial x}$ [-] at $t_{\text{end}} = 2.25$ s, when water is assumed to be compressible with $\beta = 4.05 \cdot 10^{-8}$ Pa^{-1} and using boundary conditions B-I.

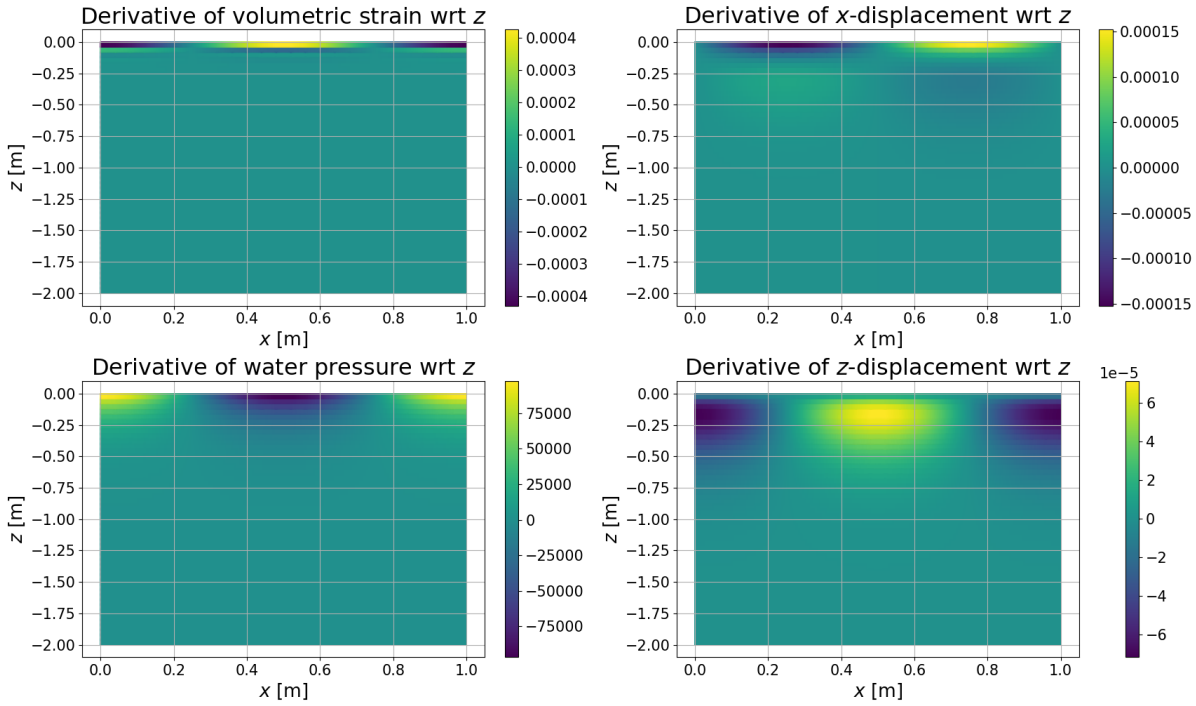

Figure 5.5: Solutions to Biot's model for $\frac{\partial \epsilon_{\text{vol}}}{\partial z}$ [m^{-1}], $\frac{\partial P}{\partial z}$ [N/m^3], $\frac{\partial u_x}{\partial z}$ [-], $\frac{\partial u_z}{\partial z}$ [-] at $t_{\text{end}} = 2.25$ s, when water is assumed to be compressible with $\beta = 4.05 \cdot 10^{-8}$ Pa^{-1} and using boundary conditions B-I.

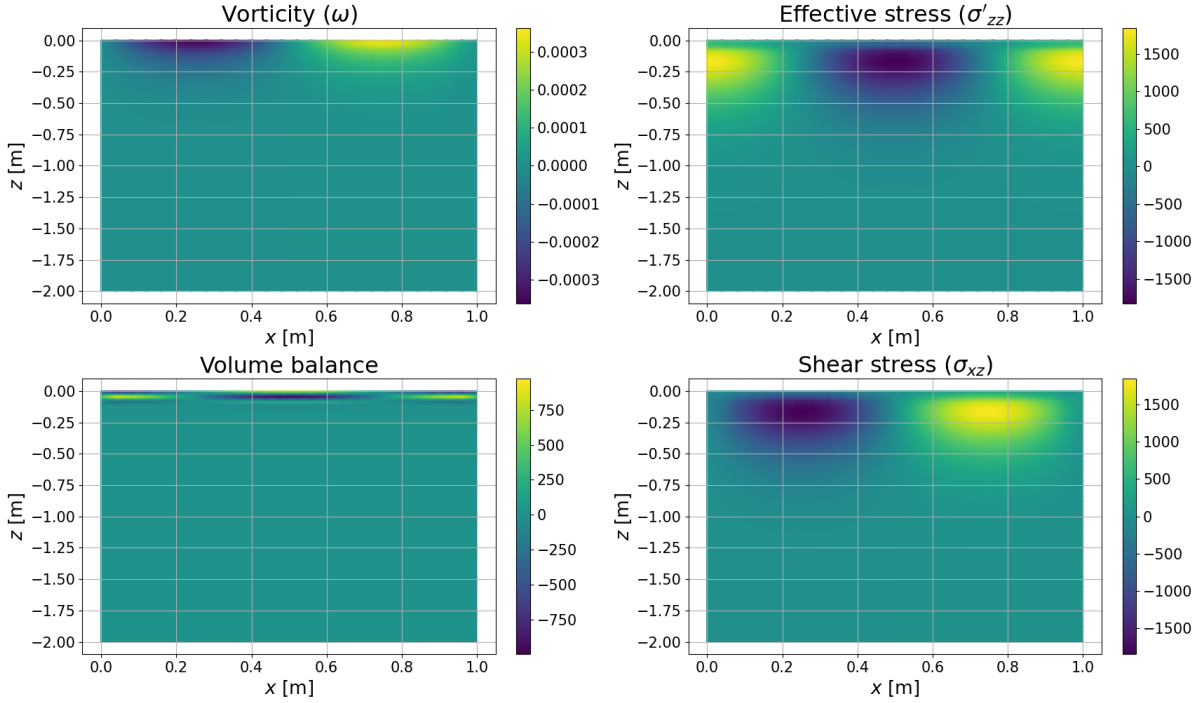

Figure 5.6: Solutions to Biot's model for ω [-], σ'_{zz} [Pa], σ_{xz} [Pa] and volume balance at $t_{\text{end}} = 2.25$ s, when water is assumed to be compressible with $\beta = 4.05 \cdot 10^{-8}$ Pa^{-1} and using boundary conditions B-I. The vorticity is expected to be zero. The volume balance is represented by the weak form of the volumetric strain equation and is satisfied if it equals 0 everywhere on the domain and its boundaries.

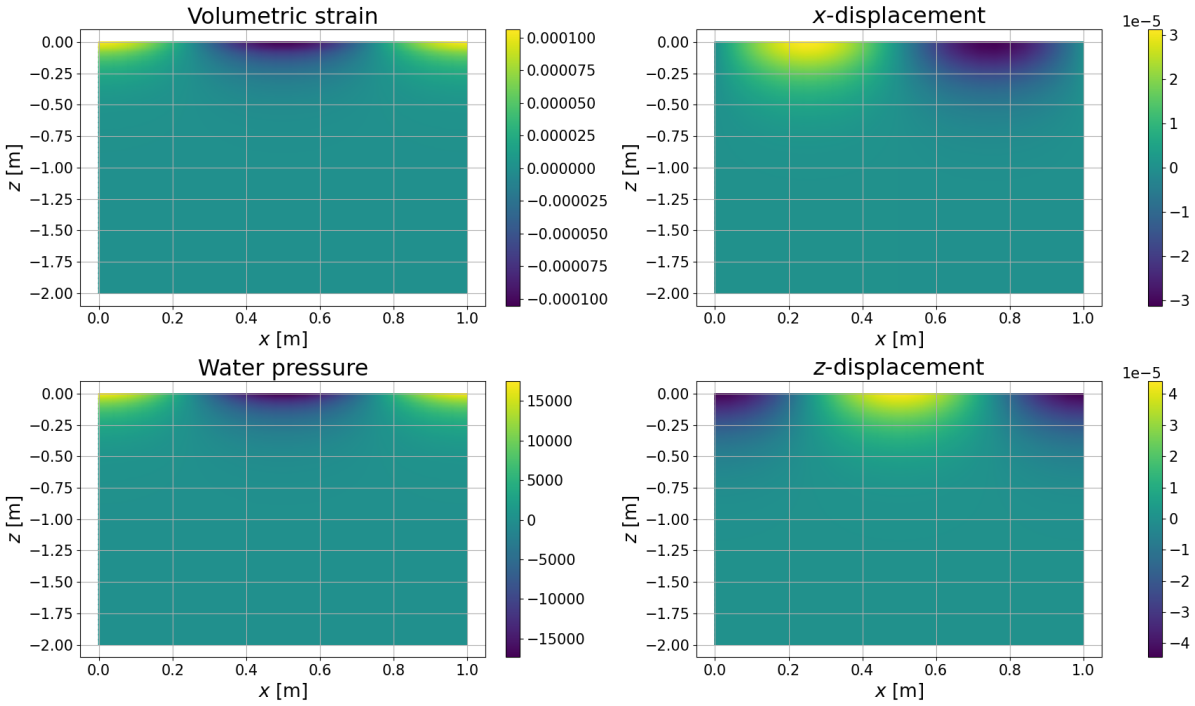

Figure 5.7: Solutions to Biot's model for ϵ_{vol} [-], P [Pa], u_x [m], u_z [m] at $t_{\text{end}} = 2.25$ s, when water is assumed to be compressible with $\beta = 4.05 \cdot 10^{-8}$ Pa^{-1} and using boundary conditions B-II. In this thesis, a negative pressure is pointing upwards (a pulling force), and a positive pressure is pointing downwards (a pushing force). The soil displacement upwards or to the right is positive and downwards or to the left is negative.

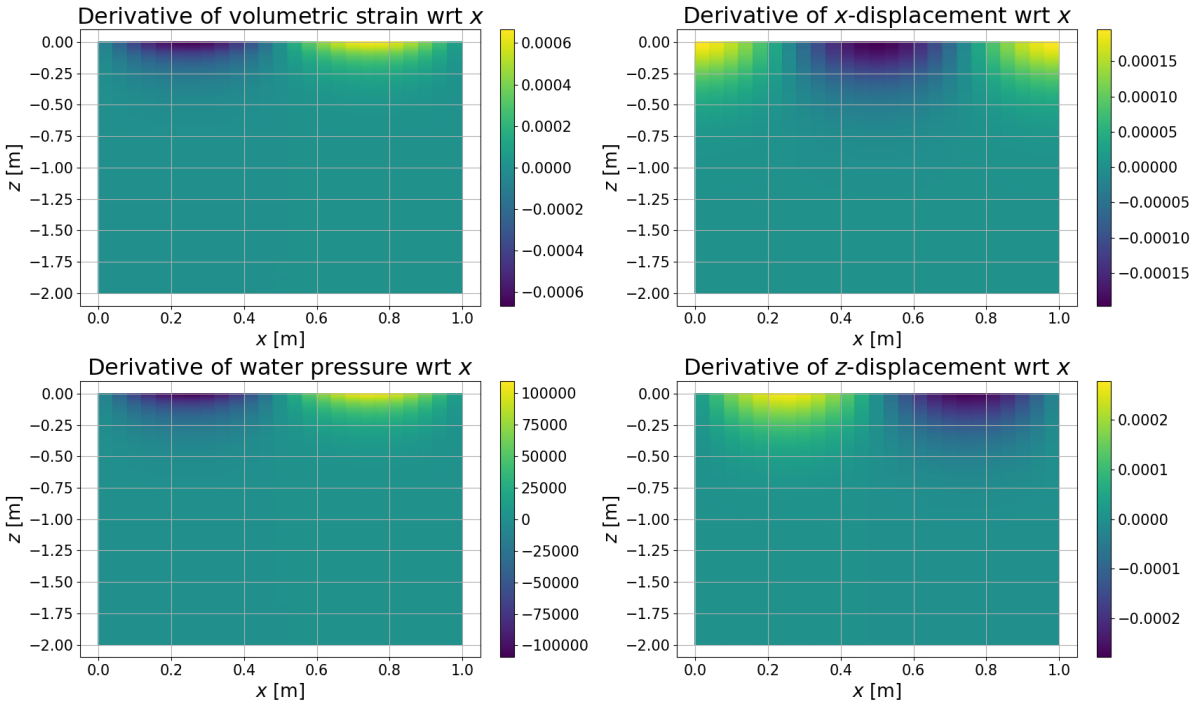

Figure 5.8: Solutions to Biot's model for $\frac{\partial \epsilon_{\text{vol}}}{\partial x}$ [m^{-1}], $\frac{\partial P}{\partial x}$ [N/m^3], $\frac{\partial u_x}{\partial x}$ [-], $\frac{\partial u_z}{\partial x}$ [-] at $t_{\text{end}} = 2.25$ s, when water is assumed to be compressible with $\beta = 4.05 \cdot 10^{-8}$ Pa^{-1} and using boundary conditions B-II.

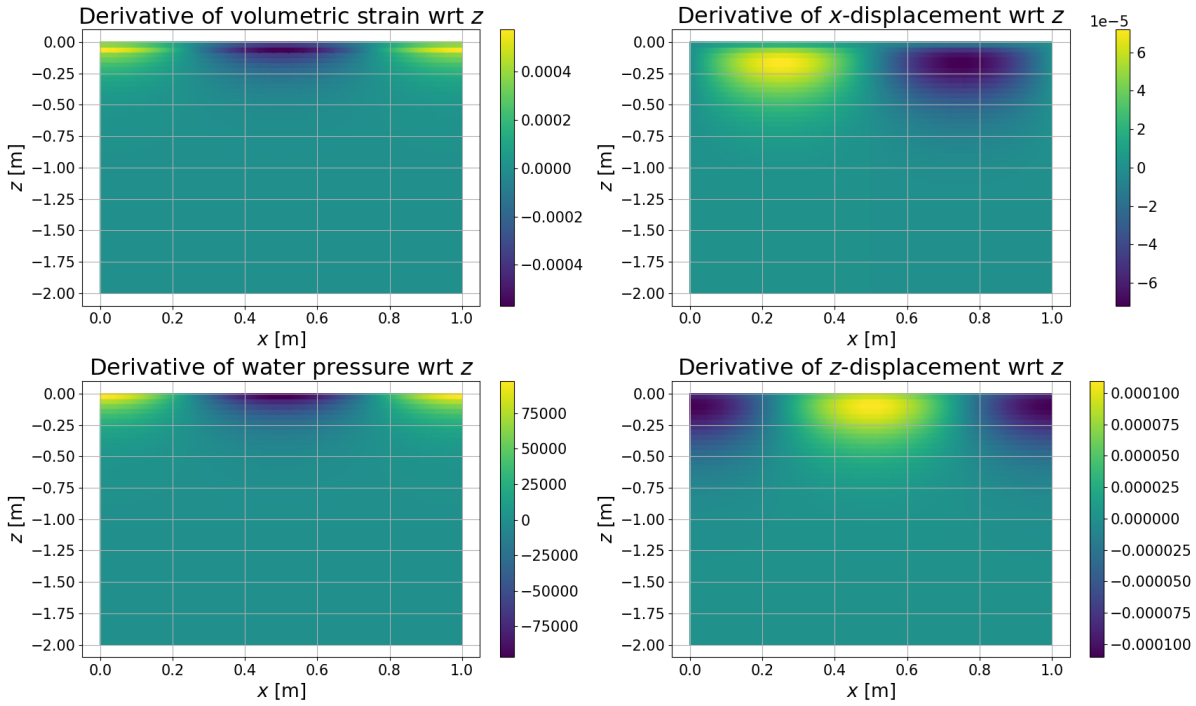

Figure 5.9: Solutions to Biot's model for $\frac{\partial \epsilon_{\text{vol}}}{\partial z}$ [m^{-1}], $\frac{\partial P}{\partial z}$ [N/m^3], $\frac{\partial u_x}{\partial z}$ [-], $\frac{\partial u_z}{\partial z}$ [-] at $t_{\text{end}} = 2.25$ s, when water is assumed to be compressible with $\beta = 4.05 \cdot 10^{-8}$ Pa^{-1} and using boundary conditions B-II.

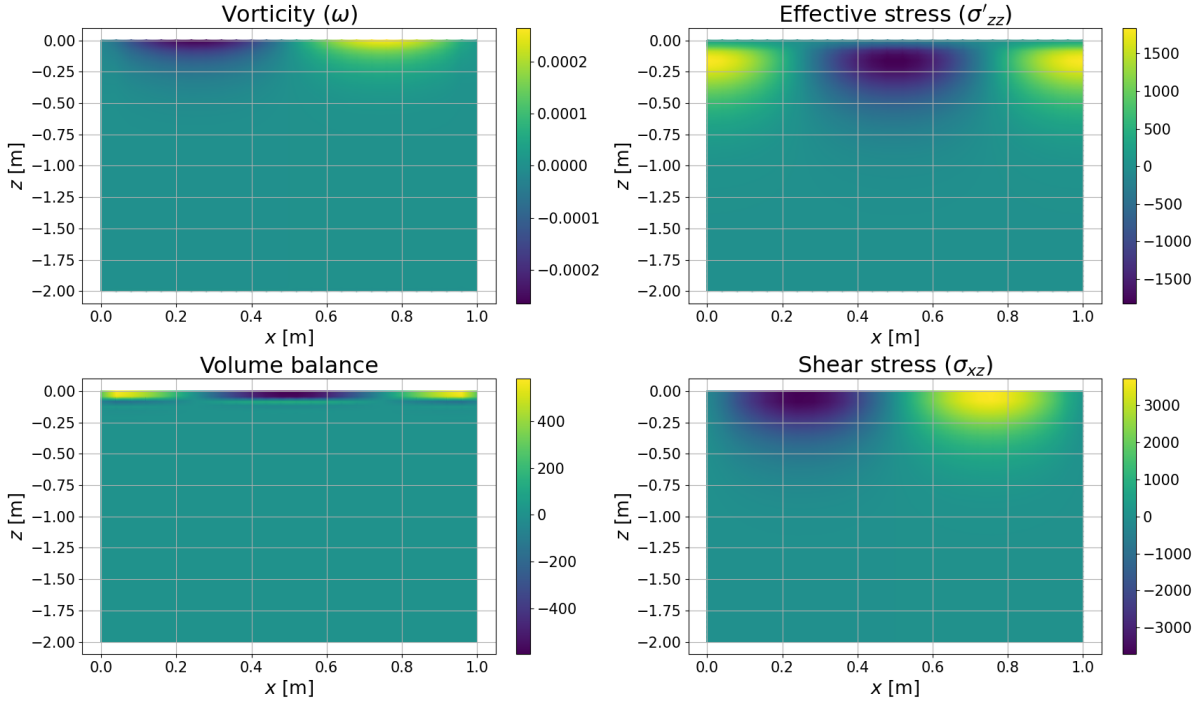

Figure 5.10: Solutions to Biot's model for ω [-], σ'_{zz} [Pa], σ_{xz} [Pa] and volume balance at $t_{\text{end}} = 2.25$ s, when water is assumed to be compressible with $\beta = 4.05 \cdot 10^{-8}$ Pa^{-1} and using boundary conditions B-II. The vorticity is expected to be zero. The volume balance is represented by the weak form of the volumetric strain equation and is satisfied if it equals 0 everywhere on the domain and its boundaries.

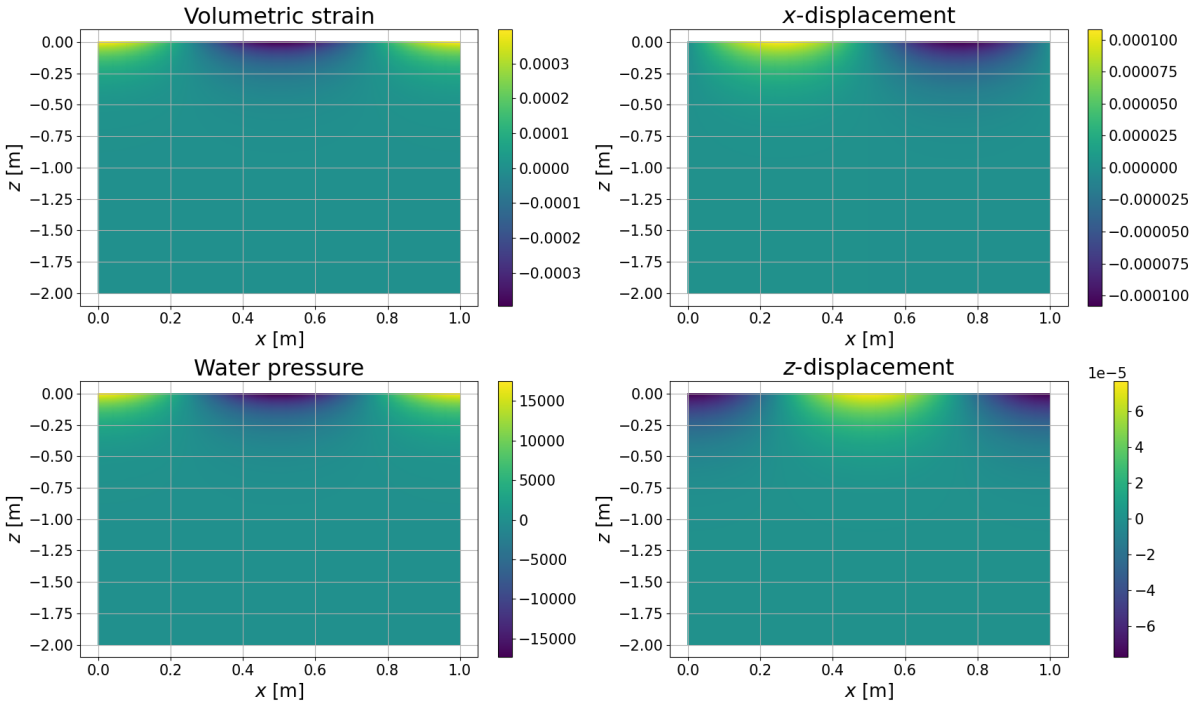

Figure 5.11: Solutions to Biot's model for ϵ_{vol} [-], P [Pa], u_x [m], u_z [m] at $t_{\text{end}} = 2.25$ s, when water is assumed to be compressible with $\beta = 4.05 \cdot 10^{-8}$ Pa^{-1} and using boundary conditions B-III. In this thesis, a negative pressure is pointing upwards (a pulling force), and a positive pressure is pointing downwards (a pushing force). The soil displacement upwards or to the right is positive and downwards or to the left is negative.

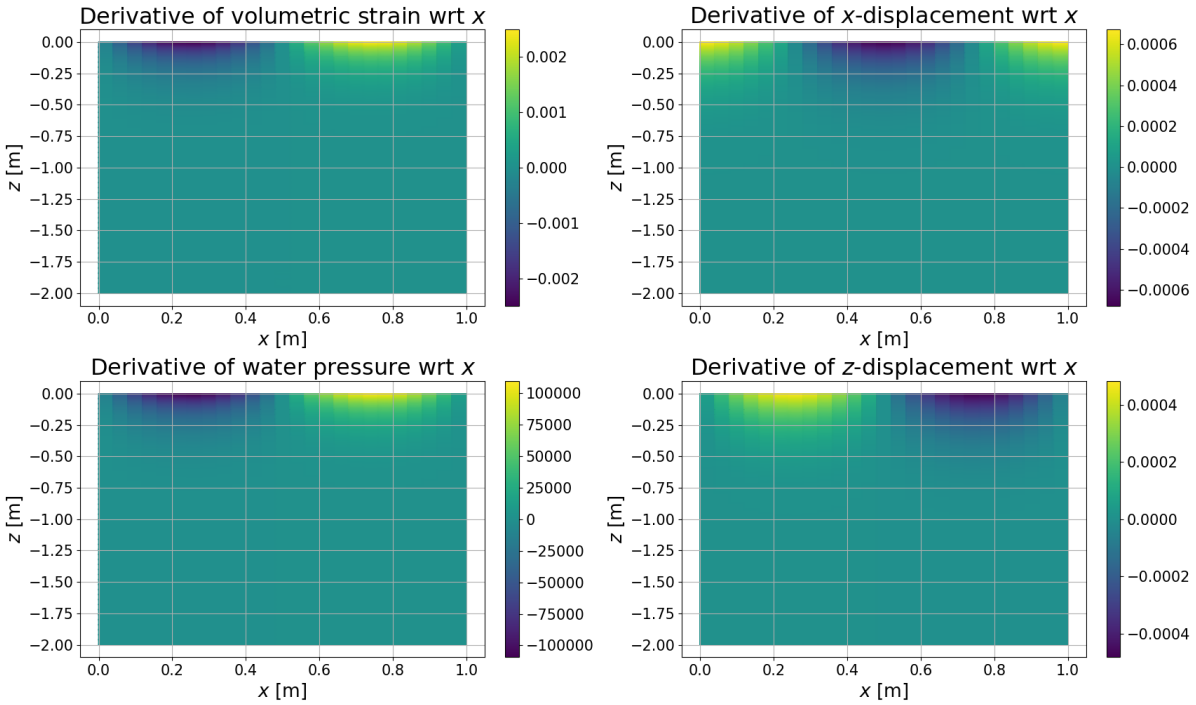

Figure 5.12: Solutions to Biot's model for $\frac{\partial \epsilon_{\text{vol}}}{\partial x}$ [m^{-1}], $\frac{\partial P}{\partial x}$ [N/m^3], $\frac{\partial u_x}{\partial x}$ [-], $\frac{\partial u_z}{\partial x}$ [-] at $t_{\text{end}} = 2.25$ s, when water is assumed to be compressible with $\beta = 4.05 \cdot 10^{-8}$ Pa^{-1} and using boundary conditions B-III.

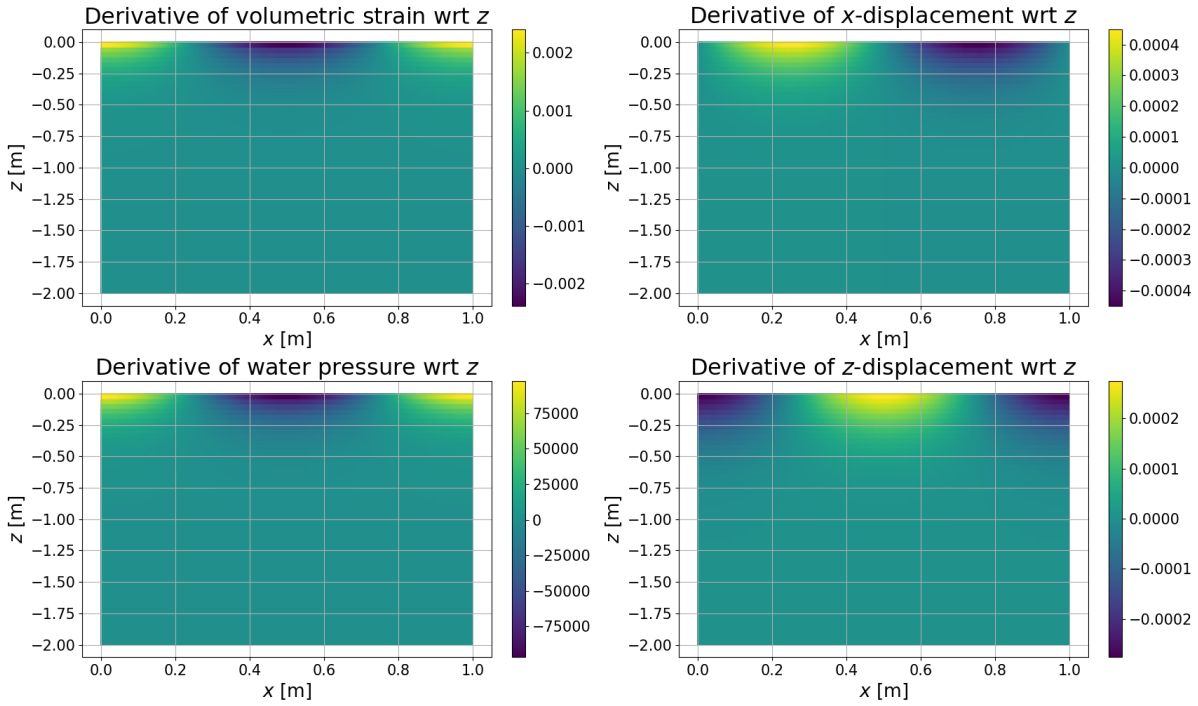

Figure 5.13: Solutions to Biot's model for $\frac{\partial \epsilon_{\text{vol}}}{\partial z}$ [m^{-1}], $\frac{\partial P}{\partial z}$ [N/m^3], $\frac{\partial u_x}{\partial z}$ [-], $\frac{\partial u_z}{\partial z}$ [-] at $t_{\text{end}} = 2.25$ s, when water is assumed to be compressible with $\beta = 4.05 \cdot 10^{-8}$ Pa^{-1} and using boundary conditions B-III.

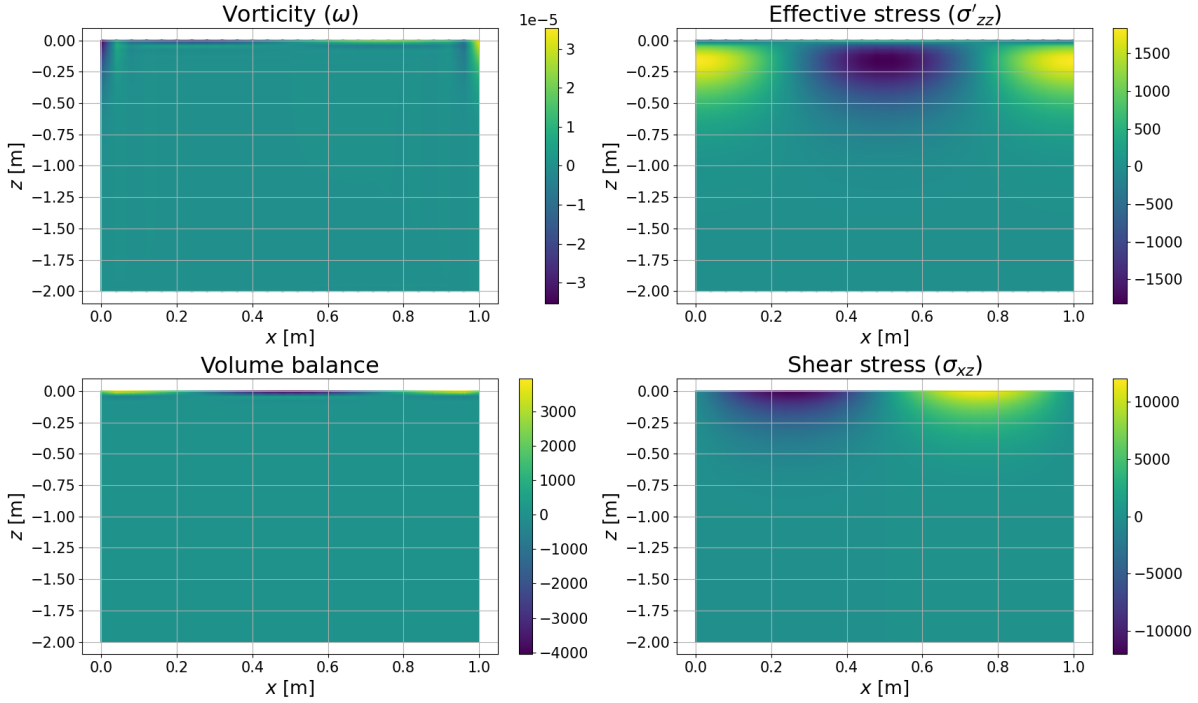

Figure 5.14: Solutions to Biot's model for ω [-], σ'_{zz} [Pa], σ_{xz} [Pa] and volume balance at $t_{\text{end}} = 2.25$ s, when water is assumed to be compressible with $\beta = 4.05 \cdot 10^{-8}$ Pa^{-1} and using boundary conditions B-III. The vorticity is expected to be zero. The volume balance is represented by the weak form of the volumetric strain equation and is satisfied if it equals 0 everywhere on the domain and its boundaries.

6

Van Damme and Den Ouden - Van der Horst model (2D)

We will now look at a new model, namely the model of Van Damme and Den Ouden - Van der Horst. This physical model is already determined in our literature report [9] and will also be stated in this chapter. The model is based on the five constitutive equations derived by [4]. These are the vorticity equation, volumetric strain equation, water pressure equation, x-displacement equation and z-displacement equation which follows from the volume balance equation and the momentum balance equations. Since this approach is based on defining a stress and a stress gradient as boundary conditions which follows from the momentum balance equation [4], it is also in line with the D'Alembert's principle of minimisation of virtual work [9]. However, it does not follow the effective stress principle of Terzaghi like Biot's model does [4].

6.1. Volume balance equation

According to [4], the volume balance equation for compressible or incompressible pore water is given by

$$p\beta\frac{\partial P}{\partial t}+\frac{\partial p}{\partial t}+\frac{\partial}{\partial x}\left(p\frac{\partial w_x}{\partial t}\right)+\frac{\partial}{\partial z}\left(p\frac{\partial w_z}{\partial t}\right)=0, \tag{6.1}$$

where t denotes time, p denotes the porosity of the medium, β denotes the compressibility of the pore water (if $\beta=0$ the water is incompressible, and if $\beta\in(0,1]$ the water is compressible), P denotes the pore water pressure and w_x and w_z denotes the 2D displacement of the pore water in x-direction and z-direction, respectively. According to [4] the volume balance equation of the incompressible particles in a porous medium is given by

$$\frac{\partial(1-p)}{\partial t}+\frac{\partial}{\partial x}\left((1-p)\frac{\partial u_x}{\partial t}\right)+\frac{\partial}{\partial z}\left((1-p)\frac{\partial u_z}{\partial t}\right)=0, \tag{6.2}$$

where u_x and u_z denote the 2D displacement of the porous medium in x-direction and z-direction, respectively. Equation (6.2) describes the change in porosity caused by the movement of incompressible particles in a porous medium. Then the volume balance equation for the porous medium is given by adding the volume balance equation of the pore water to the volume balance equation of the particles [4]

$$p\beta\frac{\partial P}{\partial t}+\frac{\partial}{\partial x}\left(p\frac{\partial(w_x-u_x)}{\partial t}\right)+\frac{\partial}{\partial z}\left(p\frac{\partial(w_z-u_z)}{\partial t}\right)+\frac{\partial\epsilon_{\text{vol}}}{\partial t}=0, \tag{6.3}$$

where $\epsilon_{\text{vol}}=\frac{\partial u_x}{\partial x}+\frac{\partial u_z}{\partial z}$ is the volumetric strain of the porous medium.

6.2. Momentum balance equations

[4] derives the momentum balance equations using D'Alembert's principle of virtual work. This principle states that for the reversible displacements the total virtual work of the imposed forces plus the inertial forces vanish [4]. The momentum balance equations are given by [4]

$$-\mu\frac{\partial}{\partial z}\left(\frac{\partial u_x}{\partial z}-\frac{\partial u_z}{\partial x}\right)-(\lambda+2\mu)\frac{\partial}{\partial x}\left(\frac{\partial u_x}{\partial x}+\frac{\partial u_z}{\partial z}\right)-\frac{\gamma_w}{K_s}\frac{\partial p(w_x-u_x)}{\partial t}=0, \tag{6.4}$$

$$2\mu\frac{\partial}{\partial x}\left(\frac{\partial u_x}{\partial z}-\frac{\partial u_z}{\partial x}\right)-(\lambda+2\mu)\frac{\partial}{\partial z}\left(\frac{\partial u_x}{\partial x}+\frac{\partial u_z}{\partial z}\right)-\frac{\gamma_w}{K_s}\frac{\partial p(w_z-u_z)}{\partial t}=0, \tag{6.5}$$

$$\frac{\partial P}{\partial x}+\frac{\gamma_w}{K_s}\frac{\partial p(w_x-u_x)}{\partial t}=0, \tag{6.6}$$

$$\frac{\partial P}{\partial z}+\frac{\gamma_w}{K_s}\frac{\partial p(w_z-u_z)}{\partial t}=0, \tag{6.7}$$

where K_s denotes the hydraulic conductivity, γ_w denotes the specific weight. We recall that λ and μ are Lamé's constant and are related to the elasticity modulus E and Poisson ratio v_p of the porous medium which are given by [10]

$$\lambda=\frac{v_pE}{(1+v_p)(1-2v_p)},$$
$$\mu=\frac{E}{2(1+v_p)}.$$

6.3. Vorticity equation

Applying the curl on the momentum balance equations, we get a constitutive equation for the vorticity [4]. Therefore, the vorticity is defined to be the curl of the displacement field which is given by $\omega=\frac{\partial u_x}{\partial z}-\frac{\partial u_z}{\partial x}$. Via substituting Equations (6.6) and (6.7) into Equations (6.4) and (6.5) the Darcy's friction terms are replaced by the pressure gradients. Substituting ϵ_{vol} and ω, this gives the following two equations

$$\frac{\partial P}{\partial x}-\mu\frac{\partial \omega}{\partial z}-(\lambda+2\mu)\frac{\partial \epsilon_{\text{vol}}}{\partial x}=0, \tag{6.8}$$

$$\frac{\partial P}{\partial z}+\mu\frac{\partial \omega}{\partial x}-(\lambda+2\mu)\frac{\partial \epsilon_{\text{vol}}}{\partial z}=0. \tag{6.9}$$

Then taking first the curl of Equations (6.8) and (6.9), and second multiplying the resulting equation with -1, gives [4]

$$\mu\left[\frac{\partial^2\omega}{\partial z^2}+\frac{\partial^2\omega}{\partial x^2}\right]=0. \tag{6.10}$$

Note that Equation (6.10) does only depend on the vorticity ω now and not on the pressure P and volumetric strain ϵ_{vol} anymore. Equation (6.10) forms the first constitutive equation.

6.4. Volumetric strain equation

Substituting ϵ_{vol} and ω and then taking the divergence of Equations (6.4) and (6.5), gives

$$-(\lambda+2\mu)\left(\frac{\partial^2\epsilon_{\text{vol}}}{\partial x^2}+\frac{\partial^2\epsilon_{\text{vol}}}{\partial z^2}\right)-\frac{\gamma_w}{K_s}\left(\frac{\partial}{\partial x}\left[p\frac{\partial(w_x-u_x)}{\partial t}\right]+\frac{\partial}{\partial z}\left[p\frac{\partial(w_z-u_z)}{\partial t}\right]\right)=0. \tag{6.11}$$

Substituting Equation (6.3) into Equation (6.11), we get

$$\frac{\gamma_w}{K_s}\frac{\partial \epsilon_{\text{vol}}}{\partial t}-(\lambda+2\mu)\left(\frac{\partial^2\epsilon_{\text{vol}}}{\partial x^2}+\frac{\partial^2\epsilon_{\text{vol}}}{\partial z^2}\right)=-\frac{\gamma_w}{K_s}p\beta\frac{\partial P}{\partial t}. \tag{6.12}$$

Note that in Equation (6.12) we account for the effects of damping. According to [4], if we would account for the acceleration terms Equation (6.12) would become a wave equation in the case of no damping, because the pore water is not part of this equation. Equation (6.12) forms the second constitutive equation.

6.5. Water pressure equation

We also need a constitutive equation describing the relation for the pore water pressures. This is done similar as for the volumetric strain. So now we take the divergence of the momentum balance equations for the pore water which are given by Equations (6.6) and (6.7). This gives a storage equation given by [4]

$$\frac{\gamma_w}{K_s} p\beta \frac{\partial P}{\partial t} - \frac{\partial^2 P}{\partial x^2} - \frac{\partial^2 P}{\partial z^2} = -\frac{\gamma_w}{K_s} \frac{\partial \epsilon_{\text{vol}}}{\partial t}. \tag{6.13}$$

Equation (6.12) forms the third constitutive equation.

6.6. Displacement equations

Beside the relations described above, it is also needed to form some relations between the horizontal and vertical displacements and the vorticity and volumetric strain. These are given by [4]

$$-\frac{\partial^2 u_x}{\partial x^2} - \frac{\partial^2 u_x}{\partial z^2} = -\frac{\partial \omega}{\partial z} - \frac{\partial \epsilon_{\text{vol}}}{\partial x}, \tag{6.14}$$

$$-\frac{\partial^2 u_z}{\partial x^2} - \frac{\partial^2 u_z}{\partial z^2} = \frac{\partial \omega}{\partial x} - \frac{\partial \epsilon_{\text{vol}}}{\partial z}. \tag{6.15}$$

Equations (6.14) and (6.15) represent the fourth and fifth constitutive equations, respectively.

6.7. Boundary conditions

The following boundary conditions are described in our literature report [9] and will be described in this subsection again.

We set three boundary conditions at the surface $z = 0$. These involve the normal stress and the shear stress.

- In the new model the shear stress is set equal to a function of time and horizontal displacement like in Biot's model, i.e. $\sigma_{xz} = \sigma_{zx} = F_{xz}$ where F_{xz} is a function depending on the horizontal displacement x and on time t. Note that the shear stress σ_{xz} is given by $\sigma_{xz} = -\mu\left(\frac{\partial u_x}{\partial z} + \frac{\partial u_z}{\partial x}\right)$ which can be rewritten as $\sigma_{xz} = \mu\omega - 2\mu\frac{\partial u_x}{\partial z}$.

- We recall that in Biot's model $\sigma_{zz} = \sigma'_{zz} + P = -\lambda\epsilon_{\text{vol}} - 2\mu\frac{\partial u_z}{\partial z} + P$ is assumed. However, according to [4], this assumption of $\sigma'_{zz} + P = F_{zz}$ gives a surface pressure that is much larger than the pressure of the waves caused by water running over the porous medium. It also violates Terzaghi's stress principle when dealing with hydrodynamic loads. Another assumption in Biot's model is $\sigma'_{zz} = 0$ with $P = F_{zz}$, which means that the water carries all the load. This is, however, physically invalid [4]. The assumption that $P = F_{zz}$ gives a solution where the pressure inside the pores is equal to the force of water flow on the surface, but the porous medium can experience a pulling force [4]. Since both assumptions give unlikely situations, the assumption is made that $P = F_{zz}$. However, then Terzaghi's stress principle is not necessarily met in the case of hydrodynamic loads, since we do not define the effective stresses at the surface.

- The vertical momentum balance equation must hold, which is given by $(\lambda + 2\mu)\frac{\partial \epsilon_{\text{vol}}}{\partial z} - \mu\frac{\partial \omega}{\partial x} - \frac{\partial P}{\partial z} = 0$.

At $z = -n_z$ we assume again that the displacement for the soil and pore water in z-direction is zero for a deep enough seabed [9] which implies that $u_z = 0$ and that there is no gradient for the pore water pressure which is defined as $\frac{\partial P}{\partial z} = 0$ [6, 7] at $z = -n_z$, respectively. Hence, there is also no gradient for the volumetric strain $\frac{\partial \epsilon_{\text{vol}}}{\partial z} = 0$ [6]. Furthermore, since $\frac{\partial u_x}{\partial z} = 0$ and $\frac{\partial u_z}{\partial x} = 0$, we have that $\omega = 0$ at $z = -n_z$.

At $x = 0$, and $x = -n_x$, the variables and their derivatives with respect to z or x are assumed to be zero, as the influence of the waves at these locations is assumed to be negligible.

- So at $z = -n_z$ we define $\omega = u_z = \frac{\partial u_x}{\partial z} = \frac{\partial P}{\partial z} = \frac{\partial \epsilon_{\text{vol}}}{\partial z} = 0$, since the influence of the waves on such a depth is assumed to be nil for these specific variables or their derivative with respect to z [4, 6].
- Similarly, at $x = 0$ and $x = -n_x$ we have $\omega = u_x = \frac{\partial u_z}{\partial x} = \frac{\partial P}{\partial x} = \frac{\partial \epsilon_{\text{vol}}}{\partial x} = 0$. These boundary conditions at $x = 0$ and $x = -n_x$ are based on the situation of a standing wave that increases and decreases the load on the soil in horizontal direction [4].

In conclusion, we have the following boundary conditions

$$\text{for } z = 0: \begin{cases} \mu\omega - 2\mu\frac{\partial u_x}{\partial z} & = F_{xz} \\ P & = F_{zz} \\ (\lambda + 2\mu)\frac{\partial \epsilon_{\text{vol}}}{\partial z} - \mu\frac{\partial \omega}{\partial x} - \frac{\partial P}{\partial z} & = 0 \end{cases}, \tag{6.16}$$

$$\text{for } z = -n_z: \left\{\omega = u_z = \frac{\partial u_x}{\partial z} = \frac{\partial P}{\partial z} = \frac{\partial \epsilon_{\text{vol}}}{\partial z} = 0\right. \quad , \tag{6.17}$$

$$\text{and for } x = 0 \text{ and } x = n_x: \left\{\omega = u_x = \frac{\partial u_z}{\partial x} = \frac{\partial P}{\partial x} = \frac{\partial \epsilon_{\text{vol}}}{\partial x} = 0\right. , \tag{6.18}$$

where F_{xz} and F_{zz} are a functions only depending on time and horizontal displacement. Their value and their gradient equal zero.

6.8. Initial conditions

Like in our literature report [9], we assume that at the start, $t = 0$, everything is at rest. Therefore, no stresses act on the surface in the beginning. Then there are no stresses and displacements at time $t = 0$ [4] which implies that the volumetric strain and pressure must be zero too. Then we have that [4]

$$\omega|_{t=0} = u_x|_{t=0} = u_z|_{t=0} = \epsilon_{\text{vol}}|_{t=0} = P|_{t=0} = 0.$$

7

Numerical model of Van Damme and Den Ouden - Van der Horst (2D)

In this chapter, the numerical approximation of the two-dimensional physical model of Van Damme and Den Ouden - Van der Horst described in Chapter 6 will be derived. We will use the Finite-Element Method for discretisation in space and the Euler method for discretisation in time which are described in Sections 7.1 and 7.2, respectively. After applying the discretisation first in space and second in time, the final numerical model is derived.

7.1. Discretisation in space

We use the Finite-Element Method to discretise the constitutive equations given by Equations (6.10), (6.12), (6.13), (6.14) and (6.15) in space. This is done by multiplying each of the five equations with its own test function and integrate over the domain. After applying integration by parts followed by the divergence theorem, substituting the trial function corresponding to the equation and rewriting the equations, we find the weak forms of the vorticity equation, volumetric strain equation, water pressure equation, x-displacement equation and z-displacement equation. The following four subsections of discretisation in space follow from our literature report [9].

In this discretisation we assume that $\Omega = (0, n_x) \times (-n_z, 0) \subseteq \mathbb{R}^2$ is the space domain and that $\mathbb{T} = (0, t_{\text{end}})$ is the time domain, with $n_x, n_z, t_{\text{end}} > 0$ [9].

Following [9], we assume that the two-dimensional domain and its boundaries and the unit vectors normal to these boundaries are given as in Figure 4.1. Recall that the normal unit vectors in two dimensions are given by

$$\eta_1 = \begin{bmatrix} 0 \\ -1 \end{bmatrix}, \quad \eta_2 = \begin{bmatrix} 1 \\ 0 \end{bmatrix}, \quad \eta_3 = \begin{bmatrix} 0 \\ 1 \end{bmatrix}, \quad \eta_4 = \begin{bmatrix} -1 \\ 0 \end{bmatrix}.$$

where the first entry represents the x-direction and the second entry represents the z-direction.

Recall that n is the dimension of the space and N_i are the basis-functions for $i = 1, \dots, n$ which form a basis for the space. When having the symbol of the volumetric strain, pore water pressure or displacement in horizontal or vertical direction, n and N_i for $i = 1, \dots, n$ are defined for the space of that unknown variable. However, we assume that n is the same for all spaces [9].

7.1.1. Vorticity equation

We will derive the weak form of the vorticity equation and its matrix-vector form. Suppose that the test and trial functions are given by

$$v^{\omega}(x,z,t) = \sum_{i=1}^{n} N_i^{\omega}(x,z)\bar{v}_i^{\omega}(t), \tag{7.1}$$

$$\omega(x,z,t) = \sum_{j=1}^{n} N_j^{\omega}(x,z)\bar{\omega}_j(t). \tag{7.2}$$

Multiplying Equation (6.10) by test function v^{ω} and integrating over the domain Ω gives

$$\int_{\Omega} v^{\omega}\mu\left[\frac{\partial^2\omega}{\partial z^2} + \frac{\partial^2\omega}{\partial x^2}\right]\mathrm{d}\Omega = 0. \tag{7.3}$$

Since $\frac{\partial^2\omega}{\partial z^2} + \frac{\partial^2\omega}{\partial x^2} = \nabla\cdot(\nabla\omega)$ with ∇ the gradient operator, we can apply integration by parts on Equation (7.3) followed by the divergence theorem. Then Equation (7.3) becomes the weak equation

$$\int_{\mathrm{d}\Omega} v^{\omega}\mu\,(\nabla\omega\cdot\boldsymbol{\eta})\,\mathrm{d}\Gamma - \int_{\Omega}\nabla v^{\omega}\cdot\mu\nabla\omega\mathrm{d}\Omega = 0, \tag{7.4}$$

where $\mathrm{d}\Omega$ contains the boundaries of domain Ω, and $\boldsymbol{\eta}$ is the unit normal vector pointing outward to the surface $\mathrm{d}\Omega$. Because of the boundary conditions given by Equations (6.16), (6.17) and (6.18), we set $v^{\omega}(x,z,t) = 0$ for $z = -n_z$, $x = 0$ and $x = n_x$. Then we get that

$$\begin{aligned}\int_{\mathrm{d}\Omega} v^{\omega}\mu\,(\nabla\omega\cdot\boldsymbol{\eta})\,\mathrm{d}\Gamma &= \int_{\mathrm{d}\Omega_1} v^{\omega}\mu\,(\nabla\omega\cdot\boldsymbol{\eta}_1)\,\mathrm{d}\Gamma + \int_{\mathrm{d}\Omega_2} v^{\omega}\mu\,(\nabla\omega\cdot\boldsymbol{\eta}_2)\,\mathrm{d}\Gamma \\ &\quad + \int_{\mathrm{d}\Omega_3} v^{\omega}\mu\,(\nabla\omega\cdot\boldsymbol{\eta}_3)\,\mathrm{d}\Gamma + \int_{\mathrm{d}\Omega_4} v^{\omega}\mu\,(\nabla\omega\cdot\boldsymbol{\eta}_4)\,\mathrm{d}\Gamma \\ &= \int_{\mathrm{d}\Omega_3} v^{\omega}\mu\frac{\partial\omega}{\partial z}\mathrm{d}\Gamma.\end{aligned} \tag{7.5}$$

After substituting the test and trial functions given by Equations (7.1) and (7.2), respectively, and boundary integral given by Equation (7.5) into Equation (7.4) we get the following Galerkin equations

$$\begin{aligned}0 &= \int_{\mathrm{d}\Omega_3}\sum_{i=1}^{n} N_i^{\omega}\bar{v}_i^{\omega}\mu\frac{\partial}{\partial z}\left(\sum_{j=1}^{n} N_j^{\omega}\bar{\omega}_j\right)\mathrm{d}\Gamma - \int_{\Omega}\nabla\left(\sum_{i=1}^{n} N_i^{\omega}\bar{v}_i^{\omega}\right)\cdot\mu\nabla\left(\sum_{i=1}^{n} N_j^{\omega}\bar{\omega}_j\right)\mathrm{d}\Omega \\ &= \sum_{i=1}^{n}\bar{v}_i^{\omega}\int_{\mathrm{d}\Omega_3} N_i^{\omega}\mu\sum_{j=1}^{n}\bar{\omega}_j\frac{\partial N_j^{\omega}}{\partial z}\mathrm{d}\Gamma - \sum_{i=1}^{n}\bar{v}_i^{\omega}\int_{\Omega}\nabla N_i^{\omega}\cdot\mu\sum_{j=1}^{n}\bar{\omega}_j\nabla N_j^{\omega}\mathrm{d}\Omega.\end{aligned} \tag{7.6}$$

Since it must hold for arbitrary $\bar{v}_i^{\omega}$ with $i = 1,\dots,n$, we have that Equation (7.6) still holds as

$$0 = \int_{\mathrm{d}\Omega_3} N_i^{\omega}\mu\sum_{j=1}^{n}\bar{\omega}_j\frac{\partial N_j^{\omega}}{\partial z}\mathrm{d}\Gamma - \int_{\Omega}\nabla N_i^{\omega}\cdot\mu\sum_{j=1}^{n}\bar{\omega}_j\nabla N_j^{\omega}\mathrm{d}\Omega \quad \text{for } i = 1,\dots,n. \tag{7.7}$$

We can write Equation (7.7) as matrix-vector multiplication,

$$(B^{\omega} - SD^{\omega})\,\bar{\boldsymbol{w}} = 0, \tag{7.8}$$

where

$$B_{ij}^{\omega} = \int_{\Omega}\mu\left(\nabla N_i^{\omega}\cdot\nabla N_j^{\omega}\right)\mathrm{d}\Omega, \quad SD_{ij}^{\omega} = \int_{\mathrm{d}\Omega_3}\mu N_i^{\omega}\frac{\partial N_j^{\omega}}{\partial z}\mathrm{d}\Gamma, \quad \bar{\boldsymbol{w}} = \begin{bmatrix}\bar{\omega}_1\\ \vdots\\ \bar{\omega}_n\end{bmatrix},$$

for $i,j = 1,\dots,n$. Equation (7.8) is our first matrix problem to solve.

7.1.2. Volumetric strain equation

We will derive the weak form of the volumetric strain equation and its matrix-vector form. Suppose that the test and trial functions are given by

$$v^\epsilon(x,z,t) = \sum_{i=1}^{n} N_i^\epsilon(x,z)\bar{v}_i^\epsilon(t), \tag{7.9}$$

$$\epsilon_{\text{vol}}(x,z,t) = \sum_{j=1}^{n} N_j^\epsilon(x,z)\bar{\epsilon}_j(t), \tag{7.10}$$

$$P(x,z,t) = \sum_{l=1}^{n} N_l^P(x,z)\bar{P}_l(t). \tag{7.11}$$

Note that ϵ_{vol} and P have a first derivative with respect to time which means that their test and trial functions have to depend on time. Multiplying Equation (6.12) by test function v^ϵ and integrating over the domain Ω gives

$$\int_\Omega v^\epsilon \left[\frac{\gamma_w}{K_s}\frac{\partial \epsilon_{\text{vol}}}{\partial t} - (\lambda+2\mu)\left(\frac{\partial^2 \epsilon_{\text{vol}}}{\partial x^2} + \frac{\partial^2 \epsilon_{\text{vol}}}{\partial z^2}\right) + \frac{\gamma_w}{K_s} p\beta \frac{\partial P}{\partial t}\right] \mathrm{d}\Omega = 0. \tag{7.12}$$

Since $\frac{\partial^2 \epsilon_{\text{vol}}}{\partial x^2} + \frac{\partial^2 \epsilon_{\text{vol}}}{\partial z^2} = \nabla \cdot (\nabla \epsilon_{\text{vol}})$, we can apply integration by parts on the $\frac{\partial^2 \epsilon_{\text{vol}}}{\partial x^2} + \frac{\partial^2 \epsilon_{\text{vol}}}{\partial z^2}$ part and then the divergence theorem. Then Equation (7.12) becomes

$$-\int_{\mathrm{d}\Omega} v^\epsilon (\lambda+2\mu)\,(\nabla \epsilon_{\text{vol}} \cdot \boldsymbol{\eta})\,\mathrm{d}\Gamma + \int_\Omega v^\epsilon \frac{\gamma_w}{K_s}\left[\frac{\partial \epsilon_{\text{vol}}}{\partial t} + p\beta\frac{\partial P}{\partial t}\right] + (\lambda+2\mu)\,(\nabla v^\epsilon \cdot \nabla \epsilon_{\text{vol}})\,\mathrm{d}\Omega = 0. \tag{7.13}$$

Using the boundary conditions given by Equations (6.16), (6.17) and (6.18), we get that

$$\begin{aligned}\int_{\mathrm{d}\Omega} v^\epsilon (\lambda+2\mu)\,(\nabla \epsilon_{\text{vol}} \cdot \boldsymbol{\eta})\,\mathrm{d}\Gamma &= \int_{\mathrm{d}\Omega_1} v^\epsilon (\lambda+2\mu)\,(\nabla \epsilon_{\text{vol}} \cdot \boldsymbol{\eta}_1)\,\mathrm{d}\Gamma + \int_{\mathrm{d}\Omega_2} v^\epsilon (\lambda+2\mu)\,(\nabla \epsilon_{\text{vol}} \cdot \boldsymbol{\eta}_2)\,\mathrm{d}\Gamma \\ &\quad + \int_{\mathrm{d}\Omega_3} v^\epsilon (\lambda+2\mu)\,(\nabla \epsilon_{\text{vol}} \cdot \boldsymbol{\eta}_3)\,\mathrm{d}\Gamma + \int_{\mathrm{d}\Omega_4} v^\epsilon (\lambda+2\mu)\,(\nabla \epsilon_{\text{vol}} \cdot \boldsymbol{\eta}_4)\,\mathrm{d}\Gamma \\ &= \int_{\mathrm{d}\Omega_3} v^\epsilon \left(\mu\frac{\partial \omega}{\partial x} + \frac{\partial P}{\partial z}\right)\mathrm{d}\Gamma.\end{aligned} \tag{7.14}$$

Substituting the test and trial functions given by Equations (7.9), (7.10) and (7.11), and the boundary integral given by Equation (7.14) into Equation (7.13) gives the following Galerkin equations

$$\begin{aligned}0 &= -\int_{\mathrm{d}\Omega_3} \sum_{i=1}^{n} N_i^\epsilon \bar{v}_i^\epsilon \left(\mu \sum_{j=1}^{n} \bar{\omega}_j \frac{\partial N_j^\omega}{\partial x} + \sum_{l=1}^{n} \bar{P}_l \frac{\partial N_l^P}{\partial z}\right)\mathrm{d}\Gamma \\ &\quad + \int_\Omega \sum_{i=1}^{n} N_i^\epsilon \bar{v}_i^\epsilon \frac{\gamma_w}{K_s}\left[\frac{\partial}{\partial t}\left(\sum_{j=1}^{n} N_j^\epsilon \bar{\epsilon}_j\right) + p\beta\frac{\partial}{\partial t}\left(\sum_{l=1}^{n} N_l^P \bar{P}_l\right)\right] + (\lambda+2\mu)\left[\nabla\left(\sum_{i=1}^{n} N_i^\epsilon \bar{v}_i^\epsilon\right)\cdot\nabla\left(\sum_{j=1}^{n} N_j^\epsilon \bar{\epsilon}_j\right)\right]\mathrm{d}\Omega \\ &= -\sum_{i=1}^{n} \bar{v}_i^\epsilon \int_{\mathrm{d}\Omega} N_i^\epsilon \left(\mu \sum_{j=1}^{n} \bar{\omega}_j \frac{\partial N_j^\omega}{\partial x} + \sum_{l=1}^{n} \bar{P}_l \frac{\partial N_l^P}{\partial z}\right)\mathrm{d}\Gamma \\ &\quad + \sum_{i=1}^{n} \bar{v}_i^\epsilon \int_\Omega \frac{\gamma_w}{K_s} N_i^\epsilon \left[\sum_{j=1}^{n} N_j^\epsilon \frac{\partial \bar{\epsilon}_j}{\partial t} + p\beta \sum_{l=1}^{n} N_l^P \frac{\partial \bar{P}_l}{\partial t}\right] + (\lambda+2\mu)\left[\nabla N_i^\epsilon \cdot \left(\sum_{j=1}^{n} \bar{\epsilon}_j \nabla N_j^\epsilon\right)\right]\mathrm{d}\Omega.\end{aligned} \tag{7.15}$$

Since it must hold for arbitrary $\bar{v}_i^{\epsilon}$ with $i = 1, \dots, n$, we have that Equation (7.15) still holds as

$$0 = -\int_{\mathrm{d}\Omega_3} N_i^{\epsilon} \left(\mu \sum_{j=1}^{n} \bar{\omega}_j \frac{\partial N_j^{\omega}}{\partial x} + \sum_{l=1}^{n} \bar{P}_l \frac{\partial N_l^{P}}{\partial z} \right) \mathrm{d}\Gamma + \int_{\Omega} \frac{\gamma_w}{K_s} N_i^{\epsilon} \left[\sum_{j=1}^{n} N_j^{\epsilon} \frac{\partial \bar{\epsilon}_j}{\partial t} + p\beta \sum_{l=1}^{n} N_l^{P} \frac{\partial \bar{P}_l}{\partial t} \right] + (\lambda + 2\mu) \left[\nabla N_i^{\epsilon} \cdot \left(\sum_{j=1}^{n} \bar{\epsilon}_j \nabla N_j^{\epsilon} \right) \right] \mathrm{d}\Omega. \tag{7.16}$$

We can write Equation (7.16) as matrix-vector multiplication,

$$A^{\epsilon\epsilon} \bar{\boldsymbol{\epsilon}}_t + A^{\epsilon P} \bar{\boldsymbol{P}}_t + B^{\epsilon} \bar{\boldsymbol{\epsilon}} - SC^{\epsilon} \bar{\boldsymbol{\omega}} - SD^{\epsilon} \bar{\boldsymbol{P}} = 0, \tag{7.17}$$

where

$$A_{ij}^{\epsilon\epsilon} = \int_{\Omega} \frac{\gamma_w}{K_s} N_i^{\epsilon} N_j^{\epsilon} \mathrm{d}\Omega, \quad A_{ij}^{\epsilon P} = \int_{\Omega} \frac{\gamma_w}{K_s} p\beta N_i^{\epsilon} N_j^{P} \mathrm{d}\Omega, \quad B_{ij}^{\epsilon} = \int_{\Omega} (\lambda + 2\mu) \left[\nabla N_i^{\epsilon} \cdot \nabla N_j^{\epsilon} \right] \mathrm{d}\Omega,$$

$$SC_i^{\epsilon} = \int_{\mathrm{d}\Omega_3} \mu N_i^{\epsilon} \frac{\partial N_j^{\omega}}{\partial x} \mathrm{d}\Gamma, \quad SD_i^{\epsilon} = \int_{\mathrm{d}\Omega_3} N_i^{\epsilon} \frac{\partial N_j^{P}}{\partial z} \mathrm{d}\Gamma, \quad \bar{\boldsymbol{\epsilon}} = \begin{bmatrix} \bar{\epsilon}_1 \\ \vdots \\ \bar{\epsilon}_n \end{bmatrix}, \quad \bar{\boldsymbol{\epsilon}}_t = \begin{bmatrix} \frac{\partial \bar{\epsilon}_1}{\partial t} \\ \vdots \\ \frac{\partial \bar{\epsilon}_n}{\partial t} \end{bmatrix}, \quad \bar{\boldsymbol{P}}_t = \begin{bmatrix} \frac{\partial \bar{P}_1}{\partial t} \\ \vdots \\ \frac{\partial \bar{P}_n}{\partial t} \end{bmatrix},$$

for $i, j = 1, \dots, n$. Equation (7.17) is our second matrix problem to solve.

7.1.3. Pressure equation

We will derive the weak form of the pressure equation and its matrix-vector form. Suppose that the test function is given by

$$v^P(x, z, t) = \sum_{i=1}^{n} N_i^P(x, z) \bar{v}_i^P(t). \tag{7.18}$$

Recall the following test and trial functions

$$\epsilon_{\mathrm{vol}}(x, z, t) = \sum_{j=1}^{n} N_j^{\epsilon}(x, z) \bar{\epsilon}_j(t), \quad P(x, z, t) = \sum_{l=1}^{n} N_l^P(x, z) \bar{P}_l(t).$$

Multiplying Equation (6.13) by test function v^P and integrating over the domain Ω gives

$$\int_{\Omega} v^P \left[\frac{\gamma_w}{K_s} p\beta \frac{\partial P}{\partial t} - \frac{\partial^2 P}{\partial x^2} - \frac{\partial^2 P}{\partial z^2} + \frac{\gamma_w}{K_s} \frac{\partial \epsilon_{\mathrm{vol}}}{\partial t} \right] \mathrm{d}\Omega = 0. \tag{7.19}$$

Since $\frac{\partial^2 P}{\partial x^2} + \frac{\partial^2 P}{\partial z^2} = \nabla \cdot (\nabla P)$, we can apply integration by parts on the $-\frac{\partial^2 P}{\partial x^2} - \frac{\partial^2 P}{\partial z^2}$ part followed by the divergence theorem. Then Equation (7.19) becomes

$$-\int_{\mathrm{d}\Omega} v^P \left(\nabla P \cdot \boldsymbol{\eta} \right) \mathrm{d}\Gamma + \int_{\Omega} v^P \frac{\gamma_w}{K_s} \left[p\beta \frac{\partial P}{\partial t} + \frac{\partial \epsilon_{\mathrm{vol}}}{\partial t} \right] + \left(\nabla v^P \cdot \nabla P \right) \mathrm{d}\Omega = 0. \tag{7.20}$$

Setting $v^P(x, z, t) = 0$ for $z = 0$ because of the boundary condition given by Equation (6.16) and using the other boundary conditions given by Equations (6.17) and (6.18), we get that

$$\begin{aligned} \int_{\mathrm{d}\Omega} v^P \left(\nabla P \cdot \boldsymbol{\eta} \right) \mathrm{d}\Gamma &= \int_{\mathrm{d}\Omega_1} v^P \left(\nabla P \cdot \boldsymbol{\eta}_1 \right) \mathrm{d}\Gamma + \int_{\mathrm{d}\Omega_2} v^P \left(\nabla P \cdot \boldsymbol{\eta}_2 \right) \mathrm{d}\Gamma \\ &\quad + \int_{\mathrm{d}\Omega_3} v^P \left(\nabla P \cdot \boldsymbol{\eta}_3 \right) \mathrm{d}\Gamma + \int_{\mathrm{d}\Omega_4} v^P \left(\nabla P \cdot \boldsymbol{\eta}_4 \right) \mathrm{d}\Gamma \\ &= 0. \end{aligned} \tag{7.21}$$

Substituting the test and trial functions given by Equations (7.18), (7.10) and (7.11) into Equation (7.20), the boundary integral given by Equation (7.21), and using the computations as for Biot's model in Section 4.1.1 gives the following Galerkin equations in matrix-vector multiplication,

$$A^{PP}\bar{\boldsymbol{P}}_t + A^{P\epsilon}\bar{\boldsymbol{\epsilon}}_t + B^P\bar{\boldsymbol{P}} = 0, \tag{7.22}$$

where

$$A_{ij}^{PP} = \int_\Omega \frac{\gamma_w}{K_s} p\beta N_i^P N_j^P \,\mathrm{d}\Omega, \quad A_{ij}^{P\epsilon} = \int_\Omega \frac{\gamma_w}{K_s} N_i^P N_j^\epsilon \,\mathrm{d}\Omega, \quad B_{ij}^P = \int_\Omega \nabla N_i^P \cdot \nabla N_j^P \,\mathrm{d}\Omega,$$
$$\bar{\boldsymbol{P}} = \begin{bmatrix} \bar{P}_1 \\ \vdots \\ \bar{P}_n \end{bmatrix}, \quad \bar{\boldsymbol{P}}_t = \begin{bmatrix} \frac{\partial \bar{P}_1}{\partial t} \\ \vdots \\ \frac{\partial \bar{P}_n}{\partial t} \end{bmatrix}, \quad \bar{\boldsymbol{\epsilon}}_t = \begin{bmatrix} \frac{\partial \bar{\epsilon}_1}{\partial t} \\ \vdots \\ \frac{\partial \bar{\epsilon}_n}{\partial t} \end{bmatrix},$$

for $i, j = 1, \dots, n$. Equation (7.22) is our third matrix problem to solve.

7.1.4. Displacement equations

We will derive the weak form of the displacement equations and its matrix-vector form. Suppose that the test function is given by

$$v^{u_x}(x,z,t) = \sum_{i=1}^n N_i^{u_x}(x,z)\bar{v}_i^{u_x}(t), \tag{7.23}$$

$$v^{u_z}(x,z,t) = \sum_{i=1}^n N_i^{u_z}(x,z)\bar{v}_i^{u_z}(t), \tag{7.24}$$

$$u_x(x,z,t) = \sum_{j=1}^n N_j^{u_x}(x,z)\bar{u}_j^{x}(t), \tag{7.25}$$

$$u_z(x,z,t) = \sum_{j=1}^n N_j^{u_z}(x,z)\bar{u}_j^{z}(t). \tag{7.26}$$

Recall the following test and trial functions

$$\epsilon_{\text{vol}}(x,z,t) = \sum_{k=1}^n N_k^\epsilon(x,z)\bar{\epsilon}_k(t), \quad \omega(x,z,t) = \sum_{l=1}^n N_l^\omega(x,z)\bar{\omega}_l(t).$$

After multiplying Equations (6.14) and (6.15) by test functions v^{u_x} and v^{u_x}, respectively, and integrating over the domain Ω we get

$$0 = \int_\Omega v^{u_x}\left[-\left(\frac{\partial^2 u_x}{\partial x^2} + \frac{\partial^2 u_x}{\partial z^2}\right) + \frac{\partial \omega}{\partial z} + \frac{\partial \epsilon_{\text{vol}}}{\partial x}\right]\mathrm{d}\Omega, \tag{7.27}$$

$$0 = \int_\Omega v^{u_z}\left[-\left(\frac{\partial^2 u_z}{\partial x^2} + \frac{\partial^2 u_z}{\partial z^2}\right) - \frac{\partial \omega}{\partial x} + \frac{\partial \epsilon_{\text{vol}}}{\partial z}\right]\mathrm{d}\Omega. \tag{7.28}$$

Since $\frac{\partial^2 u_i}{\partial x^2} + \frac{\partial^2 u_i}{\partial z^2} = \nabla \cdot (\nabla u_i)$ for $i = x, z$, applying integration by parts and the divergence theorem to Equations (7.27) and (7.28) gives

$$0 = -\int_{\mathrm{d}\Omega} v^{u_x}\left[\nabla u_x \cdot \boldsymbol{\eta}\right]\mathrm{d}\Gamma + \int_\Omega v^{u_x}\left(\frac{\partial \omega}{\partial z} + \frac{\partial \epsilon_{\text{vol}}}{\partial x}\right) + \left[\nabla v^{u_x} \cdot \nabla u_x\right]\mathrm{d}\Omega, \tag{7.29}$$

$$0 = -\int_{\mathrm{d}\Omega} v^{u_z}\left[\nabla u_z \cdot \boldsymbol{\eta}\right]\mathrm{d}\Gamma + \int_\Omega v^{u_z}\left(-\frac{\partial \omega}{\partial x} + \frac{\partial \epsilon_{\text{vol}}}{\partial z}\right) + \left[\nabla v^{u_z} \cdot \nabla u_z\right]\mathrm{d}\Omega. \tag{7.30}$$

After substituting the boundary conditions given by Equations (6.16), (6.17) and (6.18) into Equations (7.29) and (7.30), we get that

$$\begin{aligned}\int_{\mathrm{d}\Omega} v^{u_x}\left[\nabla u_x \cdot \boldsymbol{\eta}\right]\mathrm{d}\Gamma &= \int_{\mathrm{d}\Omega_1} v^{u_x}\left[\nabla u_x \cdot \boldsymbol{\eta}_1\right]\mathrm{d}\Gamma + \int_{\mathrm{d}\Omega_2} v^{u_x}\left[\nabla u_x \cdot \boldsymbol{\eta}_2\right]\mathrm{d}\Gamma \\ &\quad + \int_{\mathrm{d}\Omega_3} v^{u_x}\left[\nabla u_x \cdot \boldsymbol{\eta}_3\right]\mathrm{d}\Gamma + \int_{\mathrm{d}\Omega_4} v^{u_x}\left[\nabla u_x \cdot \boldsymbol{\eta}_4\right]\mathrm{d}\Gamma \\ &= \int_{\mathrm{d}\Omega_3} v^{u_x}\frac{1}{2}\left(\omega - \frac{1}{\mu}F_{xz}\right)\mathrm{d}\Gamma, \end{aligned} \tag{7.31}$$

$$\begin{aligned}\int_{\mathrm{d}\Omega} v^{u_z}\left[\nabla u_z \cdot \boldsymbol{\eta}\right]\mathrm{d}\Gamma &= \int_{\mathrm{d}\Omega_1} v^{u_z}\left[\nabla u_z \cdot \boldsymbol{\eta}_1\right]\mathrm{d}\Gamma + \int_{\mathrm{d}\Omega_2} v^{u_z}\left[\nabla u_z \cdot \boldsymbol{\eta}_2\right]\mathrm{d}\Gamma \\ &\quad + \int_{\mathrm{d}\Omega_3} v^{u_z}\left[\nabla u_z \cdot \boldsymbol{\eta}_3\right]\mathrm{d}\Gamma + \int_{\mathrm{d}\Omega_4} v^{u_z}\left[\nabla u_z \cdot \boldsymbol{\eta}_4\right]\mathrm{d}\Gamma \\ &= \int_{\mathrm{d}\Omega_3} v^{u_z}\frac{\lambda}{2\mu}\epsilon_{\mathrm{vol}}\mathrm{d}\Gamma. \end{aligned} \tag{7.32}$$

Substituting the test and trial functions given by Equations (7.23), (7.24), (7.25), (7.26), (7.10), (7.2) and boundary integrals given by Equations (7.31) and (7.32) into Equations (7.29) and (7.30) gives the following Galerkin equations

$$\begin{aligned} 0 = &-\int_{\mathrm{d}\Omega_3}\sum_{i=1}^{n} N_i^{u_x}\bar{v}_i^{u_x}\frac{1}{2}\left[\left(\sum_{j=1}^{n} N_j^{\omega}\bar{\omega}_j\right) - \frac{1}{\mu}F_{xz}\right]\mathrm{d}\Gamma \\ &+ \int_{\Omega}\sum_{i=1}^{n} N_i^{u_x}\bar{v}_i^{u_x}\left(\frac{\partial}{\partial z}\left(\sum_{j=1}^{n} N_j^{\omega}\bar{\omega}_j\right) + \frac{\partial}{\partial x}\left(\sum_{l=1}^{n} N_l^{\epsilon}\bar{\epsilon}_l\right)\right) + \left[\nabla\left(\sum_{i=1}^{n} N_i^{u_x}\bar{v}_i^{u_x}\right)\cdot\nabla\left(\sum_{j=1}^{n} N_j^{u_x}\bar{u}_j^{x}\right)\right]\mathrm{d}\Omega, \end{aligned} \tag{7.33}$$

$$\begin{aligned} 0 = &-\int_{\mathrm{d}\Omega_3}\sum_{i=1}^{n} N_i^{u_z}\bar{v}_i^{u_z}\left(\frac{\lambda}{2\mu}\sum_{j=1}^{n} N_j^{\epsilon}\bar{\epsilon}_j\right)\mathrm{d}\Gamma \\ &+ \int_{\Omega}\sum_{i=1}^{n} N_i^{u_z}\bar{v}_i^{u_z}\left(-\frac{\partial}{\partial x}\left(\sum_{j=1}^{n} N_j^{\omega}\bar{\omega}_j\right) + \frac{\partial}{\partial z}\left(\sum_{l=1}^{n} N_l^{\epsilon}\bar{\epsilon}_l\right)\right) + \left[\nabla\left(\sum_{i=1}^{n} N_i^{u_z}\bar{v}_i^{u_z}\right)\cdot\nabla\left(\sum_{j=1}^{n} N_j^{u_z}\bar{u}_j^{z}\right)\right]\mathrm{d}\Omega. \end{aligned} \tag{7.34}$$

Equations (7.33) and (7.34) can be written as

$$\begin{aligned} 0 = &-\sum_{i=1}^{n}\bar{v}_i^{u_x}\int_{\mathrm{d}\Omega} N_i^{u_x}\frac{1}{2}\left[\left(\sum_{j=1}^{n} N_j^{\omega}\bar{\omega}_j\right) - \frac{1}{\mu}F_{xz}\right]\mathrm{d}\Gamma \\ &+ \sum_{i=1}^{n}\bar{v}_i^{u_x}\int_{\Omega} N_i^{u_x}\left(\sum_{j=1}^{n}\bar{\omega}_j\frac{\partial N_j^{\omega}}{\partial z} + \sum_{l=1}^{n}\bar{\epsilon}_l\frac{\partial N_l^{\epsilon}}{\partial x}\right) + \left[\nabla N_i^{u_x}\cdot\left(\sum_{j=1}^{n}\bar{u}_j^{x}\nabla N_j^{u_x}\right)\right]\mathrm{d}\Omega, \end{aligned} \tag{7.35}$$

$$\begin{aligned} 0 = &-\sum_{i=1}^{n}\bar{v}_i^{u_z}\int_{\mathrm{d}\Omega}\frac{\lambda}{2\mu}N_i^{u_z}\sum_{j=1}^{n}\bar{\epsilon}_j N_j^{\epsilon}\mathrm{d}\Gamma \\ &+ \sum_{i=1}^{n}\bar{v}_i^{u_z}\int_{\Omega} N_i^{u_z}\left(-\sum_{j=1}^{n}\bar{\omega}_j\frac{\partial N_j^{\omega}}{\partial x} + \sum_{l=1}^{n}\bar{\epsilon}_l\frac{\partial N_l^{\epsilon}}{\partial z}\right) + \left[\nabla N_i^{u_z}\cdot\left(\sum_{j=1}^{n}\bar{u}_j^{z}\nabla N_j^{u_z}\right)\right]\mathrm{d}\Omega. \end{aligned} \tag{7.36}$$

Since it must hold for arbitrary $\bar{v}_i^{u_x}$ and $\bar{v}_i^{u_z}$ with $i = 1, \ldots, n$, we have that Equations (7.35) and (7.36)

still holds as

$$0 = -\int_{\mathrm{d}\Omega_3} N_i^{u_x} \frac{1}{2}\left[\left(\sum_{j=1}^{n} N_j^{\omega}\bar{\omega}_j\right) - \frac{1}{\mu}F_{xz}\right]\mathrm{d}\Gamma + \int_{\Omega} N_i^{u_x}\left(\sum_{j=1}^{n}\bar{\omega}_j\frac{\partial N_j^{\omega}}{\partial z} + \sum_{l=1}^{n}\bar{\epsilon}_l\frac{\partial N_l^{\epsilon}}{\partial x}\right) + \left[\nabla N_i^{u_x}\cdot\left(\sum_{j=1}^{n}\bar{u}_j^{x}\nabla N_j^{u_x}\right)\right]\mathrm{d}\Omega, \tag{7.37}$$

$$0 = -\int_{\mathrm{d}\Omega_3} \frac{\lambda}{2\mu}N_i^{u_z}\sum_{j=1}^{n}\bar{\epsilon}_j N_j^{\epsilon}\mathrm{d}\Gamma + \int_{\Omega} N_i^{u_z}\left(-\sum_{j=1}^{n}\bar{\omega}_j\frac{\partial N_j^{\omega}}{\partial x} + \sum_{l=1}^{n}\bar{\epsilon}_l\frac{\partial N_l^{\epsilon}}{\partial z}\right) + \left[\nabla N_i^{u_z}\cdot\left(\sum_{j=1}^{n}\bar{u}_j^{z}\nabla N_j^{u_z}\right)\right]\mathrm{d}\Omega. \tag{7.38}$$

We can write Equations (7.37) and (7.38) as matrix-vector multiplications,

$$\begin{cases} B^{u_x}\bar{\boldsymbol{u}}^{x} + (D^{u_x} - SA^{u_x})\bar{\boldsymbol{\omega}} + C^{u_x}\bar{\boldsymbol{\epsilon}} &= -\mathbf{F}^{xz} \\ (B^{u_z} - SA^{u_z})\,\bar{\boldsymbol{u}}^{z} - C^{u_z}\bar{\boldsymbol{\omega}} + D^{u_z}\bar{\boldsymbol{\epsilon}} &= 0 \end{cases}, \tag{7.39}$$

where

$$SA_{ij}^{u_x} = \int_{\mathrm{d}\Omega_3}\frac{1}{2}N_i^{u_x}N_j^{\omega}\mathrm{d}\Gamma, \quad SA_{ij}^{u_z} = \int_{\mathrm{d}\Omega_3}\frac{\lambda}{2\mu}N_i^{u_z}N_j^{\epsilon}\mathrm{d}\Gamma, \quad B_{ij}^{u_x} = \int_{\Omega}\nabla N_i^{u_x}\cdot\nabla N_j^{u_x}\mathrm{d}\Omega, \quad B_{ij}^{u_z} = \int_{\Omega}\nabla N_i^{u_z}\cdot\nabla N_j^{u_z}\mathrm{d}\Omega,$$
$$C_i^{u_x} = \int_{\mathrm{d}\Omega} N_i^{u_x}\frac{\partial N_j^{\epsilon}}{\partial x}\mathrm{d}\Omega, \quad C_i^{u_z} = \int_{\mathrm{d}\Omega} N_i^{u_z}\frac{\partial N_j^{\omega}}{\partial x}\mathrm{d}\Omega, \quad D_{ij}^{u_x} = \int_{\mathrm{d}\Omega} N_i^{u_x}\frac{\partial N_j^{\omega}}{\partial z}\mathrm{d}\Omega, \quad D_{ij}^{u_z} = \int_{\mathrm{d}\Omega} N_i^{u_z}\frac{\partial N_j^{\epsilon}}{\partial z}\mathrm{d}\Omega,$$
$$F_i^{xz} = \int_{\mathrm{d}\Omega_3} N_i^{u_x}\frac{1}{2\mu}F_{xz}\mathrm{d}\Gamma,$$

for $i, j = 1, \dots, n$. Equation (7.39) is our fourth matrix problem to solve.

7.1.5. Final FEM Model

We assume that $N_i^{\epsilon} = N_i^{\omega} = N_i^{P} = N_i^{u_x} = N_i^{u_z} =: N_i$ for all $i = 1, \dots, n$. After collecting the governing equations given by Equations (7.8), (7.17), (7.22) and (7.39), we get the following set of Galerkin equations:

$$\begin{cases} \mu\,(B - SD)\,\bar{\boldsymbol{\omega}} &= 0 \\ \frac{\gamma_w}{K_s}A\bar{\boldsymbol{\epsilon}}_t + \frac{\gamma_w}{K_s}p\beta A\bar{\boldsymbol{P}}_t + (\lambda + 2\mu)\,B\bar{\boldsymbol{\epsilon}} - \mu SC\bar{\boldsymbol{\omega}} - SD\bar{\boldsymbol{P}} &= 0 \\ \frac{\gamma_w}{K_s}A\bar{\boldsymbol{\epsilon}}_t + \frac{\gamma_w}{K_s}p\beta A\bar{\boldsymbol{P}}_t + B\bar{\boldsymbol{P}} &= 0 \\ B\bar{\boldsymbol{u}}^{x} + (D - \frac{1}{2}SA)\bar{\boldsymbol{\omega}} + C\bar{\boldsymbol{\epsilon}} &= -\boldsymbol{F}^{xz} \\ (B - SD)\,\bar{\boldsymbol{u}}^{z} - C\bar{\boldsymbol{\omega}} + D\bar{\boldsymbol{\epsilon}} &= 0 \end{cases}, \tag{7.40}$$

where $A_{ij} = \int_{\Omega} N_i N_j \mathrm{d}\Omega$, $SA_{ij} = \int_{\mathrm{d}\Omega_3} N_i N_j \mathrm{d}\Gamma$, $B_{ij} = \int_{\Omega}\nabla N_i\cdot\nabla N_j\mathrm{d}\Omega$, $C_{ij} = \int_{\Omega} N_i\frac{\partial N_j}{\partial x}\mathrm{d}\Omega$, $SC_{ij} = \int_{\mathrm{d}\Omega_3} N_i\frac{\partial N_j}{\partial x}\mathrm{d}\Gamma$, $D_{ij} = \int_{\Omega} N_i\frac{\partial N_j}{\partial z}\mathrm{d}\Omega$, $SD_{ij} = \int_{\mathrm{d}\Omega_3} N_i\frac{\partial N_j}{\partial z}\mathrm{d}\Gamma$ for all $i, j = 1, \dots, n$.
We can write Equation (7.40) as one system of matrix-vector multiplication

$$M^{t}\boldsymbol{\theta}_t + M\boldsymbol{\theta} = \boldsymbol{f}, \tag{7.41}$$

where

$$M^t = \begin{bmatrix} \emptyset & \emptyset & \emptyset & \emptyset & \emptyset \\ \emptyset & \frac{\gamma_w}{K_s}A & \frac{\gamma_w}{K_s}p\beta A & \emptyset & \emptyset \\ \emptyset & \frac{\gamma_w}{K_s}A & \frac{\gamma_w}{K_s}p\beta A & \emptyset & \emptyset \\ \emptyset & \emptyset & \emptyset & \emptyset & \emptyset \\ \emptyset & \emptyset & \emptyset & \emptyset & \emptyset \end{bmatrix} \in \mathbb{R}^{5n\times 5n}, \quad M = \begin{bmatrix} \mu\,(B-SD) & \emptyset & \emptyset & \emptyset & \emptyset \\ -\mu SC & (\lambda+2\mu)\,B & -SD & \emptyset & \emptyset \\ \emptyset & \emptyset & B & \emptyset & \emptyset \\ D-\frac{1}{2}SA & C & \emptyset & B & \emptyset \\ -C & D & \emptyset & \emptyset & (B-SD) \end{bmatrix} \in \mathbb{R}^{5n\times 5n},$$

$$\boldsymbol{\theta} = \begin{bmatrix} \bar{\boldsymbol{w}} \\ \bar{\boldsymbol{\epsilon}} \\ \bar{\boldsymbol{P}} \\ \bar{\boldsymbol{u}}^x \\ \bar{\boldsymbol{u}}^z \end{bmatrix} \in \mathbb{R}^{5n}, \boldsymbol{\theta}_t = \begin{bmatrix} \frac{\partial \bar{\boldsymbol{w}}}{\partial t} \\ \frac{\partial \bar{\boldsymbol{\epsilon}}}{\partial t} \\ \frac{\partial \bar{\boldsymbol{P}}}{\partial t} \\ \frac{\partial \bar{\boldsymbol{u}}^x}{\partial t} \\ \frac{\partial \bar{\boldsymbol{u}}^z}{\partial t} \end{bmatrix} \in \mathbb{R}^{5n}, \quad \boldsymbol{f} = \begin{bmatrix} \mathbf{0} \\ \mathbf{0} \\ \mathbf{0} \\ -\mathbf{F}^{xz} \\ \mathbf{0} \end{bmatrix} \in \mathbb{R}^{5n}. \tag{7.42}$$

Note that the Neumann boundary conditions are included. The Dirichlet boundary conditions will be included after time discretisation.

7.2. Discretisation in time

For discretising the final FEM model given by Equation (7.41) we use the Backward-Euler method like we did for Biot's model. This method is an implicit method which is needed, since some of the governing equations of the new model are not time dependent but the equations are all coupled. Recall that after applying the Backward-Euler method given by Equation (4.28) to Equation (7.41) and assuming that $\left(M^t + \Delta t M\right)$ is invertible, we get that

$$\boldsymbol{\theta}^{k+1} = \left(M^t + \Delta t M\right)^{-1}\left(M^t \boldsymbol{\theta}^k + \Delta t \boldsymbol{f}^{k+1}\right),$$

where $M^t, M, \boldsymbol{\theta}$ and $\boldsymbol{f}$ are given by Equation (7.42), Δt is the time step and k means the number of steps in time.

The Dirichlet boundary conditions are included by setting the corresponding rows to zero of matrices $\left(M^t + \Delta t M\right)$ and M^t, and the right entry in these rows of matrix M to one and of the right-hand side vector to the Dirichlet value.

8

Solving the numerical model of Van Damme and Den Ouden - Van der Horst (2D)

In this chapter, the solutions to the numerical model described in 7 are solved using two different sets of boundary conditions. Like in Biot's model we assume that $\omega(x,z) = 0$ for all $x,z \in [0,L]x[-Z,0]$. We recall that this can be proven analytically under the assumption that the influence of the acceleration terms are negligible [4].

8.1. Numerical model to solve

Assuming $\omega = 0$, we get the following discretisation in space model

$$\begin{cases} \frac{\gamma_w}{K_s} A\bar{\boldsymbol{\epsilon}}_t + \frac{\gamma_w}{K_s} p\beta A\bar{\boldsymbol{P}}_t + (\lambda + 2\mu)\, B\bar{\boldsymbol{\epsilon}} - SD\bar{\boldsymbol{P}} & = 0 \\ \frac{\gamma_w}{K_s} A\bar{\boldsymbol{\epsilon}}_t + \frac{\gamma_w}{K_s} p\beta A\bar{\boldsymbol{P}}_t + B\bar{\boldsymbol{P}} & = 0 \\ B\bar{\boldsymbol{u}}^x + C\bar{\boldsymbol{\epsilon}} & = -\boldsymbol{F}^{xz} \\ (B - SD)\,\bar{\boldsymbol{u}}^z + D\bar{\boldsymbol{\epsilon}} & = 0 \end{cases}, \tag{8.1}$$

where $A_{ij} = \int_\Omega N_i N_j \mathrm{d}\Omega$, $B_{ij} = \int_\Omega \nabla N_i \cdot \nabla N_j \mathrm{d}\Omega$, $C_{ij} = \int_\Omega N_i \frac{\partial N_j}{\partial x} \mathrm{d}\Omega$, $D_{ij} = \int_\Omega N_i \frac{\partial N_j}{\partial z} \mathrm{d}\Omega$, $SD_{ij} = \int_{\mathrm{d}\Omega_3} N_i \frac{\partial N_j}{\partial z} \mathrm{d}\Gamma$ for all $i,j = 1,\dots,n$.

After discretising system of equations (8.1) also in time, the system can be written in the following matrix-vector multiplication form

$$\boldsymbol{\theta}^{k+1} = \left(M^t + \Delta t M\right)^{-1} \left(M^t \boldsymbol{\theta}^k + \Delta t \boldsymbol{f}^{k+1}\right),$$

where

$$M^t = \begin{bmatrix} \frac{\gamma_w}{K_s} A & \frac{\gamma_w}{K_s} p\beta A & \emptyset & \emptyset \\ \frac{\gamma_w}{K_s} A & \frac{\gamma_w}{K_s} p\beta A & \emptyset & \emptyset \\ \emptyset & \emptyset & \emptyset & \emptyset \\ \emptyset & \emptyset & \emptyset & \emptyset \end{bmatrix} \in \mathbb{R}^{4n \times 4n}, \quad M = \begin{bmatrix} (\lambda + 2\mu)\, B & -SD & \emptyset & \emptyset \\ \emptyset & B & \emptyset & \emptyset \\ C & \emptyset & B & \emptyset \\ D & \emptyset & \emptyset & (B - SD) \end{bmatrix} \in \mathbb{R}^{4n \times 4n},$$

$$\boldsymbol{\theta} = \begin{bmatrix} \bar{\boldsymbol{\epsilon}} \\ \bar{\boldsymbol{P}} \\ \bar{\boldsymbol{u}}^x \\ \bar{\boldsymbol{u}}^z \end{bmatrix} \in \mathbb{R}^{4n}, \boldsymbol{\theta}_t = \begin{bmatrix} \frac{\partial \bar{\boldsymbol{\epsilon}}}{\partial t} \\ \frac{\partial \bar{\boldsymbol{P}}}{\partial t} \\ \frac{\partial \bar{\boldsymbol{u}}^x}{\partial t} \\ \frac{\partial \bar{\boldsymbol{u}}^z}{\partial t} \end{bmatrix} \in \mathbb{R}^{4n}, \quad \boldsymbol{f} = \begin{bmatrix} \boldsymbol{0} \\ \boldsymbol{0} \\ -\boldsymbol{F}^{xz} \\ \boldsymbol{0} \end{bmatrix} \in \mathbb{R}^{4n}.$$

Note that by assuming $\omega = 0$, we have a four equations and four variables instead of five. This is computational more efficient. In the next two sections are two different sets of boundary conditions for which we will solve the system above.

We found out that we also need a boundary condition at $z = 0$ for u_z, namely $\frac{\partial u_z}{\partial z} = \epsilon - \frac{\partial u_x}{\partial x}$. Otherwise the relation between ϵ and the displacements is not satisfied. However, this condition must hold by definition. Therefore, adding this boundary condition to the ones we already had is not really an extra or new boundary condition.

We will now define some terms we used for discretising with Finite-Element Method. These are the same as for Biot's model. So the geometric maps ϕ_i, $i = 1, \dots, m$ are defined by Equation (5.3).

We use piece-wise linear basis-functions in both x- and z-directions which is of degree 1 and smoothness 0 in both x- and z-directions, say $p_x = p_z = 1$ and $k_x = k_z = 0$, respectively, denoted by N_j, $j = 1, \dots, (p_x + 1)(p_z + 1)$. These basis element functions $N_j|_{\Omega_i}$ are again given by (5.4) for $i = 1, \dots, m$ and $j = 1, \dots, (p_x + 1)(p_z + 1)$.

Furthermore, for integration of a subdomain we use again 50×50 integration points, the time step is chosen as $\Delta t = 0.01$ and space steps are chosen as $\Delta x = \Delta z = 0.04$. We choose these parameter such that the computation time would be reasonable which is approximately 1.5 minutes when $t_{textend} = 2.25$. For accuracy we could decrease the step in space and decrease the step in time. However, this requires an more efficient code and better equipment for computation. We note that since the computation time of the new model is less than the computation time of Biot's model, less improvements in the code for the new model and in equipment have to be made to achieve good accuracy within reasonable computation time. Furthermore, we found that the numerical solutions behave like the analytical solution by Van Damme and Den Ouden-van der Horst. In Appendix B, we have added the analytical solutions for the volumetric strain, water pressure, vertical displacement and shear stress at $t = 2.25$ s. Note that there is a relatively small difference visible for the vertical displacement and the stresses.

The porosity, Poisson ratio, hydraulic conductivity, the shear modulus and specific weight are given by Table 5.1. The compressibility parameter β is again determined by using Equation (5.5). The parameters of Equation (5.5) are given by Table 5.2. Since, for a saturation degree of one, the compressibility parameter is practically zero and completely incompressible water would have a compressibility parameter of zero by definition, we will use zero in case of incompressible water.

We recall that λ and μ are given by Equation (2.5). At last, we set $n_x = 1$ and $n_z = 2$, i.e. $\bar{\Omega} = [0, 1] \times [-2, 0]$. Lastly, we set the stopping time t_{end} equal to 2.25 seconds at which the results will be shown.

In the next two sections we will define some sets of boundary conditions. Boundary conditions N-II is the one used in the computations in the previous sections. Boundary conditions N-I similar to N-II, only the third boundary condition at $z = 0$ of set N-I is the integration of the third boundary condition of set N-II with the integration constant being equal to zero [4]. For all sets of boundary conditions, we set $F_{zz} = 0.5\gamma_w H \cos\left(2\pi\frac{x}{L}\right)\sin\left(2\pi\frac{t}{T}\right)$, where γ_w [N/m^3] the specific weight of the pore water, H [m] is the wave height, L [m] the length of the wave, T [s] the wave period. We recall that the values of these wave parameters can be found in Table 5.3 and that the function F_{zz} at 2.25 seconds is shown in Figure 5.2. Furthermore, we set again $F_{xz} = 0$ which means that we assume that the shear stress at the surface is negligible.

8.1.1. Boundary conditions N-I

For these set boundary conditions, we first rewrite the equations of volumetric strain and water pressure in matrix vector form:

$$\frac{\gamma_w}{K_s}\begin{bmatrix} \frac{1}{\lambda+2\mu} & \frac{p\beta}{\lambda+2\mu} \\ 1 & p\beta \end{bmatrix}\frac{\partial \boldsymbol{S}}{\partial t} - \begin{bmatrix} 1 & 0 \\ 0 & 1 \end{bmatrix}\frac{\partial^2 \boldsymbol{S}}{\partial x^2} - \begin{bmatrix} 1 & 0 \\ 0 & 1 \end{bmatrix}\frac{\partial^2 \boldsymbol{S}}{\partial z^2} = \boldsymbol{0}, \tag{8.2}$$

where $\boldsymbol{S} = \begin{bmatrix} \epsilon \\ P \end{bmatrix}$, $\frac{\partial \boldsymbol{S}}{\partial t} = \begin{bmatrix} \frac{\partial \epsilon}{\partial t} \\ \frac{\partial P}{\partial t} \end{bmatrix}$, $\frac{\partial^2 \boldsymbol{S}}{\partial x^2} = \begin{bmatrix} \frac{\partial^2 \epsilon}{\partial x^2} \\ \frac{\partial^2 P}{\partial x^2} \end{bmatrix}$ and $\frac{\partial^2 \boldsymbol{S}}{\partial z^2} = \begin{bmatrix} \frac{\partial^2 \epsilon}{\partial z^2} \\ \frac{\partial^2 P}{\partial z^2} \end{bmatrix}$.

Then the eigenvalues of the first matrix are $p\beta + \frac{1}{\lambda+2\mu}$ and 0 [4]. Since the eigenvalue 0 refers to a steady state [4], we will investigate the case for the other eigenvalue. Then according to [4] Equation (8.2) is now given by

$$\frac{\gamma_w}{K_s}\left(p\beta + \frac{1}{\lambda + 2\mu}\right)\frac{\partial S}{\partial t} - \frac{\partial^2 S}{\partial x^2} - \frac{\partial^2 S}{\partial z^2} = 0, \tag{8.3}$$

where $\epsilon = \frac{S}{\lambda+2\mu}$ and $P = S$. So now we can determine two variables by solving one one-dimensional equation which is computational more efficient. Note that by Equation (8.3) the vertical and horizontal momentum balance equations are automatically satisfied by the latter relation between ϵ, P and S. Furthermore, note that the boundary conditions regarding ϵ and P given by Equations (6.16), (6.17) and (6.18) can be rewritten into terms of S without contradiction.

Assuming $\omega = 0$, we define boundary conditions N-I as

$$\text{for } z = 0: \begin{cases} -2\mu\frac{\partial u_x}{\partial z} & = F_{xz} \\ S & = F_{zz} \\ \frac{\partial u_z}{\partial z} & = \epsilon - \frac{\partial u_x}{\partial x} \end{cases},$$
$$\text{for } z = -n_z: \left\{u_z = \frac{\partial u_x}{\partial z} = \frac{\partial S}{\partial z} \quad = 0\right.,$$
$$\text{and for } x = 0 \text{ and } x = n_x: \left\{u_x = \frac{\partial u_z}{\partial x} = \frac{\partial S}{\partial x} \quad = 0\right..$$

8.1.2. Boundary conditions N-II

Assuming $\omega = 0$, we define boundary conditions N-II as

$$\text{for } z = 0: \begin{cases} -2\mu\frac{\partial u_x}{\partial z} & = F_{xz} \\ P & = F_{zz} \\ (\lambda + 2\mu)\frac{\partial \epsilon_{\text{vol}}}{\partial z} - \frac{\partial P}{\partial z} & = 0 \\ \frac{\partial u_z}{\partial z} & = \epsilon - \frac{\partial u_x}{\partial x} \end{cases},$$
$$\text{for } z = -n_z: \left\{\omega = u_z = \frac{\partial u_x}{\partial z} = \frac{\partial P}{\partial z} = \frac{\partial \epsilon_{\text{vol}}}{\partial z} = 0\right.,$$
$$\text{and for } x = 0 \text{ and } x = n_x: \left\{\omega = u_x = \frac{\partial u_z}{\partial x} = \frac{\partial P}{\partial x} = \frac{\partial \epsilon_{\text{vol}}}{\partial x} \quad = 0\right..$$

8.2. Solution to numerical model

In this section we assume that the water is slightly compressible and set $\beta = 4.05 \cdot 10^{-8}$. The solutions to completely incompressible water, i.e. $\beta = 0.5 \cdot 10^{-9}$ following Equation (5.5), we get approximately the same results in two dimensions. So there are no differences in behavior near the surface which were noticeable when zoomed in for the new model. This can be expected since $4.05 \cdot 10^{-8}$ is already close to $0.5 \cdot 10^{-9}$. Even when we increase the compressibility to $\beta = 10^{-6}$, no changes in behaviour are noticeable. Therefore, we show the results for $\beta = 4.05 \cdot 10^{-8}$ like Biot's model.

In Figures 8.1, 8.2 and 8.3 the solutions for $\epsilon_{\text{vol}}, P, u_x$ and u_z, and their derivatives with respect to x and z using boundary conditions N-I are shown. In Figure 8.4 also the vorticity, effective stress, volume balance equation (in form of the weak form of the volumetric strain equation given by Equation (7.17)), and shear stress are shown for boundary conditions N-I. In Figures 8.5, 8.6 and 8.7 the solutions for $\epsilon_{\text{vol}}, P, u_x$ and u_z, and their derivatives with respect to x and z using boundary conditions N-II are shown. In Figure 8.8 also the vorticity, effective stress, volume balance equation and shear stress are shown for boundary conditions N-II.

We recall that when checking whether the volume is conserved, we are actually checking whether the volumetric strain equation given by Equation (6.12) is satisfied. The reason for this is that in Biot's model the volumetric equation is not part of the governing equations and is thus not automatically satisfied while the volume is only conserved if the solutions to the momentum equations are also solutions to the storage equation (i.e. pressure equation) given by Equation (6.12) and the volumetric strain equation given by Equation (6.12). Therefore, when we say that the volume balance is zero, we mean that

the volumetric strain equation is satisfied which results again in the volume being conserved (volume balance).

Then we find that the results to the new model using boundary conditions N-I and N-II give very similar results. The only difference is a relatively small constant when looking closely at the relation between the volumetric strain and the dynamic water pressure due to integration. Comparing Figures 8.1 and 8.5 does not show this very clearly. In other words, using boundary conditions N-I we have $(\lambda + 2\mu)\epsilon = P$ while using boundary conditions N-II we have $(\lambda + 2\mu)\epsilon \approx P - 1.4 \cdot 10^3$. Notice that they differ a constant at the surface and thus the derivatives with respect to x and z of both equations are the same, i.e. $(\lambda + 2\mu)\frac{\partial \epsilon}{\partial N-I} = \frac{\partial P}{\partial N-I}$ for $i = x, z$ holds on whole domain when using boundary conditions N-I and N-II. Therefore, the results of the displacements are exactly the same, since there equations depend on the derivative of ϵ with respect to x or z.

When looking at the relation between volumetric strain and the displacements, we find that approximately the relation $\epsilon = \frac{\partial u_x}{\partial x} + \frac{\partial u_z}{\partial z}$ holds when using boundary conditions N-I and N-II. Recall that the relation between the vorticity and the displacements is given by $\omega = \frac{\partial u_x}{\partial z} - \frac{\partial u_z}{\partial x}$ and that we assumed $\omega = 0$. Therefore, we want to find that $\frac{\partial u_x}{\partial z} - \frac{\partial u_z}{\partial x} = 0$. In Figures 8.4 and 8.8 it can be seen that $\frac{\partial u_x}{\partial z} - \frac{\partial u_z}{\partial x} \approx 0$. The error made is probably due to the Finite-Element Method itself and can decrease when increasing the number of subdomains and/or the order and/or smoothness of the finite-element functions. Furthermore, for both boundary conditions sets the volume balance is almost everywhere 0, and the shear stress is indeed zero at the surface $z = 0$. The fact that the solutions do not give exactly the expected solutions is probably due to computational errors of the Finite-Element Method and rounding errors.

Note that the boundary conditions can also be found in Figures 8.1, 8.2 and 8.3 for boundary condition N-I and in Figures 8.5, 8.6 and 8.7 for boundary condition N-II. Indeed, in the right top and bottom subplots of Figures 8.1 and 8.5 one can see that $u_x = 0$ at the left and right boundary and $u_z = 0$ at the bottom boundary and in the left bottom subplot one can see that P is indeed again a cosine in x-direction at the top boundary. Furthermore, in the left bottom subplot one can see that P is indeed a cosine in x-direction at the top boundary. Since we assumed that the pressure downwards is positive pressure and thus negative pressure is a pulling force, the water pressure subplots of the new model agree with the hydrodynamic load shown in Figure 5.2. Since negative z-displacement means displacement downwards in the soil, the solution of the z-displacement behaves like expected as positive pressure causes displacement downwards into the sandy bed. In Figures 8.2 and 8.6 one can also find that $\frac{\partial P}{\partial x} = 0$ and $\frac{\partial \epsilon}{\partial x} = 0$ at $x = 0, L$. In Figures 8.3 and 8.7 one can find that $\frac{\partial u_x}{\partial z} = 0$ at $z = 0, -n_z$, $\frac{\partial P}{\partial z} = 0$ and $\frac{\partial \epsilon}{\partial z} = 0$ at $z = -n_z$

In conclusion, the model using boundary conditions N-I and N-II give similar results, only the value of ϵ differs by a constant in space, especially at the top boundary $z = 0$.

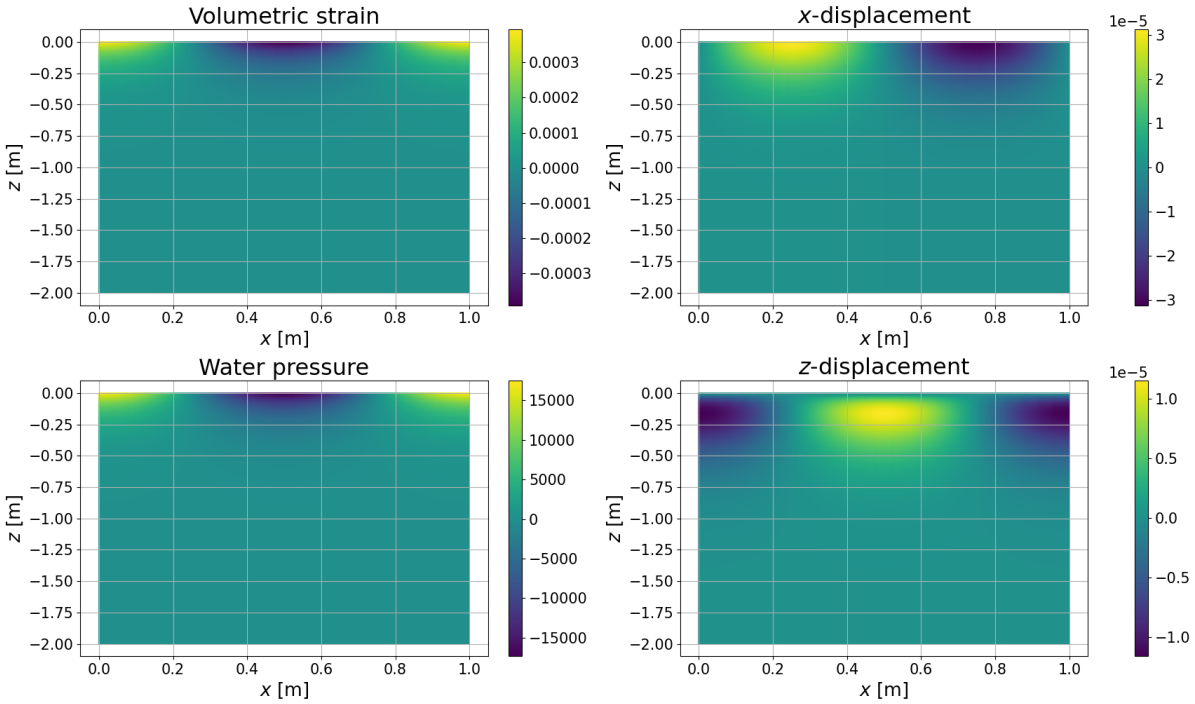

Figure 8.1: Solutions to the new model for ϵ_{vol} [-], P [Pa], u_x [m], u_z [m] at $t_{\text{end}} = 2.25$ s, when water is assumed to be compressible with $\beta = 4.05 \cdot 10^{-8}$ Pa^{-1} and using boundary conditions N-I. In this thesis, a negative pressure is pointing upwards (a pulling force), and a positive pressure is pointing downwards (a pushing force). The soil displacement upwards or to the right is positive and downwards or to the left is negative.

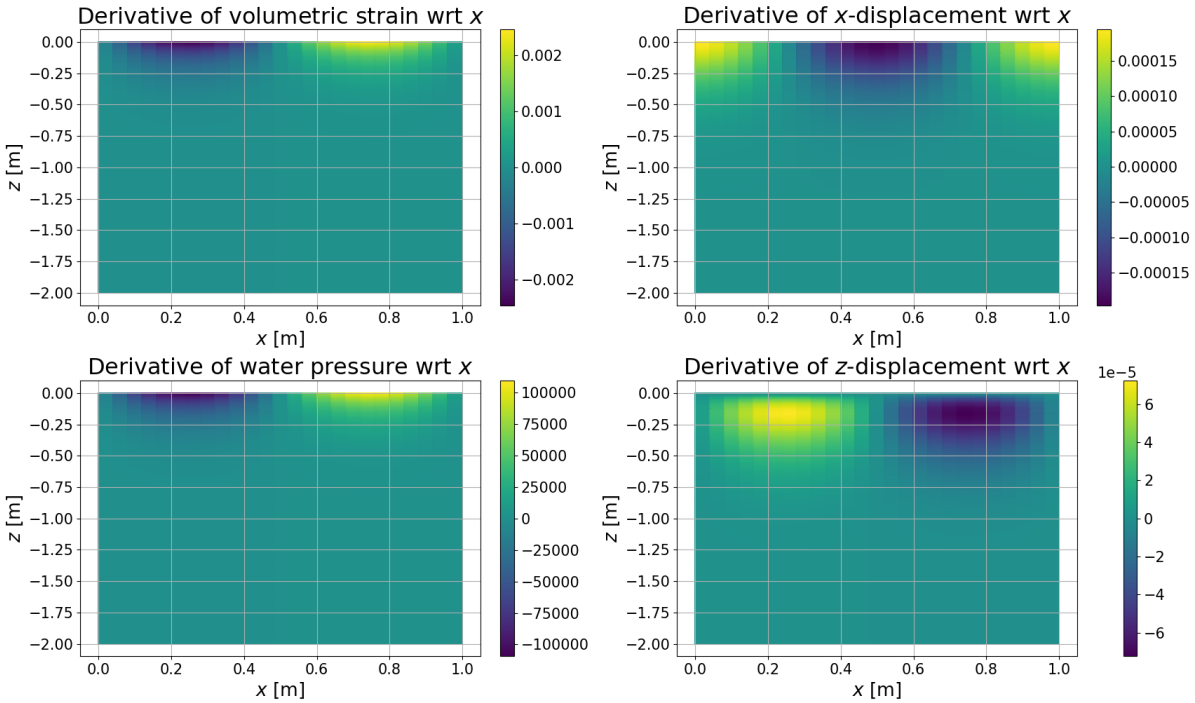

Figure 8.2: Solutions to the new model for $\frac{\partial \epsilon_{\text{vol}}}{\partial x}$ [m^{-1}], $\frac{\partial P}{\partial x}$ [N/m^3], $\frac{\partial u_x}{\partial x}$ [-], $\frac{\partial u_z}{\partial x}$ [-] at $t_{\text{end}} = 2.25$ s, when water is assumed to be compressible with $\beta = 4.05 \cdot 10^{-8}$ Pa^{-1} and using boundary conditions N-I.

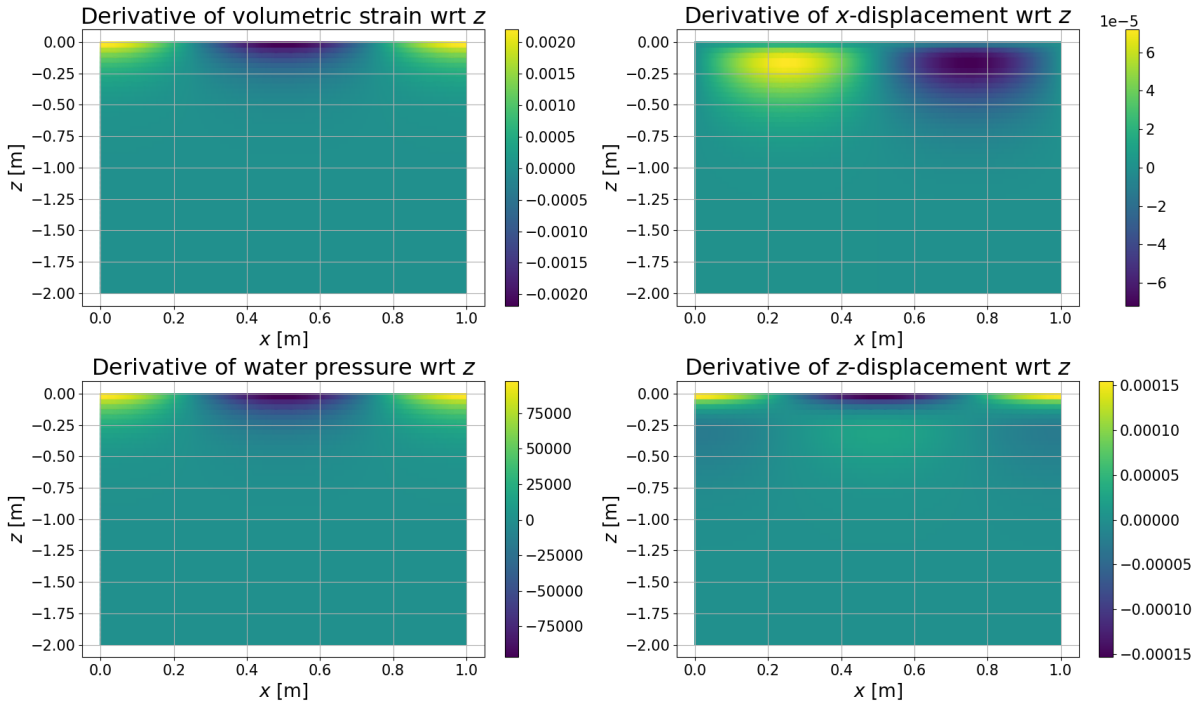

Figure 8.3: Solutions to the new model for $\frac{\partial \epsilon_{\text{vol}}}{\partial z}$ [m^{-1}], $\frac{\partial P}{\partial z}$ [N/m^3], $\frac{\partial u_x}{\partial z}$ [-], $\frac{\partial u_z}{\partial z}$ [-] at $t_{\text{end}} = 2.25$ s, when water is assumed to be compressible with $\beta = 4.05 \cdot 10^{-8}$ Pa^{-1}and using boundary conditions N-I.

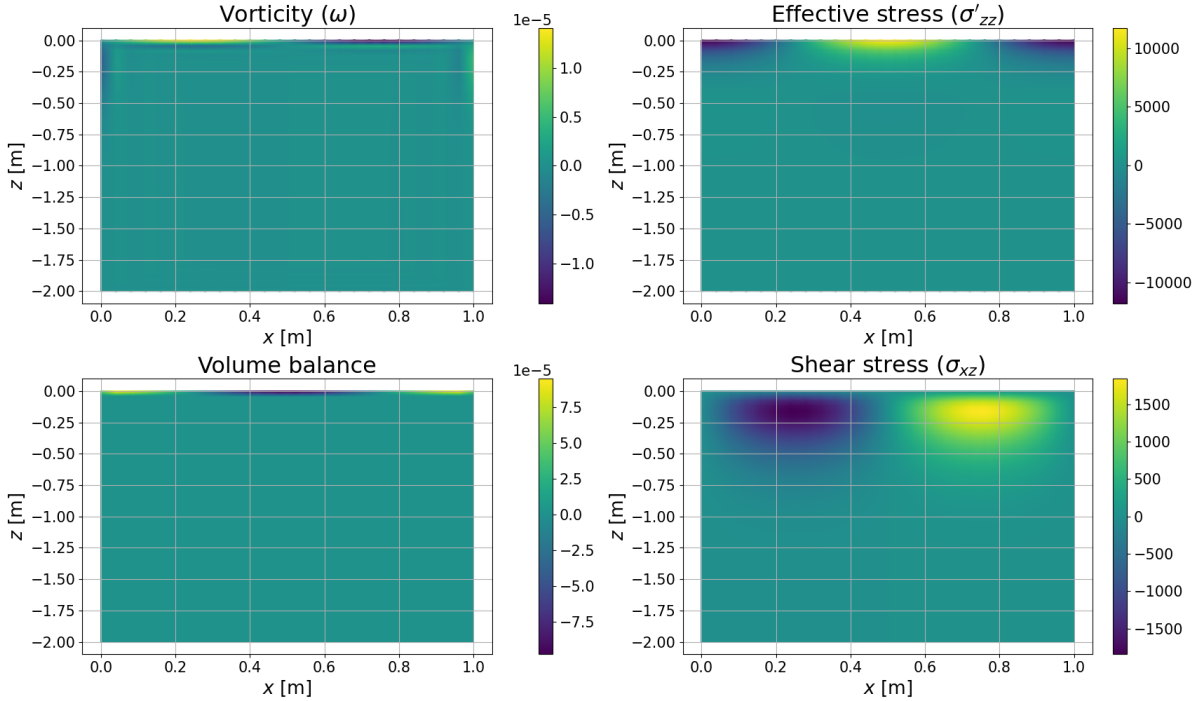

Figure 8.4: Solutions to the new model for ω [-], σ'_{zz} [Pa], σ_{xz} [Pa] and volume balance at $t_{\text{end}} = 2.25$ s, when water is assumed to be compressible with $\beta = 4.05 \cdot 10^{-8}$ Pa^{-1} and using boundary conditions N-I. The vorticity is expected to be zero. The volume balance is calculated using the weak form of the volumetric strain equation, which is given by Equation (7.17), and is satisfied if it equals 0 everywhere on the domain and its boundaries.

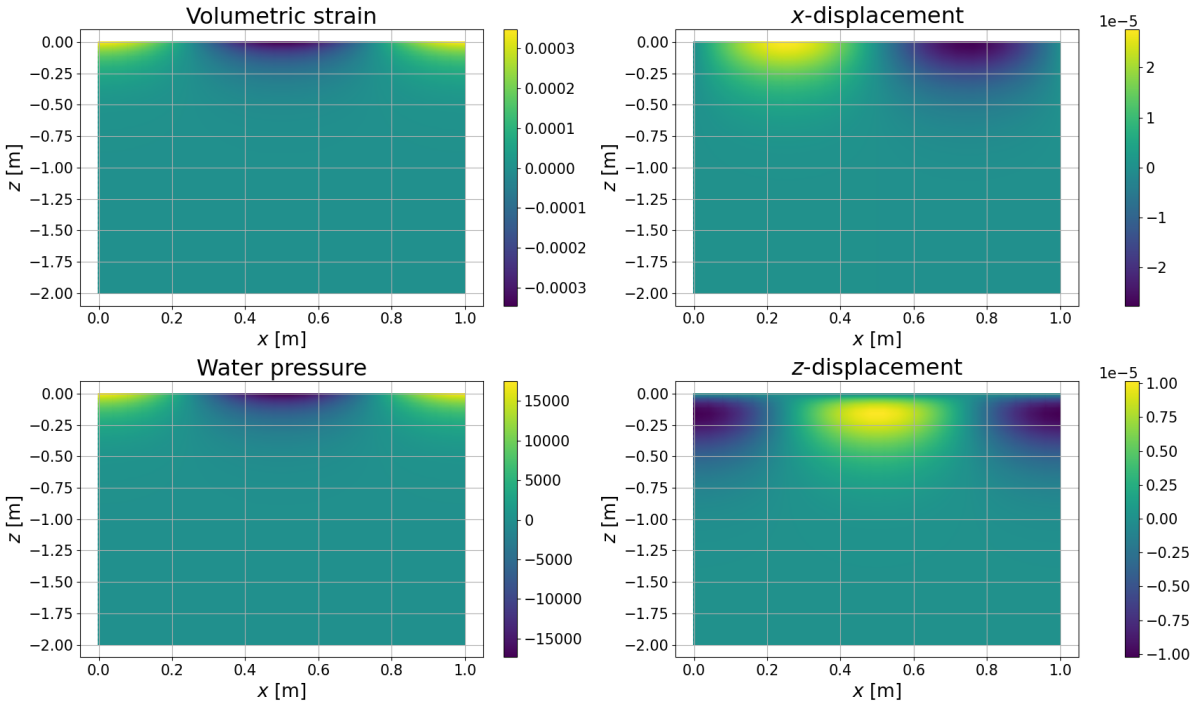

Figure 8.5: Solutions to the new model for ϵ_{vol} [-], P [Pa], u_x [m], u_z [m] at $t_{\text{end}} = 2.25$ s, when water is assumed to be compressible with $\beta = 4.05 \cdot 10^{-8}$ Pa^{-1} and using boundary conditions N-II. In this thesis, a negative pressure is pointing upwards (a pulling force), and a positive pressure is pointing downwards (a pushing force). The soil displacement upwards or to the right is positive and downwards or to the left is negative.

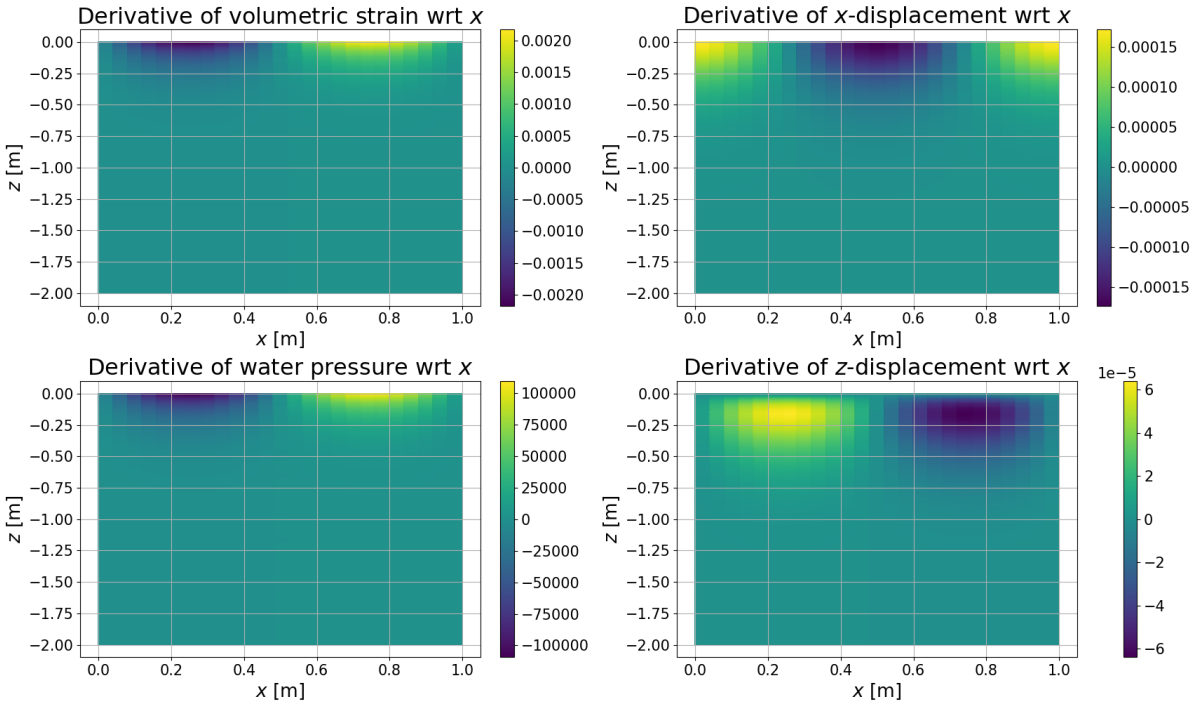

Figure 8.6: Solutions to the new model for $\frac{\partial \epsilon_{\text{vol}}}{\partial x}$ [m^{-1}], $\frac{\partial P}{\partial x}$ [N/m^3], $\frac{\partial u_x}{\partial x}$ [-], $\frac{\partial u_z}{\partial x}$ [-] at $t_{\text{end}} = 2.25$ s, when water is assumed to be compressible with $\beta = 4.05 \cdot 10^{-8}$ Pa^{-1} and using boundary conditions N-II.

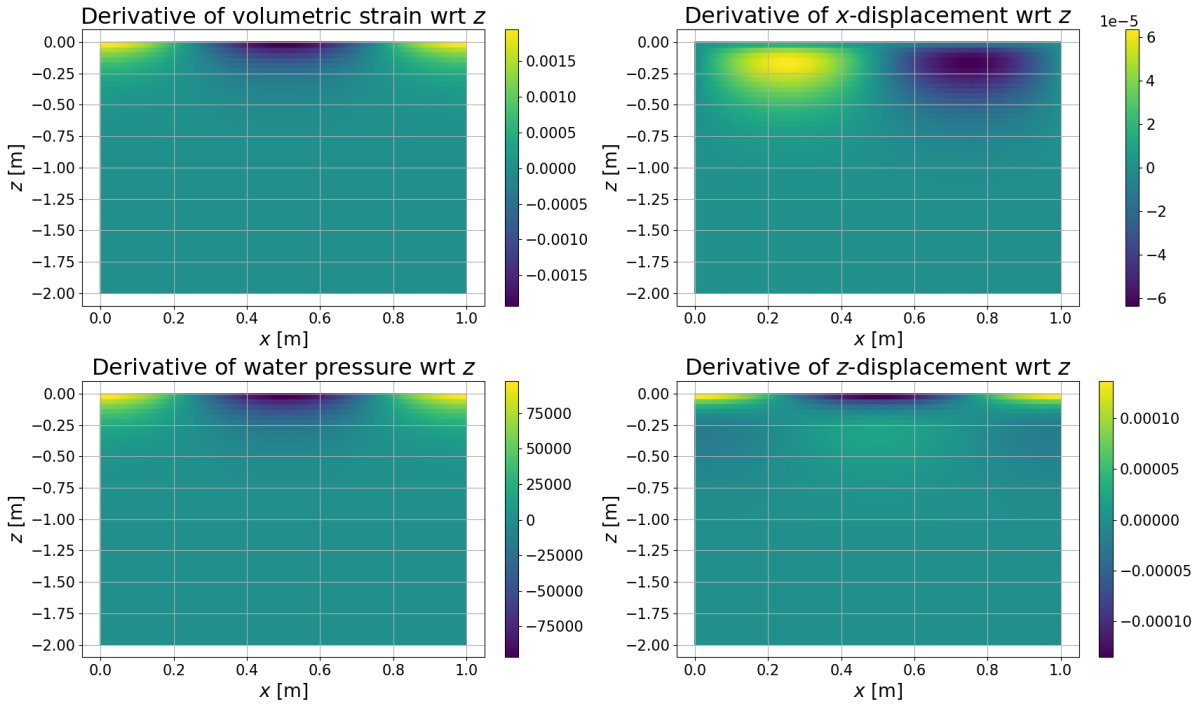

Figure 8.7: Solutions to the new model for $\frac{\partial \epsilon_{\text{vol}}}{\partial z}$ [m^{-1}], $\frac{\partial P}{\partial z}$ [N/m^3], $\frac{\partial u_x}{\partial z}$ [-], $\frac{\partial u_z}{\partial z}$ [-] at $t_{\text{end}} = 2.25$ s, when water is assumed to be compressible with $\beta = 4.05 \cdot 10^{-8}$ Pa^{-1}and using boundary conditions N-II.

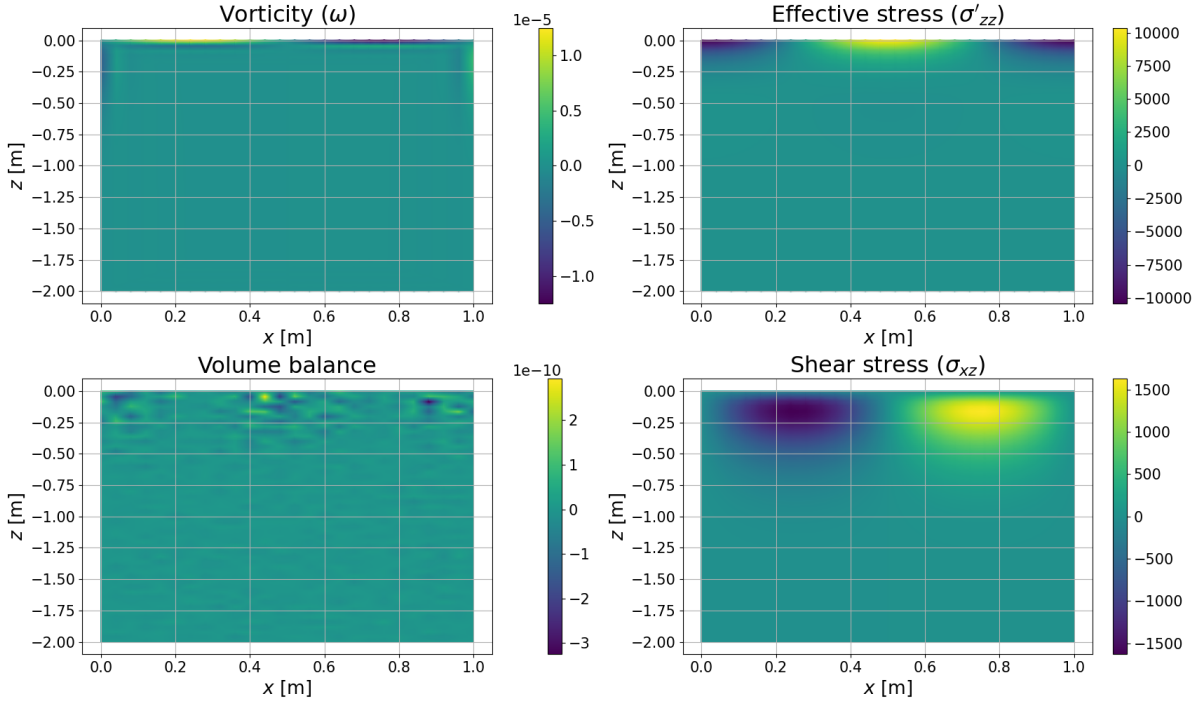

Figure 8.8: Solutions to the new model for ω [-], σ'_{zz} [Pa], σ_{xz} [Pa] and volume balance at $t_{\text{end}} = 2.25$ s, when water is assumed to be compressible with $\beta = 4.05 \cdot 10^{-8}$ Pa^{-1} and using boundary conditions N-II. The vorticity is expected to be zero. The volume balance is calculated using the weak form of the volumetric strain equation, which is given by Equation (7.17), and is satisfied if it equals 0 everywhere on the domain and its boundaries.

9

Comparison of Biot's model and New model

A main difference between the models lies in their boundary conditions at the surface. Biot's model aligns with the effective stress principle of Terzaghi which states that the total stress acting on a porous medium has to be equal to the pore water pressures added to the effective stresses [2, 3, 4] whereby the effective stresses are set to zero. However, it turns out that the volume and momentum balance equations are not satisfied everywhere. On the other hand, the new model is based on maintaining valid momentum balance equations within the computational domain and its boundaries but does not satisfy the effective stress principle of Terzaghi at the surface in case of hydrodynamic load [4]. The new model also has an extra governing equation, namely the volumetric strain equation which we also referred to as (a form of) the volume balance equation.

In this section we want to determine why the results of Biot's model do not satisfy the volume and momentum balance equations and do not satisfy all (boundary) conditions. A reason could be because of the equations of the model and/or the boundary conditions. Therefore, we will determine the results for the new model, while setting the effective stress equal to zero at $z = 0$ instead of the vertical momentum balance equation at $z = 0$. We will also determine the results of Biot's model while setting the vertical momentum balance equation at $z = 0$ instead of the effective stress equal to zero at $z = 0$. We assume that the water is slightly compressible and set $\beta = 4.05 \cdot 10^{-8}$. The two-dimensional solutions to completely incompressible water, i.e. $\beta = 0$, are really similar to the case with $\beta = 4.05 \cdot 10^{-8}$ with only some minor differences in behavior near the surface, which are only noticeable when zoomed, in for Biot and no significant differences in behavior are found for the new model. Therefore, again we only show the results when setting $\beta = 4.05 \cdot 10^{-8}$. We also set the stopping time $t_{\text{end}} := 2.25$.

When setting the effective stress equal to zero at $z = 0$ instead of the vertical momentum balance equation at $z = 0$ in the new model, we find in Figures 9.1, 9.2 and 9.3 that now the relation between ϵ and P, given by the vertical and horizontal momentum balance equation, is not satisfied. However, the other conditions seem to be satisfied, i.e. $\omega = 0$ everywhere, $\sigma_{xz} = 0$ at $z = 0$ and the volume balance equation seem to hold. This is shown in Figure 9.4. However, note that the values for the volumetric strain and displacements are very small and could be considered as zero which is the steady state of Biot's model. Therefore, the values of these solutions are expected to be small but in perspective they are still large. Furthermore, movement of the soil is expected after 2.25 seconds as there is still a force acting on the surface.

Since in Biot's model the formula for volumetric strain is first order and thus the vertical momentum balance equation can not easily be used as a boundary condition for the integration of the Galerkin equations, we use the boundary condition $(\lambda + 2\mu)\epsilon = P$ at $z = 0$ which also holds for the new model using boundary conditions N-I. Since our version of Biot's model does not directly use the volumetric strain as variable, we rewrite this latter equation to

$$(\lambda + 2\mu)\left(\frac{\partial u_x}{\partial x} + \frac{\partial u_z}{\partial z}\right) = P, \tag{9.1}$$

and use it as boundary condition for u_z. Since the results hold for all three sets of boundary conditions (with Equation (9.1) instead of the effective stress equal to zero as boundary condition for u_z at $z = 0$) defined for Biot's model, we only show the results for boundary conditions B-II of Biot with Equation (9.1). In Figures 9.5, 9.6, 9.7 we find that the vertical and horizontal momentum balance equations and $(\lambda + 2\mu)\epsilon = P$ hold almost everywhere. When we take a closer look at the surface $z = 0$ it seems there is still some instability but it rapidly converges to the wanted relation between the volumetric strain and water pressure. Also the vorticity is approximately zero everywhere with some oscillation at the surface and the shear stress is found to be closer to zero at $z = 0$ which can be seen in the top left and bottom right subplots of Figure 9.8, respectively. Only the volume balance equation still does not hold which is expected since this equation is not used in Biot's model which is shown in the bottom left subplot of Figure 9.8.

In conclusion, it seems that the numerical discretisation of Biot's model is more unstable than that of the new model. It also seems that the boundary condition $\sigma'_{zz} = 0$ at $z = 0$ tends to give a solution that does not satisfy all assumptions and conditions. The new model with its boundary conditions including the vertical momentum balance equation instead of setting the effective stress equal to zero, gives the results that satisfy our assumptions and conditions most.

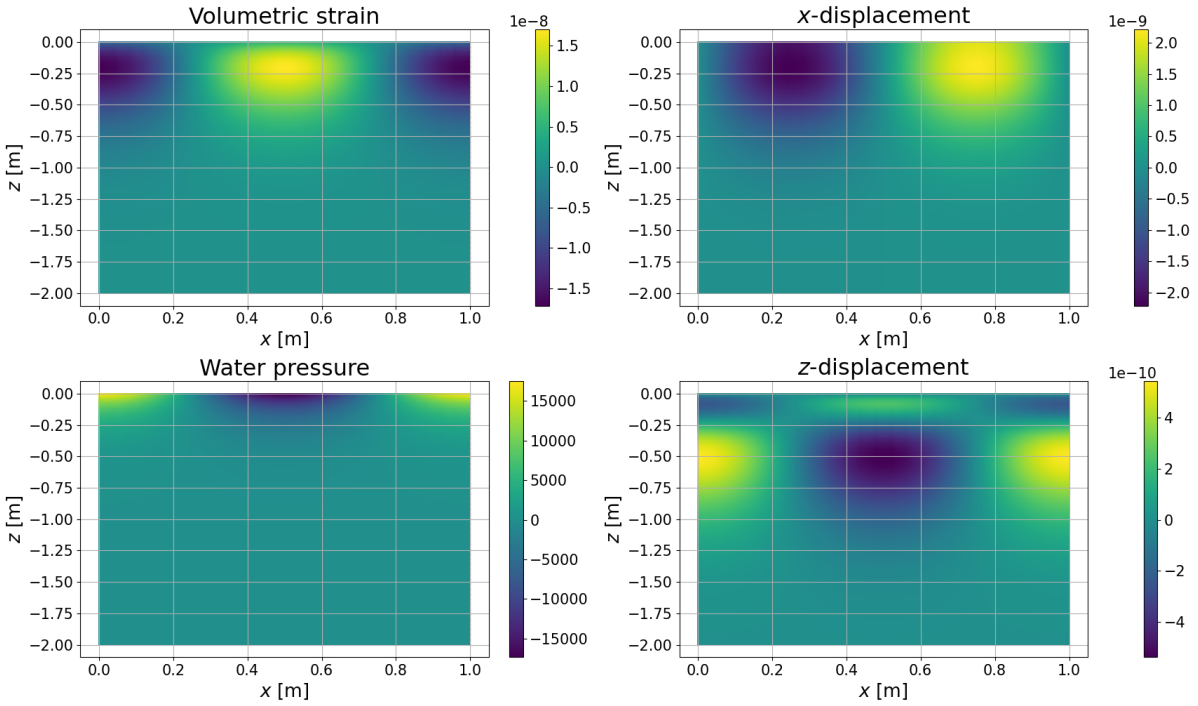

Figure 9.1: Solutions to the new model ϵ_{vol} [-], P [Pa], u_x [m], u_z [m] at $t_{\text{end}} = 2.25$ s, when water is assumed to be compressible with $\beta = 4.05 \cdot 10^{-8}$ Pa^{-1} and using boundary conditions set B-II of Biot's model instead of boundary conditions set N-II of the new model.

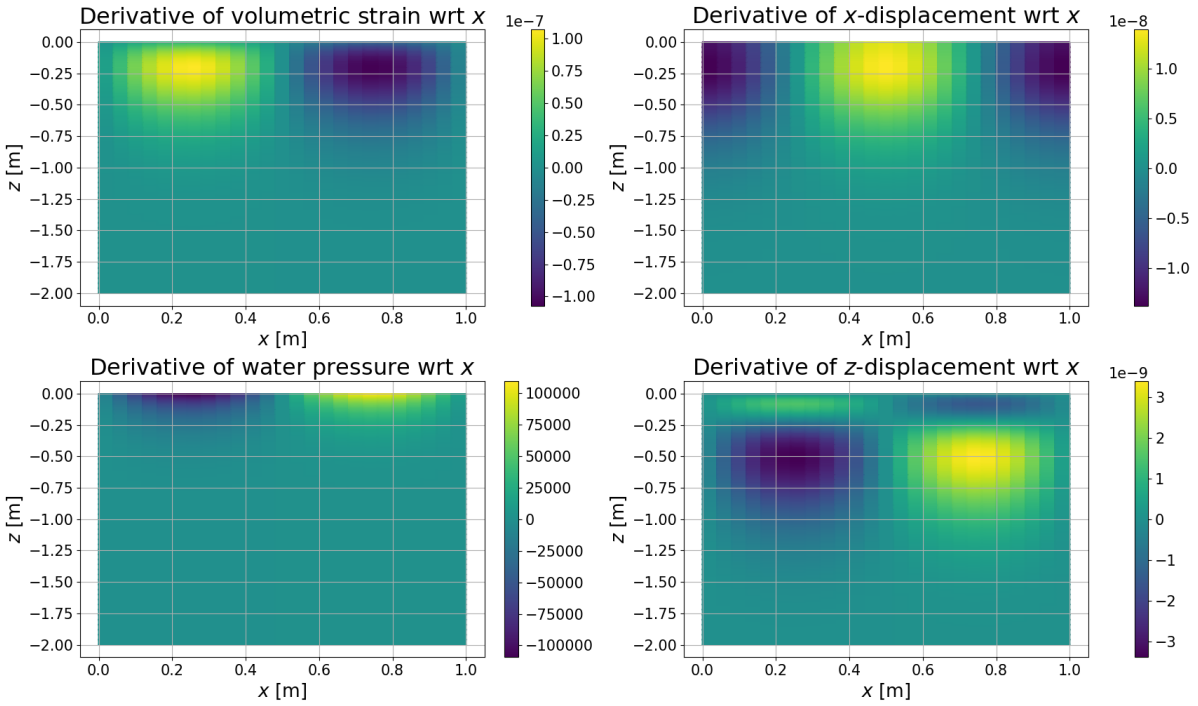

Figure 9.2: Solutions to the new model for $\frac{\partial \epsilon_{\text{vol}}}{\partial x}$ [m^{-1}], $\frac{\partial P}{\partial x}$ [N/m^3], $\frac{\partial u_x}{\partial x}$ [-], $\frac{\partial u_z}{\partial x}$ [-] at $t_{\text{end}} = 2.25$ s, when water is assumed to be compressible with $\beta = 4.05 \cdot 10^{-8}$ Pa^{-1} and using boundary conditions set B-II of Biot's model instead of boundary conditions set N-II of the new model.

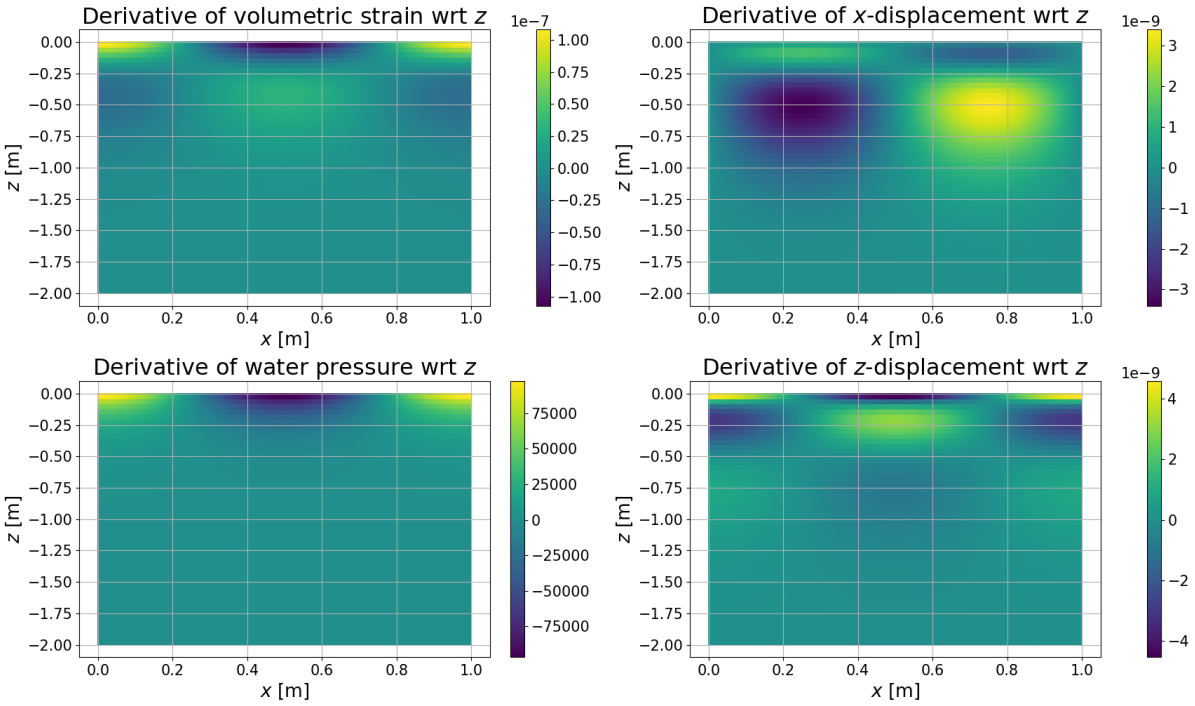

Figure 9.3: Solutions to the new model for $\frac{\partial \epsilon_{\text{vol}}}{\partial z}$ [m^{-1}], $\frac{\partial P}{\partial z}$ [N/m^3], $\frac{\partial u_x}{\partial z}$ [-], $\frac{\partial u_z}{\partial z}$ [-] at $t_{\text{end}} = 2.25$ s, when water is assumed to be compressible with $\beta = 4.05 \cdot 10^{-8}$ Pa^{-1} and using boundary conditions set B-II of Biot's model instead of boundary conditions set N-II of the new model.

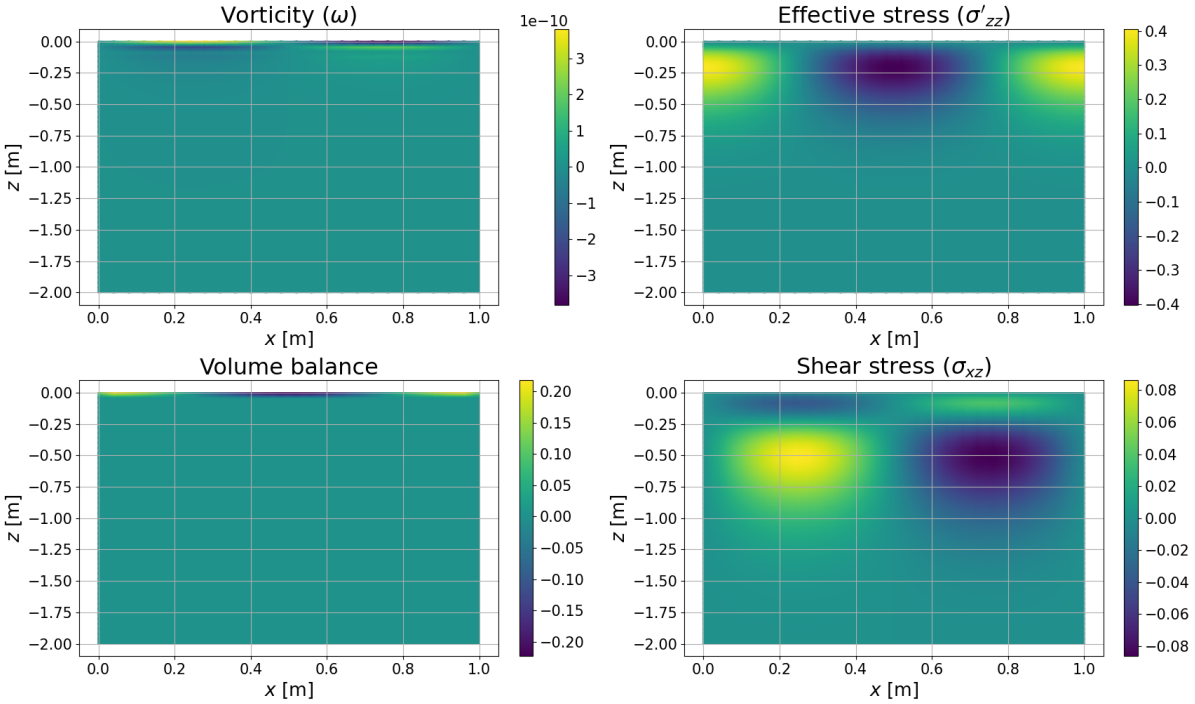

Figure 9.4: Solutions to the new model for ω [-], σ'_{zz} [Pa], σ_{xz} [Pa] and volume balance at $t_{\text{end}} = 2.25$ s, when water is assumed to be compressible with $\beta = 4.05 \cdot 10^{-8}$ Pa^{-1} and using boundary conditions set B-II of Biot's model instead of boundary conditions set N-II of the new model.

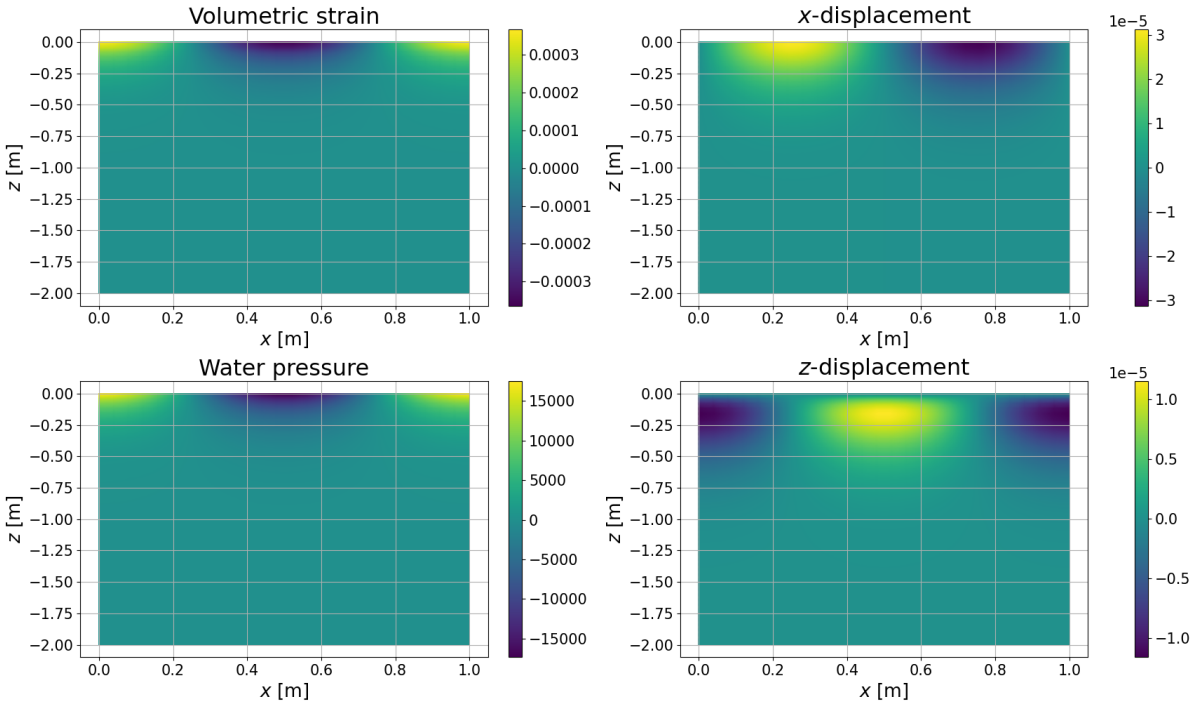

Figure 9.5: Solutions to Biot's model ϵ_{vol} [-], P [Pa], u_x [m], u_z [m] at $t_{\text{end}} = 2.25$ s, when water is assumed to be compressible with $\beta = 4.05 \cdot 10^{-8}$ Pa^{-1} and using boundary conditions set N-II of the new model instead of boundary conditions set B-II of Biot's model.

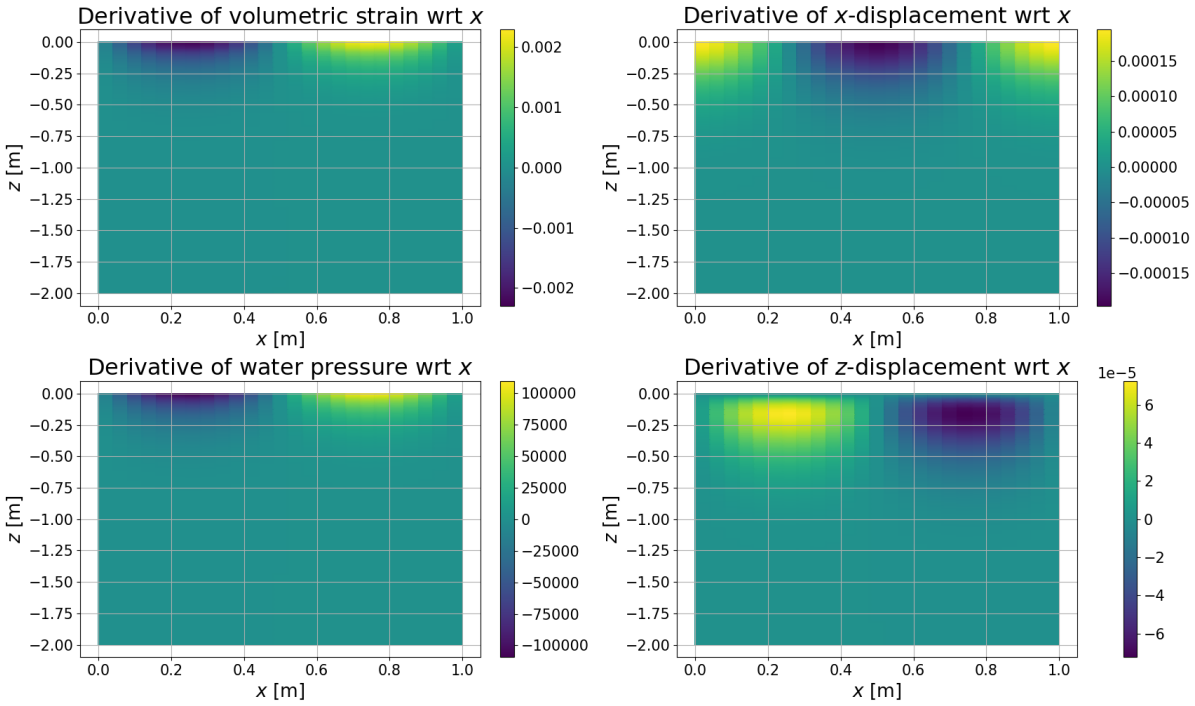

Figure 9.6: Solutions to Biot's model for $\frac{\partial \epsilon_{\text{vol}}}{\partial x}$ [m^{-1}], $\frac{\partial P}{\partial x}$ [N/m^3], $\frac{\partial u_x}{\partial x}$ [-], $\frac{\partial u_z}{\partial x}$ [-] at $t_{\text{end}} = 2.25$ s, when water is assumed to be compressible with $\beta = 4.05 \cdot 10^{-8}$ Pa^{-1} and using boundary conditions set N-II of the new model instead of boundary conditions set B-II of Biot's model.

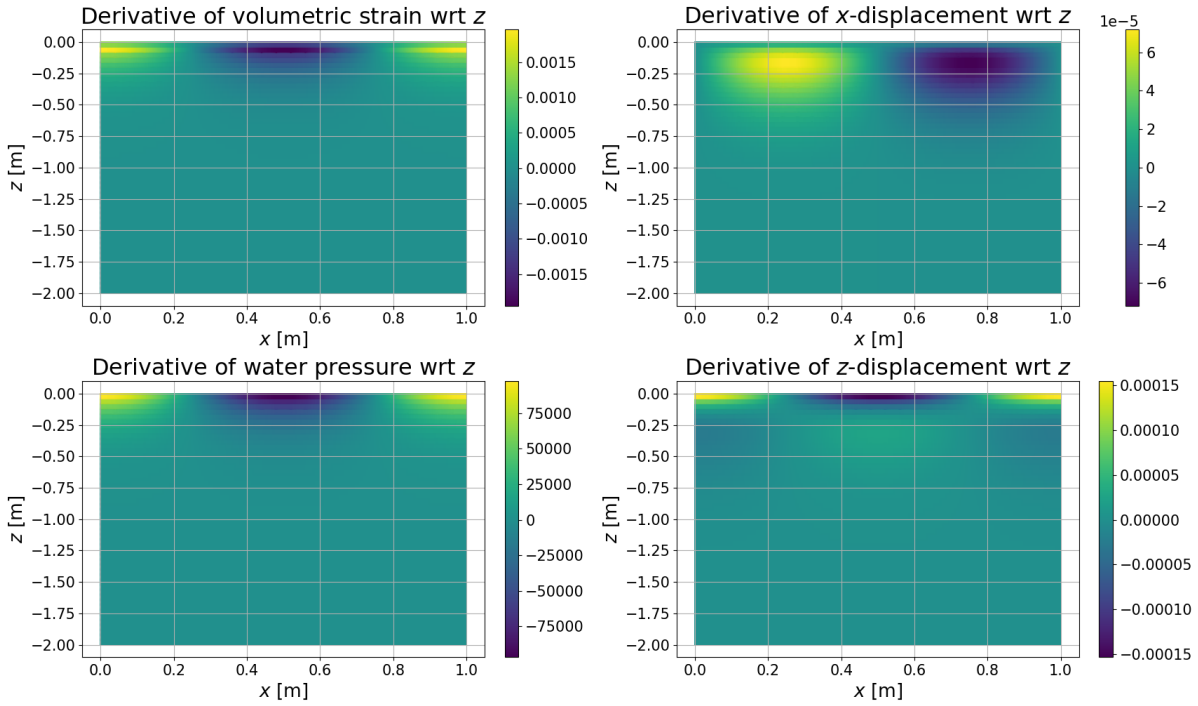

Figure 9.7: Solutions to Biot's model for $\frac{\partial \epsilon_{\text{vol}}}{\partial z}$ [m^{-1}], $\frac{\partial P}{\partial z}$ [N/m^3], $\frac{\partial u_x}{\partial z}$ [-], $\frac{\partial u_z}{\partial z}$ [-] at $t_{\text{end}} = 2.25$ s, when water is assumed to be compressible with $\beta = 4.05 \cdot 10^{-8}$ Pa^{-1} and using boundary conditions set N-II of the new model instead of boundary conditions set B-II of Biot's model.

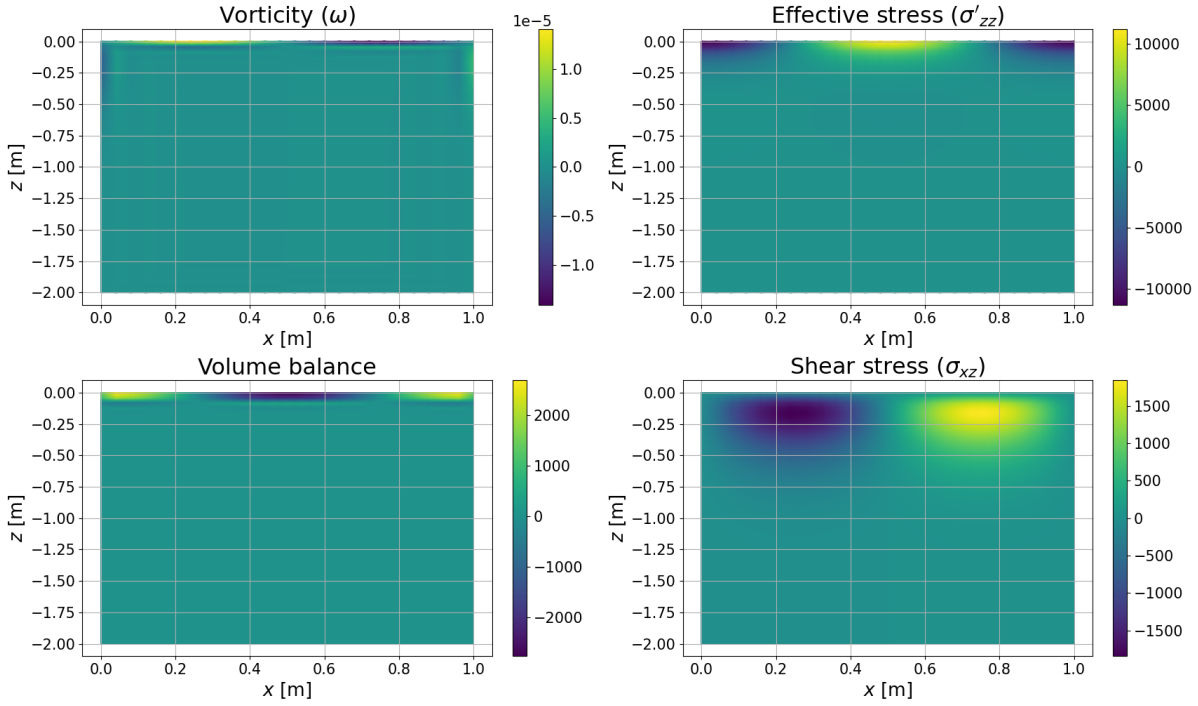

Figure 9.8: Solutions to Biot's model for ω [-], σ'_{zz} [Pa], σ_{xz} [Pa] and volume balance at $t_{\text{end}} = 2.25$ s, when water is assumed to be compressible with $\beta = 4.05 \cdot 10^{-8}$ Pa^{-1} and using boundary conditions set N-II of the new model instead of boundary conditions set B-II of Biot's model.

10

One-dimensional validation of the new model

In this chapter the new model will be compared with two experimental datasets:

1. A dataset obtained from a one-dimensional set up with a vertical cylinder with first a sand deposit of 1.8 metres thick and then 0.2 metres water above the sand.

2. A dataset of the water pressure at a location along the center line of the Twente Canal when a ship passes by.

The validation the new model will happen in one-dimension, since the first experiment is already a set up in one-dimension. Furthermore, the second experiment can be reduced to a one-dimensional problem, because the length of the canal is very long and the impact of the width of the canal on the approximation of the solution in the middle of the width of the Twente canal is expected to be negligible since the ship sails lengthwise. Therefore, we will now derive the one-dimensional version of the new model first. This was also done in our literature report [9].

10.1. Van Damme and Den Ouden - Van der Horst (1D)

Setting all derivatives with respect to x to zero, i.e. $\frac{\partial}{\partial x} = 0$, in the equations of the new model described in Chapter 6 and following a similar approach of numerical discretisation (see also our literature report [9]) we derive the one-dimensional numerical descretisation of the new model to solve, namely

$$\begin{cases} \frac{\gamma_w}{K_s}\frac{\partial \epsilon_{\text{vol}}}{\partial t} - (\lambda + 2\mu)\frac{\partial^2 \epsilon_{\text{vol}}}{\partial z^2} & = -\frac{\gamma_w}{K_s} p\beta \frac{\partial P}{\partial t} \\ \frac{\gamma_w}{K_s} p\beta \frac{\partial P}{\partial t} - \frac{\partial^2 P}{\partial z^2} & = -\frac{\gamma_w}{K_s}\frac{\partial \epsilon_{\text{vol}}}{\partial t} \\ \frac{\partial u_z}{\partial z} & = \epsilon_{\text{vol}} \end{cases}, \text{ for } z \in \Omega \text{ and } t \in \mathbb{T} \tag{10.1}$$

with boundary conditions

$$\begin{cases} P(0,t) & = F_{zz}(t) \\ (\lambda + 2\mu)\,\epsilon_{\text{vol}}(0,t) & = P(0,t) \end{cases}, \quad \begin{cases} u_z(-n_z,t) & = 0 \\ \frac{\partial P(-n_z,t)}{\partial z} & = 0 \\ \frac{\partial \epsilon_{\text{vol}}(-n_z,t)}{\partial z} & = 0 \end{cases}, \text{ for } t \in \mathbb{T} \tag{10.2}$$

and initial conditions

$$\epsilon_{\text{vol}}(z,0) = P(z,0) = u_z(z,0) = 0 \text{ for } z \in \Omega. \tag{10.3}$$

Using the boundary conditions given by (10.2), the weak equations of the new model in one-dimension given by Equation (10.1) can be stated as

$$\begin{cases} -N_i^{\epsilon}(0)\frac{\partial P(0,t)}{\partial z} + \int_{-n_z}^{0} N_i^{\epsilon}\frac{\gamma_w}{K_s}\left[\frac{\partial \epsilon_{\text{vol}}}{\partial t} + p\beta\frac{\partial P}{\partial t}\right] + (\lambda+2\mu)\left(\frac{\partial v^{\epsilon}}{\partial z}\cdot\frac{\partial \epsilon_{\text{vol}}}{\partial z}\right)\mathrm{d}z & = 0 \\ \int_{-n_z}^{0} N_i^{P}\frac{\gamma_w}{K_s}\left[\frac{\partial \epsilon_{\text{vol}}}{\partial t} + p\beta\frac{\partial P}{\partial t}\right] + \left(\frac{\partial v^{P}}{\partial z}\cdot\frac{\partial P}{\partial z}\right)\mathrm{d}z & = 0 \\ \int_{-n_z}^{0} N_i^{u}\frac{\partial u_z}{\partial z}\mathrm{d}z & = \int_{-n_z}^{0} N_i^{u}\epsilon_{\text{vol}}\mathrm{d}z \end{cases}, \quad (10.4)$$

Substituting one-dimensional trial functions into Equation (10.4) we get the following one-dimensional Galerkin equations in matrix-vector form

$$\begin{cases} \frac{\gamma_w}{K_s}A\bar{\boldsymbol{\epsilon}}_t + \frac{\gamma_w}{K_s}p\beta A\bar{\boldsymbol{P}}_t + (\lambda+2\mu)B\bar{\boldsymbol{\epsilon}} - SC\bar{\boldsymbol{P}} & = \boldsymbol{0} \\ \frac{\gamma_w}{K_s}A\bar{\boldsymbol{\epsilon}}_t + \frac{\gamma_w}{K_s}p\beta A\bar{\boldsymbol{P}}_t + B\bar{\boldsymbol{P}} & = \boldsymbol{0} \\ C\bar{\boldsymbol{u}}^{z} & = A\bar{\boldsymbol{\epsilon}} \end{cases}, \quad (10.5)$$

where $A_{i,j} = \int_{-n_z}^{0} N_i N_j \mathrm{d}z, B_{i,j} = \int_{-n_z}^{0} \frac{\partial N_i}{\partial z}\frac{\partial N_j}{\partial z}\mathrm{d}z, C_{i,j} = \int_{-n_z}^{0} N_i \frac{\partial N_j}{\partial z}\mathrm{d}z.$ and $SC_{i,j} = N_i(0)\frac{\partial N_j(0)}{\partial z}$.

We can write Equation (10.5) as two systems of matrix-vector multiplication

$$\begin{cases} M^t\boldsymbol{S}_t + M\boldsymbol{S} & = \boldsymbol{f} \\ C\bar{\boldsymbol{u}}^{z} & = A\bar{\boldsymbol{\epsilon}} \end{cases}, \quad (10.6)$$

where

$$M^t = \begin{bmatrix} \frac{\gamma_w}{K_s}A & \frac{\gamma_w}{K_s}p\beta A \\ \frac{\gamma_w}{K_s}A & \frac{\gamma_w}{K_s}p\beta A \end{bmatrix}, \quad M = \begin{bmatrix} (\lambda+2\mu)B & -SC \\ \emptyset & B \end{bmatrix}, \quad \boldsymbol{S} = \begin{bmatrix} \bar{\boldsymbol{\epsilon}} \\ \bar{\boldsymbol{P}} \end{bmatrix}, \quad \boldsymbol{S}_t = \begin{bmatrix} \frac{\partial \bar{\boldsymbol{\epsilon}}}{\partial t} \\ \frac{\partial \bar{\boldsymbol{P}}}{\partial t} \end{bmatrix}, \quad \boldsymbol{f}(t) = \begin{bmatrix} \boldsymbol{0} \\ \boldsymbol{F}(t) \end{bmatrix}. \quad (10.7)$$

Like in our literature report [9], the Dirichlet boundary conditions are included in the numerical model by setting the corresponding rows of matrices M^t and M to zero and then putting pivots in these same rows of M. Furthermore, setting $F_i = 0$ for $i = 1, \dots, n-1$ and $F_n = F_{zz}$ we get that $\bar{P}_n = F_n = F_{zz}$ and $\bar{u}_0^z = 0$. After applying the time integration given by Equation (4.30) to Equation (10.6) using $M^t, M, \boldsymbol{S}$ and $\boldsymbol{f}$ given by Equation (10.7) and assuming that matrix $\left(M^t + \Delta t M\right)$ and C are invertible like in our literature report [9], we get that

$$\begin{cases} \boldsymbol{S}^{k+1} & = \left(M^t + \Delta t M\right)^{-1}\left(M^t\boldsymbol{S}^k + \Delta t\boldsymbol{f}^{k+1}\right) \\ \bar{\boldsymbol{u}}_{\boldsymbol{z}}{}^{k+1} & = C^{-1}A\bar{\boldsymbol{\epsilon}}^{k+1} \end{cases}.$$

Note that we assumed the alternative boundary conditions which are described in Section 5.2 of our literature report [9], since then we get a unique solution instead of infinitely many, namely

$$\int_{\Omega}(\lambda+2\mu)\frac{\partial^2 \epsilon}{\partial z^2}\mathrm{d}\Omega = \int_{\Omega}\frac{\partial^2 P}{\partial z^2}\mathrm{d}\Omega \Leftrightarrow (\lambda+2\mu)\epsilon = P + d_1 z + d_2 \quad (10.8)$$

for $d_1(t), d_2(t) \in \mathbb{R}$. Since $\frac{\partial \epsilon}{\partial z} = \frac{\partial P}{\partial z} = 0$, we find that constant $d_1(t) = 0$ for all $t \in \mathbb{T}$. However, since $d_2(t)$ is arbitrary we still have infinitely many solutions. Therefore, we chose $d_2(t) = 0$ for all $t \in \mathbb{T}$ to find a unique solution. This choice of constant feels natural, because then the solution of the two-dimensional model with boundary conditions N-I (approximately interchangeable with the two-dimensional model with boundary conditions N-II) will converge to the solution of the one-dimensional model when the horizontal distance of the domain is chosen to be infinitely large. Furthermore, note that when the wave length L goes to infinity, the shear stress goes to a constant value which in line with the boundary conditions for the new model in two dimensions is zero and the normal stress due to the wave becomes a function only depending on time. At the surface this would mean that $\sigma_{xz}(x,t) := F_{xz}(x,t) \Longrightarrow 0$ and $\sigma_{zz}(x,t) := F_{zz}(x,t) \Longrightarrow F_{zz}(t)$ as $L \Longrightarrow \infty$.

Since the shear stress goes to zero and the normal stress due to the wave only depends on time as $L \Longrightarrow \infty$, there are no alterations in x-directions and thus the displacement in x-direction and all derivatives with respect to x vanish, i.e. $u_x \Longrightarrow 0$ and $\left(\frac{\partial \cdot}{\partial x}\right) \Longrightarrow 0$ as $L \Longrightarrow \infty$. Substituting these findings,

we get the one-dimensional model described in the 1D chapters of our literature report [9]. Following our literature report, in one dimension we use piece-wise linear basis-functions N_i of degree $p_z = 1$ and smoothness $k = 0$ called hat functions. These are given by

$$N_i = \begin{cases} \frac{z - z_{i-1}}{z_i - z_{i-1}}, & \text{if } z \in [z_{i-1}, z_i] \\ \frac{z_{i+1} - z}{z_{i+1} - z_i}, & \text{if } z \in [z_i, z_{i+1}] \end{cases},$$

for $i = 1, \dots, (p_z + 1)$. Furthermore, for integration of a subdomain we use 1000 integration points, the time step is chosen as $\Delta t = 0.01$ and the stepsize is chosen as $\Delta z = 0.001$.

10.2. Experiment 1: Variation of relative density and degree of saturation

In the first experiment, the one-dimensional set up is a vertical cylinder with a 1.8m thick layer of (nearly) saturated sand covered by a 0.2m thick layer of water [8]. A schematic diagram of the equipment is given by Figure 10.1, where pore pressure gauge P0 is installed at the surface of the sandy bed and pore pressure gauges P1-P10 are installed in the sandy deposit.

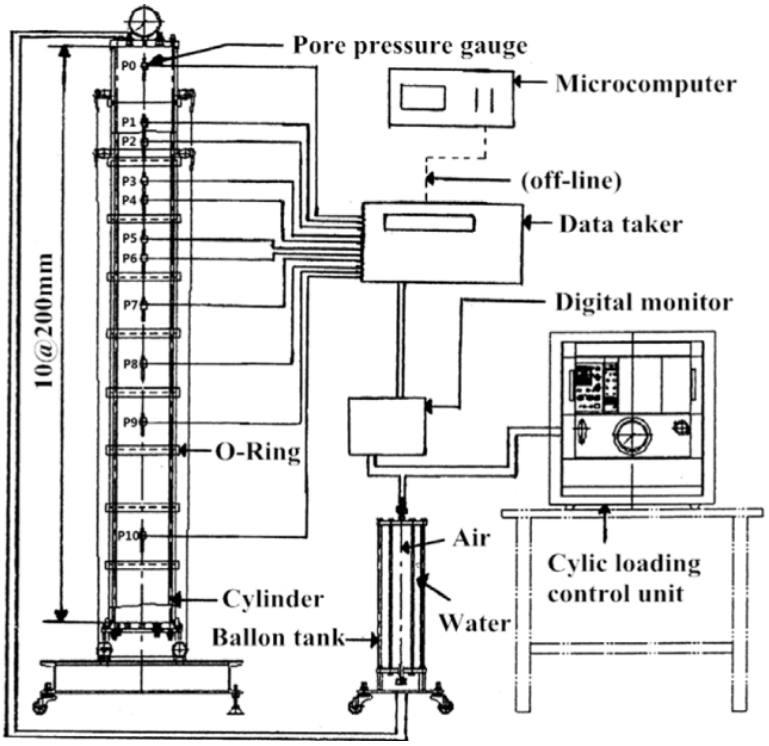

Figure 10.1: A schematic diagram of the equipment used for the one-dimensional cylinder experiment [8]. This figure is from (Liu et al., 2015).

For comparison of the new model with the data of [8], we set $F_{zz}(t) = 0.5\gamma_w H \cos\left(2\pi\frac{x}{L}\right)\sin\left(2\pi\frac{t}{T}\right) + \gamma_w D$, where the wave period T, wave height H, water depth D and number of waves N_c are given by Table 10.1. Note that in Equation (10.3) the initial condition $P(z, 0)$ is set equal to 0 as used everywhere else in this paper and in our literature report [9]. Since the water pressure in the steady state equals $\gamma_w D$, we add this solution to the transient solution of the water pressure at the end. Another approach would be setting the initial value of the water pressure equal to $\gamma_w D$. However, then the initial condition of the volumetric strain and vertical displacement need to be adjusted too. The steady state of the volumetric strain and vertical displacement would be given by $\epsilon(z) = \frac{\gamma_w D}{\lambda + 2\mu}$ and $u_z(z) = \frac{\gamma_w D}{\lambda + 2\mu}(z + n_z)$ for all $t \in \mathbb{T}$ when choosing $d_2 = 0$ in Equation (10.8) [9]. Since we only compare the water pressure, we chose the first approach. The values for the hydraulic conductivity K_s, porosity p, Poisson ratio v_p,

shear modulus μ, specific weight of water γ_w, relative density D_r and the depth of the soil h for dense and loose sand with a high or low degree of saturation are given by Table 10.2. Table 10.3 gives the values of the parameters for calculating the compressibility parameter β using Equation (5.5), namely the degree of saturation, the compressibility of pure water and the absolute pressure in the water. We will look at the numerical solution for the water pressure when the load on the surface is maximal, i.e. $(\max_t(F_{zz}(t)))$. In Figure 10.2 dense sand and loose sand is visualised.

Table 10.1: Parameters of the waves for subplots (a)-(d) [8].

Wave properties	**Symbols**	**Values**			
		(a)	**(b)**	**(c)**	**(d)**
Wave period [s]	T	15	9	9	9
Wave height [m]	H	3.5	2.5	3.5	1.23
Water depth [m]	D	5.2	5.2	5.2	5.2
Number of waves	N_c	10	10	10	10

Table 10.2: Parameters of one layer of sandy deposit based on [8].

Soil properties	**Symbols**	**Values**		
		Dense sand and high saturation	**Loose sand and high saturation**	**Loose sand and low saturation**
Hydraulic conductivity [m/s]	K_s	$1.4 \cdot 10^{-3}$	$2.1 \cdot 10^{-4}$	$1.8 \cdot 10^{-4}$
Porosity	p	0.384	0.425	0.425
Poisson ratio	v_p	0.3	0.3	0.3
Shear modulus [Pa]	μ	$1.27 \cdot 10^6$	$1.27 \cdot 10^7$	$1.27 \cdot 10^7$
Specific weight of water [N/m^3]	γ_w	9810	9810	9810
Relative density [-]	D_r	73.8	46.7	46.7
Depth of soil [m]	n_z	1.8	1.8	1.8

Table 10.3: Parameters of compressibility equation given by Equation (5.5).

Soil properties	**Symbols**	**Values**		
		Dense sand and high saturation	**Loose sand and high saturation**	**Loose sand and low saturation**
Degree of saturation [8]	s	1.0	1.0	0.994
Compressibility [10] of pure water [Pa^{-1}]	β_0	$0.5 \cdot 10^{-9}$	$0.5 \cdot 10^{-9}$	$0.5 \cdot 10^{-9}$
Absolute pressure [10] in the water [Pa]	P_0	10^5	10^5	10^5

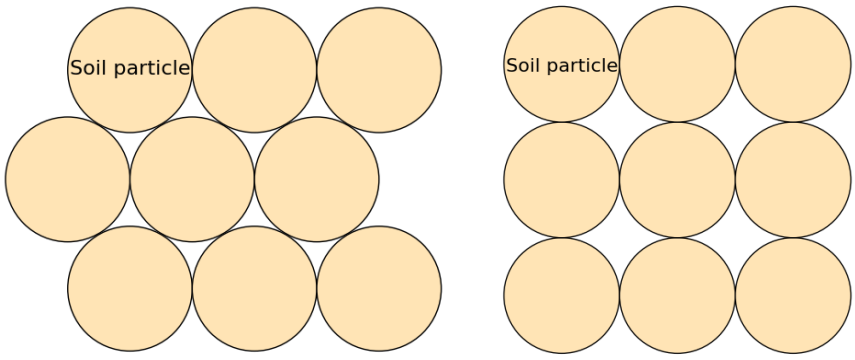

(a) Dense sand. (b) Loose sand.

Figure 10.2: Particles of sand.

In Figure 10.3 the normalised pore water pressure ($|P|/P_0$ with P_0 the initial amplitude) is plotted against the normalised depth (z/h) for loose sand with a high degree of saturation and dense sand with a high degree of saturation for several different properties of the waves given by Table 10.1. Since we want to stop at the time with most load ($\max_t(F_{zz}(t))$), we have that the stopping time $t_{\text{end}} = (N_c + 0.25)\,T$. Because the soil permeability is an experimental value [8], we have fitted our numerical solution to the data in Figure 10 from [8]. According to [8], the wave period and wave height will enlarge the influence of the relative density. Note that the wave height enhances the influence of the relative density more than the wave period when looking at the data which makes sense since the wave period is in a sine-function and the wave height is part of the amplitude of the load at the surface due to the waves. Furthermore, it holds that when the relative density is large, the soil permeability is small in any wave conditions [8]. The soil permeability values that give a good fit are given by $K_s = 1.4 \cdot 10^{-3}$ m/s for the dense sand and $K_s = 2.1 \cdot 10^{-4}$ m/s for the loose sand. However, we would expect the soil permeability to be larger for loose sand than for dense sand. When we take a closer look at the parameters given by [8], we also notice that the shear modulus is larger for loose sand than for dense sand while we would expect vice versa. If the values of the shear modulus in the paper are indeed swapped, then we would get the same solutions for ($\mu = 1.27 \cdot 10^7$, $K_s = 2.1 \cdot 10^{-4}$ m/s) for the dense sand and ($\mu = 1.27 \cdot 10^6$, $K_s = 1.4 \cdot 10^{-3}$ m/s) for the loose sand. In all subplots we find that at each depth, the water pressure is lower for a higher relative density which follows the data. Then we find that for wave properties (a) and (c) with the soil properties of the loose and dense sand with a high degree of saturation, the numerical solution fits the data from [8] quite well which can be seen in subplots 10.3a and 10.3c for the different relative densities. However, for the wave properties (b) and (d) we do find that the water pressure decreases over depth, but not as fast as the data from Figure 10 of [8]. It could be that the influence of the relative density due to the wave height and/or wave period is not well described yet in the model. Another reason for change of the difference in numerical solution and data for different wave heights could be caused by secondary terms that are more likely to happen for a certain wave height. For smaller wave heights, we have smaller loadings on the surface which means that the secondary terms have more influence on the behavior of the soil.

In Figure 10.4 the normalised pore water pressure ($|P|/P_0$) is plotted against the normalised depth (z/h) for loose sand with a low degree of saturation and for loose sand with a high degree of saturation for several different properties of the waves given by Table 10.1. Again, since we want to stop at the time with most load ($\max_t\{F_{zz}(t)\}$), we have that the stopping time $t_{\text{end}} = (N_c + 0.25)\,T$. Then we find that, like the data suggested, the pressure inside the soil diminishes more rapidly in the case of sand with a low degree of saturation than in the case of sand with a high degree of saturation. Furthermore, we find that for wave properties (a) and (c) and soil properties of the loose sand with a low degree of saturation and the loose sand with a high degree of saturation, the numerical solution fits the data of Figure 11 in [8] quite well which can be seen in subplots 10.4a and 10.4c for the different degrees of saturation. For soil properties (b) we also find numerical solutions that behave similar to the data. For the different degrees of saturation, especially subplot (d) stands out. According to [8], the influence of the degree of saturation decreases when the wave height and/or wave period decrease. Therefore, it could be that the influence of the degree of saturation is not yet linked well to the wave height and/or wave period in the model.

In Figure 10.5 the normalised pore water pressure ($|P|/P_0$) is plotted against the normalised depth (z/h) for loose sand with a a high degree of saturation. For the wave parameters, we use the values of (c) given by 10.1,i.e. $T = 9$, $H = 3.5$, $D = 5.2$, $N_c = 10$. Note that we again have a stopping time $t_{\text{end}} = (N_c + 0.25)\,T$ which equals 92.25 in this case. Then we find that the numerical solution for water pressure overall fits the data from Figure 4 in [8] quite well except for the lower part of the soil.

Another reason for the differences in value for Figures 10.3, 10.4 and 10.5 could be the assumption of constant soil properties in the new model [8]. A possibility is that the thickness of the sandy deposit was changing over time during the experiments due to liquefaction [8]. Another possibility could be that the relative density is not constant over depth [8]. Since the new model assumes constant soil properties, the difference between the numerical solution and the data could be caused by these phenomena. Lastly, errors in numerical discretisation and/or in the experimental data measured by [8] could also contribute to the difference in value.

In conclusion, most numerical solutions for water pressure overall agrees well with the data from [8]. There are some significant differences between the numerical solution and the data which could be caused by the assumption of constant soil parameters or simply by errors of the numerical discretisation

and data.

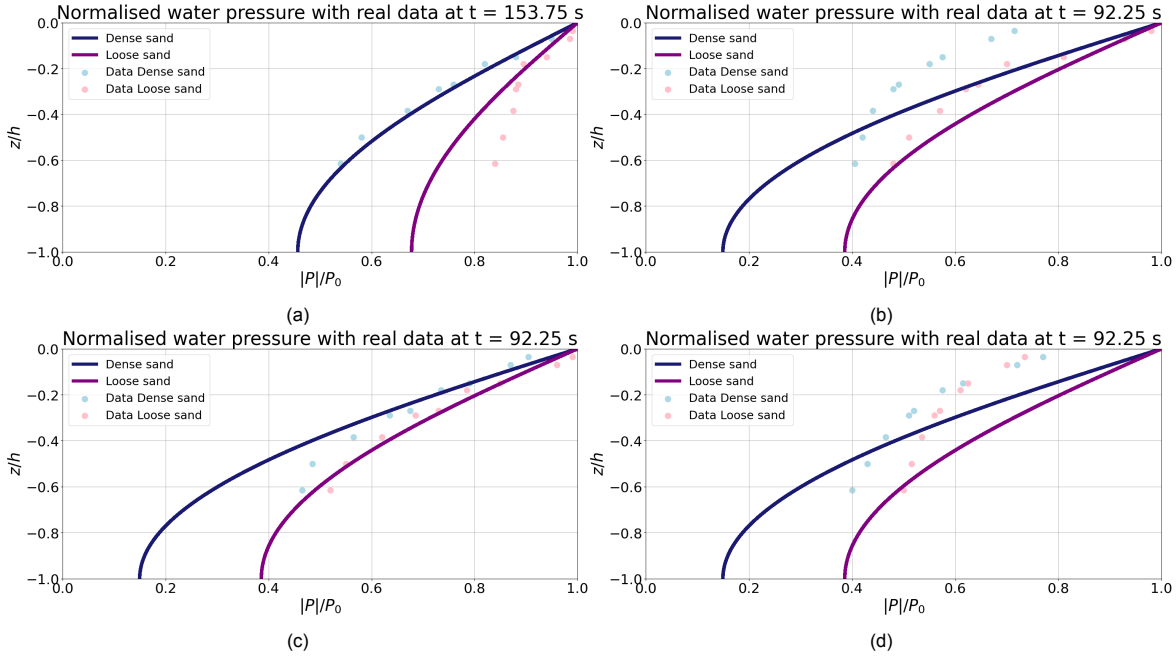

Figure 10.3: The normalised pore water pressure against the normalised depth together with the experimentally measured data from Figure 10 of [8] for different relative densities: for dense sand 73.8 and for loose sand 46.7 (i.e. different shear moduli: for dense sand $\mu = 1.27 \cdot 10^6$ and for loose sand $\mu = 1.27 \cdot 10^7$). The wave parameters corresponding to each subplot are given by Table 10.1. The water was assumed to be incompressible, so $\beta = 0.5 \cdot 10^{-9}$.

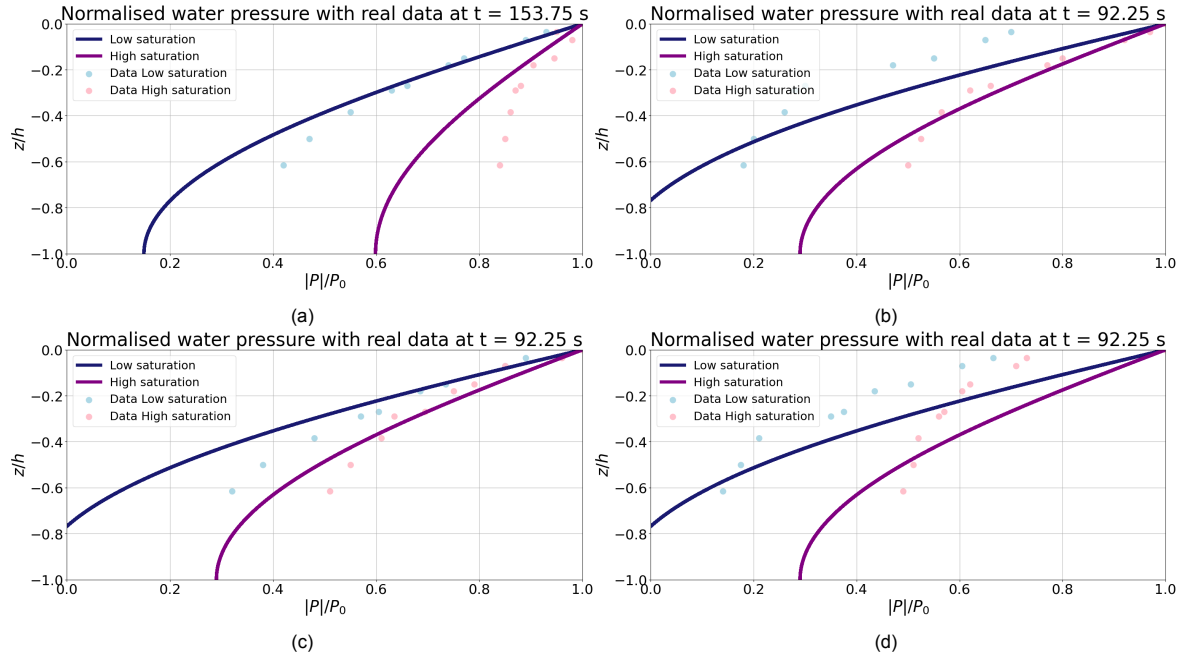

Figure 10.4: The normalised pore water pressure against the normalised depth together with the experimentally measured data from Figure 11 of [8] for different degrees of saturation (Low saturation: $s = 0.994$, high saturation: $s = 1.0$). The compressibility parameter is then calculated using equation (5.5). The wave parameters corresponding to each subplot are given by Table 10.1. The sand here is assumed to be loose with a relative density 46.7%.

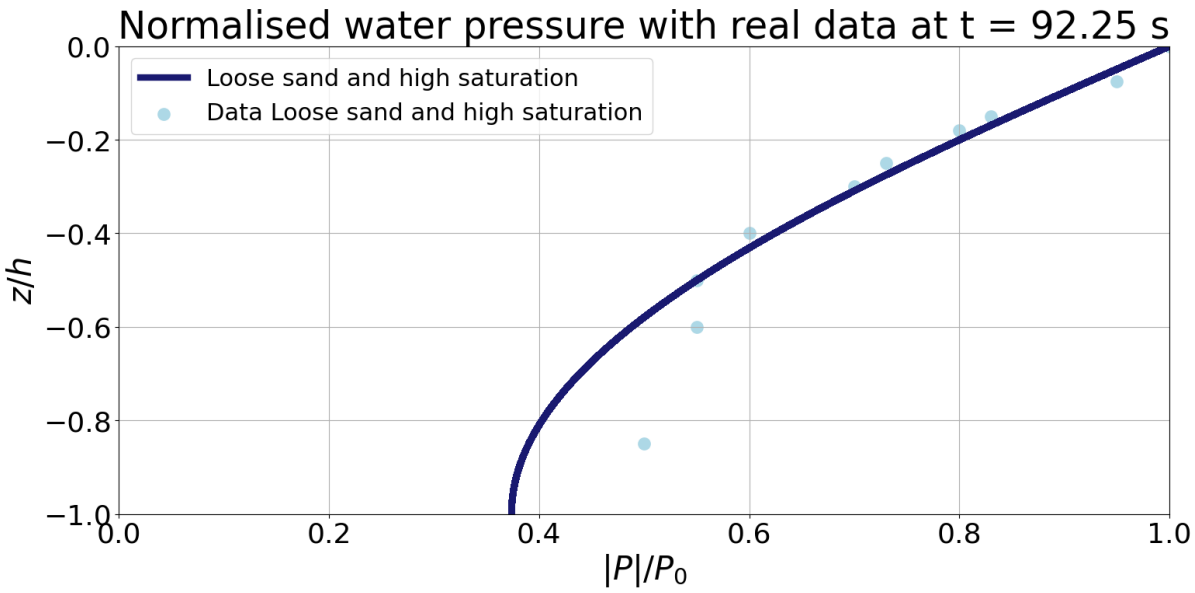

Figure 10.5: The normalised pore water pressure against the normalised depth together with the experimentally measured data from Figure 4a of [8].

10.3. Experiment 2: A passing ship

We will now look at the second experiment: the effect of a ship passing by on the water pressure. The set up is shown in Figure 10.6 where a ship is passing by above the pressure sensors from right to left. We will focus on validating the new model in one dimension (depth) with the data of Zaat [12]. In the experiments described by the paper [12], ten centimetres of the riverbed is dredged and a sand-bentonite-mix (SBM) is added above the sandy ground under the water of the canals of Twente. Therefore, we will take into account that two layers are involved in the riverbed. There are four pressure sensors placed on or in the riverbed, namely two (P1 and P3) at the surface of the river bed ($z = 0$ [m]) and two (P2 and P4) in the riverbed of which one is placed at a depth of thirty centimetres ($z = -0.3$ [m]). The depth of the other sensor is not fully known, but the paper [12] writes that sensor P2 measures lower water pressure than sensor P4. According to [12], return flows arise when a ship passes by. These return flows causes the water level and the water pressure to decrease. This means that P2 would be buried closer to the surface than P4. The difference is estimated at 0.1 metres, so sensors P2 and P4 lay at $z = -0.2$ [m] and at $z = -0.3$ [m], respectively. Note that this latter is stated in the text of [12]. However, in the figures of [12] it seems that the sensors P2 and P4 are swapped. For example, see Figure 1 in [12]. Since we agree with the reasoning of P2 measuring lower water pressure means being buried shallower, we assume the presence of a mistake in the legend of the figures in [12]. Therefore, in our figures based on the figures in [12] P2 and P4 are illustrated in the colors yellow and orange, respectively. The locations of the pressure sensors can be found in Figure 10.7.

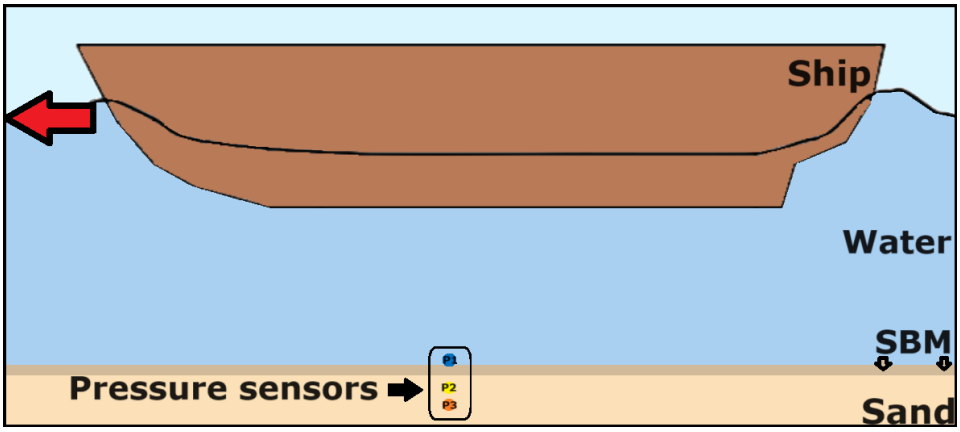

Figure 10.6: A passing ship above the pressure sensors based on [12].

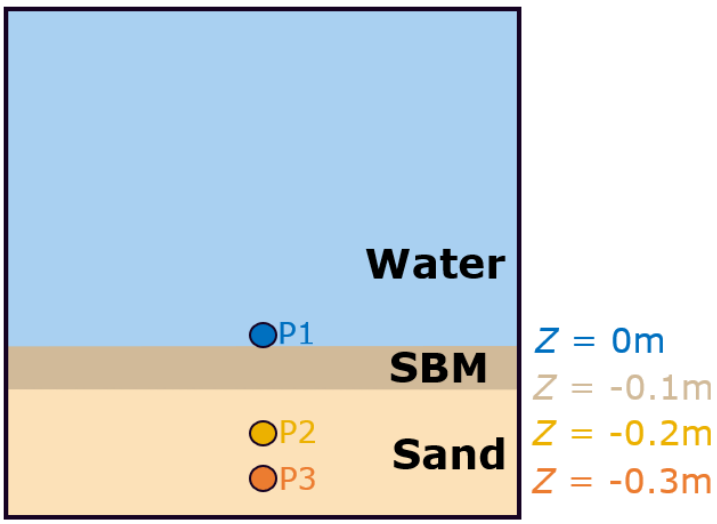

Figure 10.7: Locations of the pressure sensors based on [12].

We use the soil properties porosity, poisson ratio, shear modulus, specific weight of water, effective grain size and the dept of the soil that are given by Table 10.4 and the soil properties regarding the compressibility of the soil are given by Table 10.5. These values are based on us fitting the numerical solution to the data given by [12]. Note that like for case 1 we assume that the water is incompressible. Furthermore, the hydraulic conductivity can be approximated by the following equation of Allen Hazen [13]: $K_s = c \cdot d_{10}^2$ [cm/s], where c is Hazen's coefficient and d_{10} is the effective grain size [mm]. We will use $c = 1.0$ which is often chosen in civil engineering problems, like we did in our literature report [9]. The load on the surface is set equal to the water pressure measurements by sensor P1, i.e. the water pressure data of sensor P1 are used as boundary condition at the surface.

Note that the water pressure measured by the sensors does not equal 0 in steady state. However, since we set the initial condition of the water pressure (and other variables) equal to zero which is stated in Equation (10.3), we will determine the steady state with initial conditions being equal to zero and adding the steady state corresponding to the depth of the sensors P1, P2 and P4 to the transient solution like we did for case 1 in the previous section. Lastly, to compare the numerical solution to the data, the data in metres water column is converted to data in Pascal by a multiplication of factor $\gamma_w g$.

Table 10.4: Parameters of two layers of different soils: SBM at suface and a sand below.

Soil properties	**Symbols**	**Values**	
		Sand	**SBM**
Porosity [-]	p	0.44	0.4
Poisson ratio [-]	v_p	0.3	0.3
Shear modulus [Pa]	μ	$1.0 \cdot 10^5$	$2.0 \cdot 10^5$
Specific weight of water [N/m^3]	γ_w	10^4	10^4
Effective grain size [mm]	d_{10}	0.23	0.3
Depth of the layer [m]	h	0.1	1.9
Total depth of soil deposit [m]	n_z	2.0	2.0

Table 10.5: Parameters of compressibility equation given by Equation (5.5).

Soil properties	**Symbols**	**Values**	
		Sand	**SBM**
Degree of saturation	s	1.0	1.0
Compressibility [10] of pure water [Pa^{-1}]	β_0	$0.5 \cdot 10^{-9}$	$0.5 \cdot 10^{-9}$
Absolute pressure [10] in the water [Pa]	P_0	10^5	10^5

We present four comparisons between the numerical results of the new model and the data obtained by reading the corresponding graph in [12] given by Figures 10.8a, 10.8b, 10.8c and 10.8d. In Figure 10.8a, a ship is passing by on 26-10-2021 (DD-MM-YYYY) at 09:13:30 (HH:MM:SS). In Figures 10.8b, 10.8c and 10.8d, a ship is passing by on 27-10-2021 at 17:49:28, 28-10-2021 at 15:41:56 and 01-11-2021 at 09:01:03, respectively. Then we find that the numerical results of the new model for the water pressure fits the data quite well. The water pressure indeed drops when the ship is passing by the pressure sensors and over time it goes back to the steady state it had before the ship passing by. However, there are some minor differences in value of the numerical solution and data, especially around the peaks and troughs. This latter could be caused by numerical error, since we used basis element functions of degree 1 and smoothness 0 to find the numerical solution. Higher order and/or higher smoothness would probably give a better approximation around the peaks and troughs. Also note that the difference between the numerical solution and the data can be smaller but also larger, since the data is obtained from reading the graphs [12]. Furthermore, there can be some experimental errors. In conclusion, the numerical solutions behave similar to the data but may differ significantly in value, especially around the peaks and troughs.

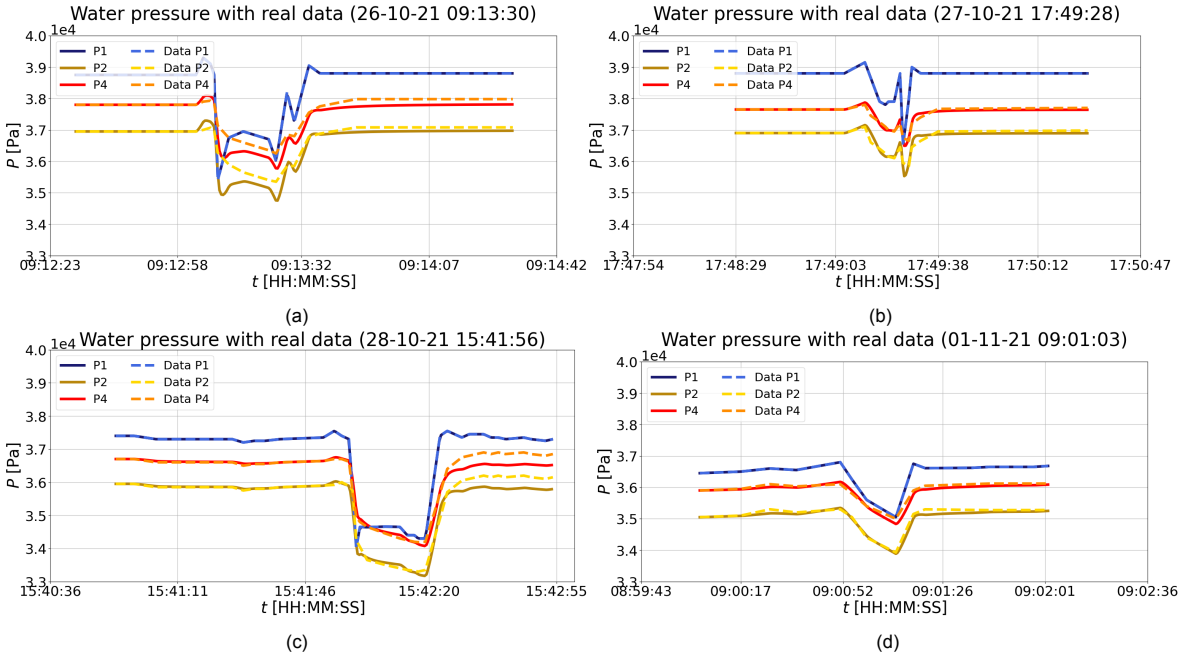

Figure 10.8: The time in HH:MM:SS against the pore water pressure in Pascal is plotted together with the experimentally measured data of [12] for different times and dates. There are three lines plotted, namely one for the depth of each of the three pressure sensors: P1, P2, P3 at $z = 0, -0.2, -0.3$ m, respectively. The soil properties are given by Tables 10.4 and 10.5.

11 Discussion

The aim of this master thesis was

1. to describe the response of porous media to transient hydraulic loads using numerical methods like the Finite-Element Method, and
2. to apply it to a one-dimensional case whereby a sandbed is subjected to waves.

Currently, changes in pore water pressure in porous media subjected to transient hydraulic loads are typically predicted using Biot's model. Biot's model considers compressible pore water, assumes zero effective stresses on the surface of the seabed, and assumes that the wave load is completely carried by the pore water pressure only. A new model proposed by van Damme and Den Ouden-Van der Horst suggests that transient hydraulic loads acting on a porous medium affect both the pore water pressure and the effective stresses in soils. Note that this makes sure that the momentum balance equations are satisfied throughout the computational domain and its boundaries. However, this model does not satisfy Terzaghi's effective stress principle at the soil surface in the sense that the sum of the effective stresses and pore water pressure does not equal the hydraulic load, whereas Biot's model is in line with this principle.

In Chapter 2 the stress and strain relations in a linear elastic medium are explained.

In Chapter 3 Biot's model is introduced in two dimensions. Here the governing equations, boundary conditions and initial conditions are described.

In Chapter 4 a numerical approach is applied to Biot's equations to solve them. Section 4.1 shows that the Finite-Element Method is used for spatial discretization. The Finite-Element Method is flexible in terms of computational domain and different types of boundary conditions that can be included. By approximating the unknown variables with a linear combination of basis functions, the weak equations can be rewritten as Galerkin equations. These equations are then solved using the Backward-Euler time discretization method which is described in Section 4.2. The Backward-Euler method is an implicit method which is needed, since some of the governing equations are not time dependent but the equations are all coupled. Furthermore, an implicit method is unconditionally stable which we prioritize over accuracy.

In Chapter 5 we derived the numerical results of Biot's model for three different sets of boundary conditions. We assumed that the soil particles of the porous media are incompressible and that the water particles are slightly compressible, namely a compressibility of $4.05 \cdot 10^{-8}$ Pa^{-1}. The numerical results were similar to those obtained for incompressible water, but a bit more oscillating near the surface when zoomed in. For incompressible water a compressibility parameter of $0.5 \cdot 10^{-9}$ Pa^{-1} is assumed. Furthermore, we assume that the vorticity is zero beforehand. In Section 5.1 three different sets of boundary conditions are described for Biot's model. In Section 5.2 for each set of boundary conditions we found a solution for the volumetric strain, water pressure, horizontal displacement and vertical displacement of Biot's equations in two dimensions with the assumption of one homogeneous layer of soil. Also the vorticity, effective stress in z-direction, shear stress and volume balance were determined. Depending on the set of boundary conditions, we get a solution for the volumetric strain, water pressure and displacements which does not satisfy all assumptions and (boundary) conditions.

The three sets of boundary conditions for Biot's model differ in one condition at the surface, namely the first states that the shear stress equals zero, the second states the derivative of the horizontal displacement with respect to the depth equals zero and the third states that the vorticity equals zero. Since the vorticity is assumed to be zero everywhere, we would expect that the first two sets of boundary conditions give the same results. The third set is to investigate whether the assumption of vorticity being zero everywhere is indeed satisfied. However, for a zero shear stress boundary condition the solutions are not vorticity free, do not satisfy the volume balance equation everywhere and also the momentum balance equations are not satisfied. For the boundary condition given by the derivative of horizontal displacement with respect to z being equal to zero at the surface, the results are still not vorticity free and do not satisfy the volume balance equation everywhere. Also the momentum balance equations are still not satisfied. Furthermore, the shear stress is not found to be zero at the surface which we expected when assuming vorticity to be zero everywhere. The boundary conditions given by the vorticity being zero at the surface, gives results that do satisfy the momentum balance equations. However, the solutions are still not vorticity free, the volume balance is not satisfied everywhere and the shear stress is not found to be zero at the surface.

In Chapter 6 the two-dimensional model of Van Damme and Den Ouden-Van der Horst introduced. Here the governing equations, boundary conditions and initial conditions are described.

In Chapter 7 a numerical approach is applied to model of Van Damme and Den Ouden-Van der Horst to find a solution. In Section 7.1, the Finite-Element Method is used for spatial discretization. By approximating the unknown variables with a linear combination of basis functions, the weak equations can be rewritten as Galerkin equations. These equations are then solved using the Backward-Euler method for time discretization which is described in Section 7.2. Note that this discretisation is the same as for Biot.

In Chapter 8 we derived the numerical results of the model of Van Damme and Den Ouden-Van der Horst for two different sets of boundary conditions. We assumed again that the soil particles of the porous media are incompressible and that the water particles are slightly compressible, namely a compressibility of $4.05 \cdot 10^{-8}$ Pa^{-1}. The numerical results, when assuming incompressible water, seem the same. For incompressible water a compressibility parameter of $0.5 \cdot 10^{-9}$ Pa^{-1} is assumed. Furthermore, we assume again that the vorticity is zero. In Section 8.1 two different sets of boundary conditions are described for the new model. In Section 8.2, for two different sets of boundary conditions we solved the new model for the volumetric strain, water pressure, horizontal displacement and vertical displacement in two dimensions with the assumption of one homogeneous layer of soil. Furthermore, the vorticity, effective stress in vertical direction, shear stress and volume balance were also determined. The two sets of boundary conditions for the new model differ in one condition at the surface, namely the first states that the volumetric strain times a constant equals the pore water pressure and the second states that the vertical momentum balance equation must hold at the surface. In these boundary condition sets, we also simplified the shear stress condition at the surface to the derivative of vertical displacement with respect to the depth being zero, which follows from the vorticity being zero. We expect similar results for both, since when the first boundary conditions set holds the second boundary conditions set also automatically holds. Indeed, we find very similar results for both boundary conditions sets. Only their solutions for the volumetric strain differ by a constant in space. They both satisfy all their boundary conditions, the vorticity and the volume balance are approximately zero everywhere and the shear stress is zero at the surface.

In Chapter 9 we did compare Biot's model and the new model of Van Damme and Den Ouden-Van der Horst further. Here, we exchanged the boundary condition at the surface that was different, namely the effective stress being equal to zero versus the vertical momentum balance equation. We did this comparison to investigate the stability of both models and the influence of the boundary conditions. Overall, we found that the results of the new model were slightly more stable in behaviour than Biot's model. Furthermore, we found that the influence of the assumption of the effective stress being zero at the surface is such that the solutions do not seem to satisfy all conditions we expect. These expectations are that the solutions satisfy their boundary conditions, are vorticity free and satisfy the volume balance equation. When setting the vertical momentum balance equation at the surface, these are all satisfied.

In Chapter 10 we validated the new model in one dimension. The new model is compared with experimental data from two different experiments: (1) measuring data in a one-dimensional set up with a vertical cylinder with first a sand deposit of 1.8 m thick and then 0.2 m water above the sand, and (2)

measuring data when a ship passes by in the Twente Canal. For both experiments pressure sensors were used to determine the water pressure at several levels above or in the soil. For the first experiment a certain function is assumed as input for the load at the surface while for the second experiment the measured input at the surface of the riverbed is used as input for the load. Furthermore, the one-dimensional version of the new model is used for approximation of the solution, since the set up of the first experiment is one-dimensional and the second experiment can be reduced to a one-dimensional problem. Overall, the new model in one-dimension fits both datasets quite well and when the value of the numerical solution of the water pressure differs with the data, the behaviour of the numerical solution over space and/or time is similar. For the first experiment this means that the water pressure decreases with an increase in relative density or a decrease in degree of saturation. For the second experiment it means that the water pressure in the soil is less impacted by the load at the surface when the depth is increasing.

12

Conclusions and recommendations

We came to the following conclusions based on this study.

	Model of Biot	**Model of Van Damme and Den Ouden-Van der Horst**
1.	Biot's model in this thesis exists of three constitutive equations: for the dynamic water pressure, displacement in horizontal direction and displacement in vertical direction.	The model of Van Damme and Den Ouden-Van der Horst exists of five consitutive relations: for the dynamic water pressure, displacement in horizontal direction, displacement in vertical direction, volumetric strain and vorticity.
2.	Numerical solutions are derived for the dynamic water pressure, displacement in horizontal direction and displacement in vertical direction in line with Terzaghi's stress principle by using the Finite-Element method for discretising in space and the Backward-Euler method for discretising in time.	Numerical solutions are derived for the dynamic water pressure, displacement in horizontal direction, displacement in vertical direction and volumetric strain in line with d'Alemberts principle of minimum energy using the Finite-Element method for discretising in space and the Backward-Euler method for discretising in time.
3.	In Biot's model the hydrodynamic loads are carried by the pore water and the effective stress is set equal to zero at the surface.	In the new model the pressure, the effective stress or the normal stress is defined at the surface.
4.	Biot's model is based on the assumption of compressible water.	In the new model the water can be assumed to be compressible or incompressible.
5.	Momentum and volume balance equations are not satisfied.	Momentum and volume balance equations are (approximately) satisfied.
6.	The assumption vorticity free is not satisfied.	The assumption vorticity free is (approximately) satisfied.
7.	Biot's model is more difficult to solve numerically.	The new model is easier to solve numerically.
8.	The solution to the new model for the dynamic pore water pressure is similar to the solution to Biot's model. However, the solutions to the new model for the other variables as volumetric strain and displacements can differ significantly. It is not possible yet to tell which model is right which might differ per physical problem. Since these variables can not be measured or are difficult to be measured, it is not possible to compare the numerical results for variables as volumetric strain and displacements to experimental data.	

For further research we suggest the following extensions of this study.

- Investigate the case when having multiple layers of different kinds of soil more, since there are many assumptions regarding the intersections between these layers to consider.
- Compare the (numerical) solutions of Biot's model and the model of Van Damme and Den Ouden-Van der Horst based on physics, mathematics and data of experiments more extensively.
- Extend the one-dimensional and two-dimensional model by adding the acceleration terms as an extension. This could provide insights into the validity of our assumption of the acceleration terms being negligible.
- Improve computation time and accuracy of the numerical methods by making the code more efficient and the steps in space and time smaller, respectively.
- Choose the computational domain in different shapes. In this master thesis, we assumed a rectangular grid in two dimensions. However, in reality the layers of the seabed are not necessarily rectangular but can be multiple shapes like diagonal or wavy.

.

A

Numerical solutions to Biot's model with water that is very compressible (2D)

We set the compressibility parameter $\beta = 10^{-6}$. The numerical solutions to Biot's model for the volumetric strain ϵ_{vol}, pore water pressure P, horizontal displacement u_x and vertical displacement u_z, and their derivatives with respect to x or z are shown in Figures A.1, A.2 and A.3. The vorticity ω, effective stress σ'_{zz}, shear stress σ_{xz} and the volume balance are shown in A.4.

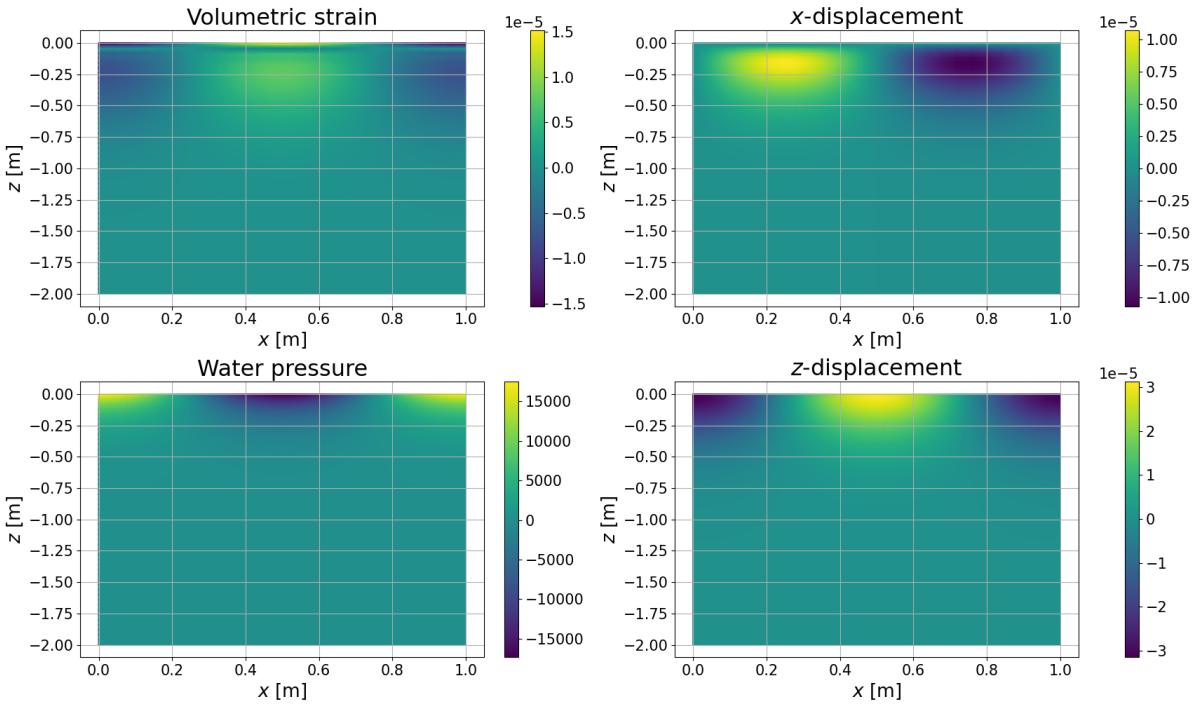

Figure A.1: Solutions to Biot's model for ϵ_{vol} [-], P [Pa], u_x [m], u_z [m] at $t_{\text{end}} = 2.25$ s, when water is assumed to be compressible with $\beta = 10^{-6}$ Pa^{-1} and using boundary conditions B-I which is given in Section 5.1.1. The other used parameters for the soil, the water and the waves are given by Tables 5.1, 5.2 and 5.3, respectively. In this thesis, a negative pressure is pointing upwards (a pulling force), and a positive pressure is pointing downwards (a pushing force). The soil displacement upwards or to the right is positive and downwards or to the left is negative.

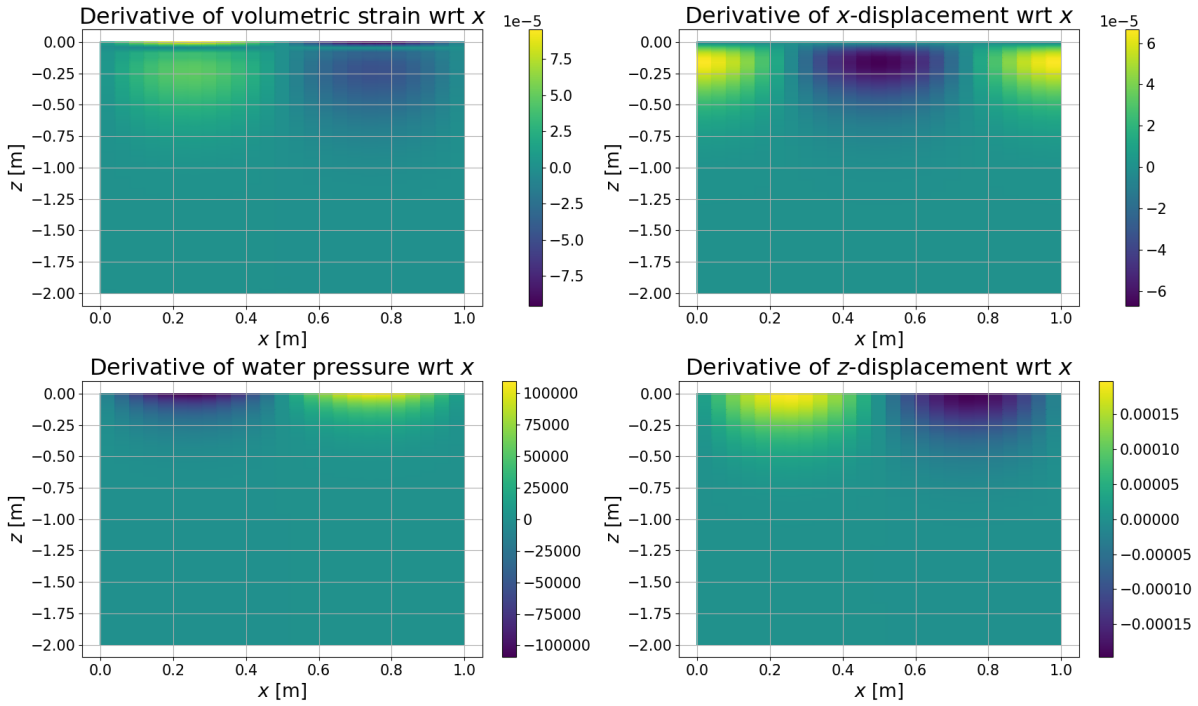

Figure A.2: Solutions to Biot's model for $\frac{\partial \epsilon_{\text{vol}}}{\partial x}$ [m^{-1}], $\frac{\partial P}{\partial x}$ [N/m^3], $\frac{\partial u_x}{\partial x}$ [-], $\frac{\partial u_z}{\partial x}$ [-] at $t_{\text{end}} = 2.25$ s, when water is assumed to be compressible with $\beta = 10^{-6}$ Pa^{-1} and using boundary conditions B-I which is given in Section 5.1.1. The other used parameters for the soil, the water and the waves are given by Tables 5.1, 5.2 and 5.3, respectively.

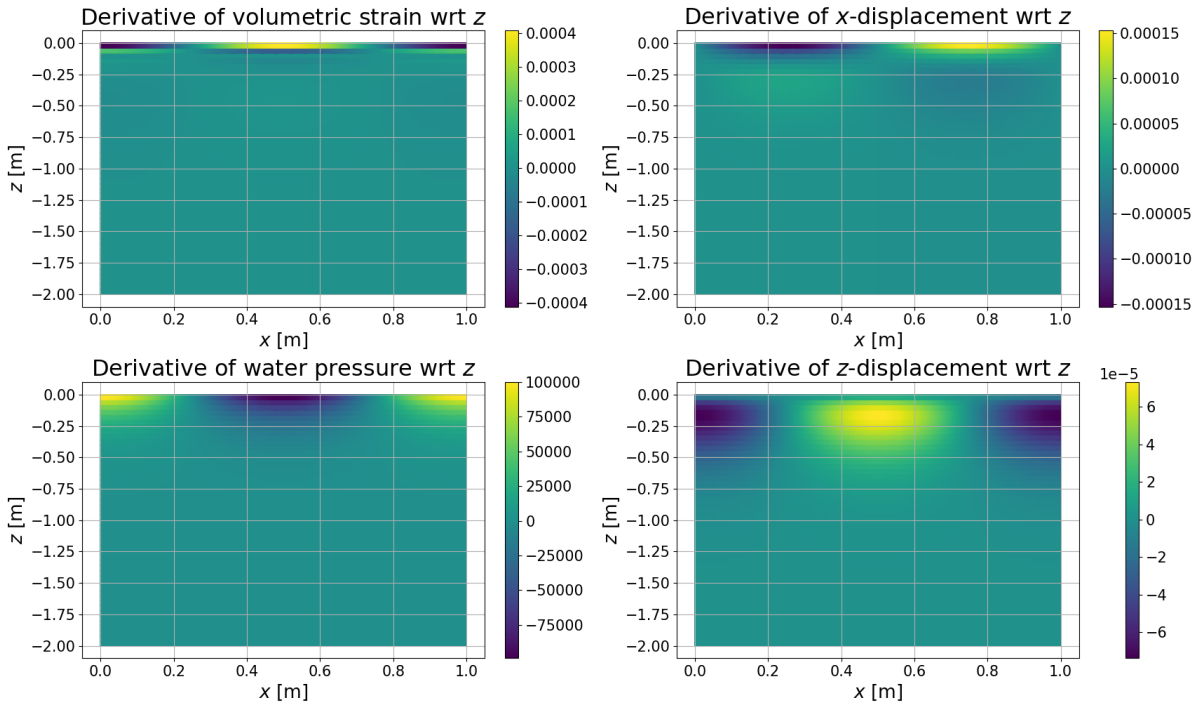

Figure A.3: Solutions to Biot's model for $\frac{\partial \epsilon_{\text{vol}}}{\partial z}$ [m^{-1}], $\frac{\partial P}{\partial z}$ [N/m^3], $\frac{\partial u_x}{\partial z}$ [-], $\frac{\partial u_z}{\partial z}$ [-] at $t_{\text{end}} = 2.25$ s, when water is assumed to be compressible with $\beta = 10^{-6}$ Pa^{-1} and using boundary conditions B-I which is given in Section 5.1.1. The other used parameters for the soil, the water and the waves are given by Tables 5.1, 5.2 and 5.3, respectively.

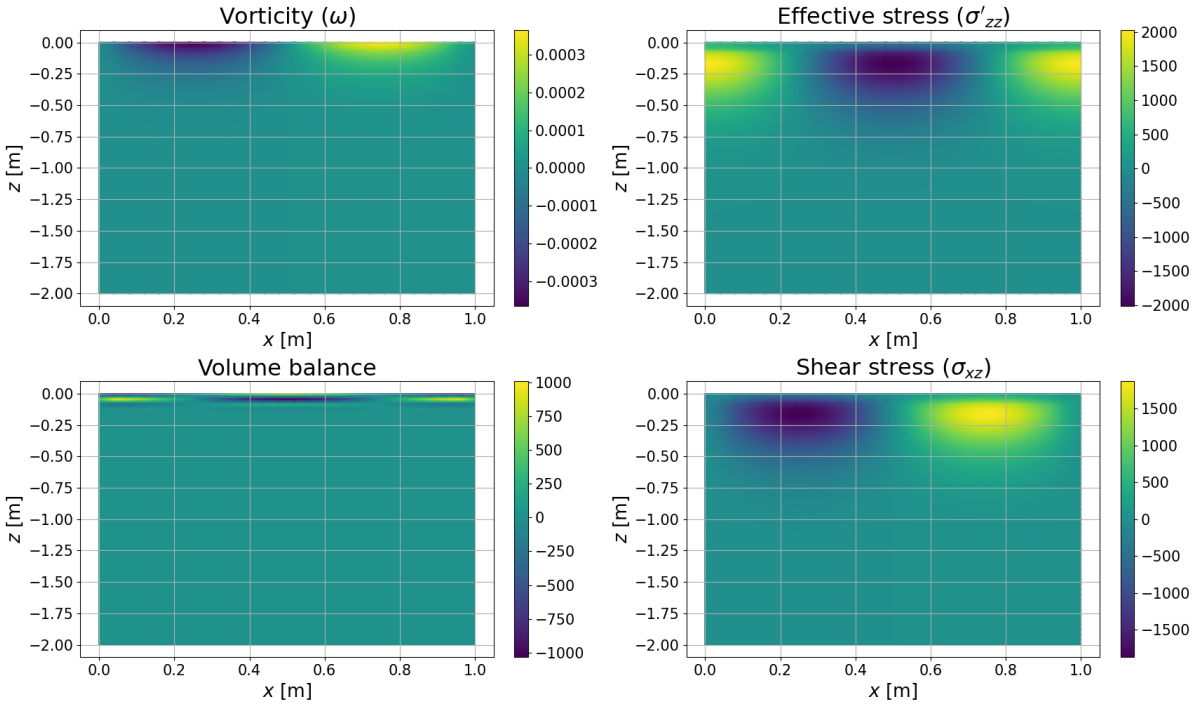

Figure A.4: Solutions to Biot's model for ω [-], σ'_{zz} [Pa], σ_{xz} [Pa] and volume balance at $t_{\text{end}} = 2.25$ s, when water is assumed to be compressible with $\beta = 10^{-6}$ Pa^{-1} and using boundary conditions B-I which is given in Section 5.1.1. The other used parameters for the soil, the water and the waves are given by Tables 5.1, 5.2 and 5.3, respectively. The vorticity is expected to be zero. The volume balance is represented by the weak form of the volumetric strain equation and is satisfied if it equals 0 everywhere on the domain and its boundaries.

B

Analytical solutions to the model of Van Damme and Den Ouden-Van der Horst (2D)

The compressibility parameter for solving the model of Van Damme and Den Ouden-van der Horst (new model) analytically is $\beta = 0.5 \cdot 10^{-9}$ which is the compressibility of pure water. Therefore, the water is practically incompressible. The two-dimensional analytical solutions to the new model for the volumetric strain ϵ_{vol}, pore water pressure P, vertical displacement u_z and shear stress σ_{xz} are shown in Figure B.1 and are obtained from Van Damme and Den Ouden-Van der Horst [4].

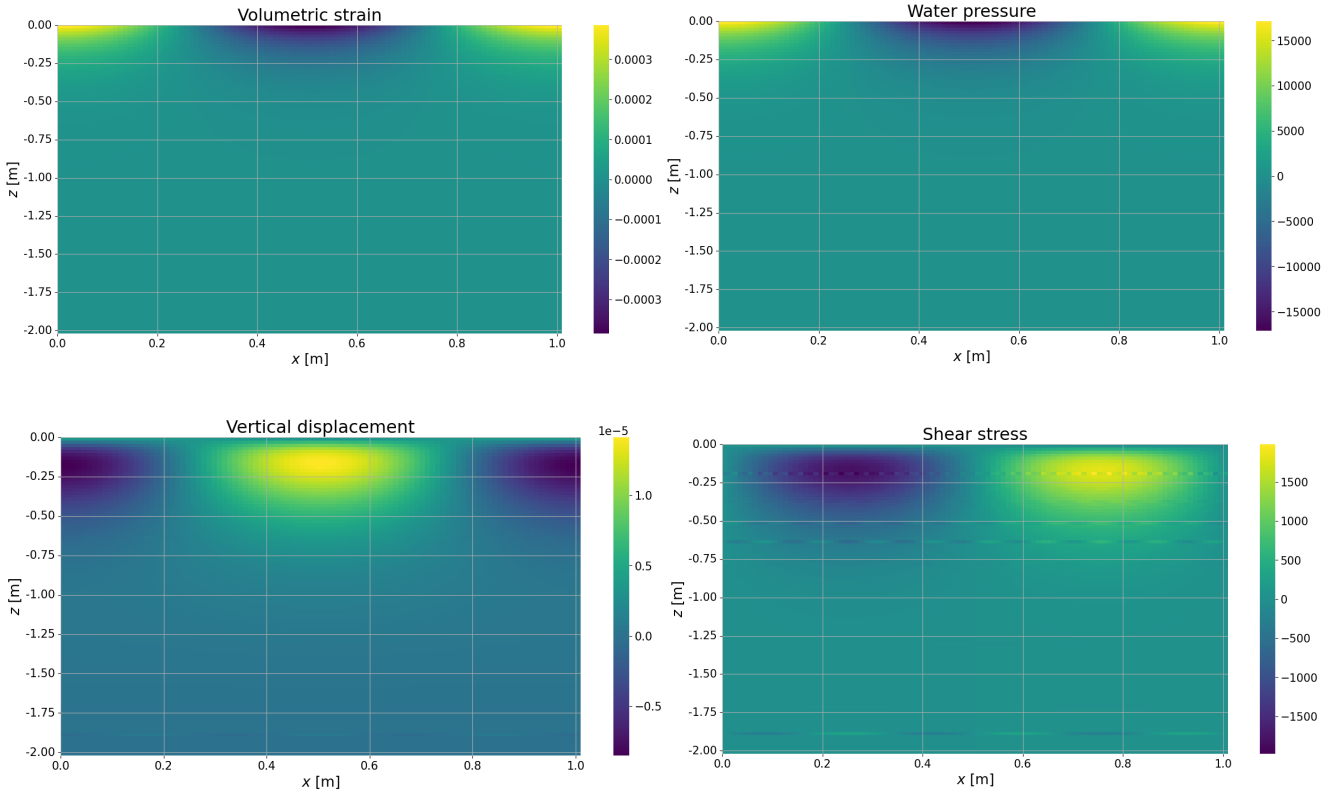

Figure B.1: Solutions to New model for ϵ_{vol} [-], P [Pa], u_z [m], σ'_{zz} [Pa] and σ_{xz} [Pa] at $t_{\text{end}} = 2.25$ s, when water is assumed to be incompressible with $\beta = 0.5 \cdot 10^{-9}$ Pa^{-1} and using boundary conditions N-I which is given in Section 8.1.1. The other used parameters for the soil, the water and the waves are given by Tables 5.1, 5.2 and 5.3, respectively.

Bibliography

[1] Willemsen, P., Klein Breteler, M., Doeleman, M., Borsje, B., & van Maren, B. (2023). *Bijdrage van kweldervegetatie aan het waterkeringssysteem* (tech. rep.). Deltares. 11205132-002-HYE-0010

[2] Biot, M. (1956). Theory of propagation of elastic waves in a fluid-saturated porous solid i. low-frequency range. *The Journal of the Acoustical Society of America*, *28*(2), 168–178.

[3] Verruijt, A. (2006). *Offshore soil mechanics*.

[4] Van Damme, M., & Den Ouden-Van der Horst, D. (2023). An alternative process-based approach to predicting the response of water saturated porous media to hydrodynamic loads. *Journal of Porous Media*. https://doi.org/10.1615/JPorMedia.2023045106

[5] Cai, Y., & Sun, H. (2017). *Solutions for biot's poroelastic theory in key engineering fields*. Butterworth-Heinemann.

[6] Mersie, M. (2021). *Overtopping failure in levees* (Master's thesis). TU Delft and Rijkswaterstaat.

[7] Ye, J., & Jeng, D.-S. (2011). Effects of bottom shear stresses on the wave-induced dynamic response in a porous seabed: Poro–wssi (shear) model. *Acta Mech. Sin.*, *27*(6), 898–910. https://doi.org/10.1007/s10409-011-0469-1

[8] Liu, B., Jeng, D.-S., Ye, G., & Yang, B. (2015). Laboratory study for pore pressures in sandy deposit under wave loading. *Ocean Engineering*, *106*, 207–219. https://doi.org/https://doi.org/10.1016/j.oceaneng.2015.06.029

[9] Klein, F. (2023). *Compressible vs. incompressible pore water in fully-saturated poroelastic soil: Literature report* (Master's thesis). TU Delft and Rijkswaterstaat.

[10] Verruijt, A. (2010). *Soil mechanics*.

[11] Van Damme, M., & Den Ouden-Van der Horst, D. (2022). Methodology for calculating the response of porous media for evaluating grass response to overtopping loads. *Proceedings of 4th International Seminar on Dam Protections against Overtopping*.

[12] Zaat, L. (2022). *Analyse meetdata kanaalafdichting met zbm* (tech. rep.). RWS.

[13] Salarashayeri, A., & Siosemarde, M. (2012). Prediction of soil hydraulic conductivity from particle-size distribution. *International Journal of Geological and Environmental Engineering*, *6*(1).